

A modular nonlinear stochastic finite element formulation for uncertainty estimation.



Yanis Ammouche
St Hugh's College
University of Oxford

A thesis submitted for the degree of
Doctor of Philosophy
Trinity 2023

Acknowledgements

Pour commencer, je voudrais sincèrement remercier mon superviseur Antoine d'avoir cru en moi et de m'avoir donné l'opportunité d'étudier à Oxford, chose que je n'aurais jamais imaginé, même dans mes rêves les plus audacieux. Je te remercie de tout tes conseils pour le futur, du temps que tu m'as consacré, et des projets plus intéressants les uns que les autres dans lesquels tu m'as impliqués. Ta constante disponibilité et ta force de travail digne d'une mongoose sous amphétamines auront été des éléments déterminant dans la (possible) réussite de ce doctorat. En bref, la thèse présentée dans ce rapport, mais aussi mes futurs travaux te doivent énormément.

I kindly acknowledge the EPSRC Prosperity Partnership Grant EP/S005072/1 for their financial support during this project.

My warmest thoughts go to the members of the group when I arrived, very intimidated, in 2019. In particular, Céline, who facilitated my adaptation to the group, for always being incredibly positive, supportive, kind, and funny (the list could go on forever). I am also very grateful to Miren, for being always helpful, altruistic and more importantly frank, a quality that is rare nowadays. Speaking of qualities, it has been hard to find some about Sahand... Despite your horrible imitation of the french accent, your sense of humour composed of way-over-the-line jokes have been greatly appreciated. I wish you'd have stayed in the group a bit longer... Ciara, please know that you were the cement of the group. Your bubblyness, your organisation skills were key to the cohesion of the group. I will never forget our ice-skating sessions and I wish you a happy wedding to you and your fantastic boyfriend Alex. Last but not least, I'd like to express my sincere thanks to Sara, who has been sometimes incredibly patient to me (remember Barcelona), and a very good co-worker. To all of you guys: I hope you'll have a life full of happiness, success and no stress.

I would also like to pay tribute to Van Dung Nguyen, probably the best researcher I've ever met and worked with (sorry Antoine...). I am still impressed by how quickly you manage to make anything work, and how easily you understand incredibly abstract and theoretical concepts. Your patience and coding advice have been incredibly useful. Please know that part of the work presented below would have not been there without you. My kindest regards to you!

Casey, I am still in awe of how skillful you are, capable of imitating many accents, speaking french fluently and also sending microscopes from UK to any part of the world. Thanks so much for all the proofreading you've done and your constructive conversations. Each and every second by your side were amazing, full of laugh and joy of life. Please never lose your enthusiasm, that makes you such a unique person (in a good way).

Thanks to Phoebe, for proofreading a lot of things I sent to you. I admire your kindness and your energy, always smiling even when you feel disheartened. With you, the group could not be in safer hands. I'd like to deeply acknowledge Yuyang's contribution to my work, you are certainly one of the most hardworking, but also sweetest person I have ever met. Lizzie, I strongly appreciate your help during the end of my PhD and your ice-skating skills that are second to none. Thanks to Kin, Thalès, Aaron, beautiful Tom, Khariton, Alice (being stuck with you in Oslo was not that bad, trust me), Peihao, Jimmy for the day-to-day interactions.

I am also thankful to all the good souls I met in St Hugh's. Wei, you've been a fantastic friend, and changed my perception of human interactions to an extent you cannot imagine. During my journey in Oxford, there has definitely been an after and before I met you. My warmest thought to Kiana, to whom I owe my best months in Oxford and the Colonel, always there to share food and life thoughts :). A particular thanks to the Thursday doughnuts squad, always ready to eat sweet stuff: Pauline, Kathy, Jared, Lauren, Siyu, Sophie, Daphné (who is probably one of the best person I have met). Special shout-out to Marin, a tough yet sweet person, with a strong sense of moral and a questionable sense of humour. St-Hugh's could not hope to have a better Junior Dean than you, I swear. Prachi, know your Chai tea is unmatched in Oxford :).

I want to express how grateful I am to the Hugh's football team. In particular, Roma, to whom I have a special thought in these rough times, you're one of the first person I befriended during the pandemic and I wish I would have met you sooner. Thanks to Antonio, one of the funniest person I have ever met, Tim (to whom I apologise for all the stories he had to listen), Captain Barney, reliable off and on the pitch, Captain Dennis, one of the best players I have ever met, and a very good soul. Many thanks to Solomon, Rex (who became prime Cafu in 2022), Ludwig, Johannes, Gonzalo (I wish I'd have talked to you more often) Mark and Albie. Also, as some people knew, I had a double life with the Jesus College football team, and I want to thank Marco (for being a formidable captain and human being), Ryan, Adrien (amazing person but unfortunately is not aware of it) and Burno Sram. My most sincere apologies if I forget anyone, the list could actually go on forever.

Ma sincère gratitude à mes parents, Mohand et Khédoudja que je n'ai jamais oublié durant ces trois ans, même si le peu d'appel que je vous ai donnés laisse

penser le contraire. Tout mon parcours, je le dois à vous, n'en doutez pas une seule seconde. Merci de m'avoir toujours accueilli les bras ouverts avec énormément de nourriture délicieuse. Je tiens aussi à remercier mes soeurs, Sonia pour sa constante communication et son aide logistique, Lila pour m'avoir accueilli durant la période de quarantaine et Nadia ainsi que Myriam pour nos interactions dans la capitale. J'espere vous retrouver tous bientôt. Je pense aussi à toi Kamel, tu as beaucoup fait pour m'aider et je ne l'oublie pas. Petite dédicaces à mes nieces Farah, Camélia, Lehna, Jasmine et au petit Arilès. Big up à toi Juju !

Abstract

The Monte Carlo method is widely used for the estimation of uncertainties in mechanical engineering design. However, while flexible, this method remains impractical in terms of computational time and scalability. In 1990's Ghanem and Spanos introduced a more efficient approach. Albeit code intrusive, this framework has the advantage of being sampling independent, provides accurate output statistics and is modular in terms of operation. However, this method has traditionally been limited to linear elasticity.

This thesis aims to extend the Galerkin Stochastic Finite Element Method (GSFEM) to a wider range of industry-relevant applications. First, Wavelet expansions are incorporated in the GSFEM. This new feature enables capturing discontinuous surface responses. The flexibility of this approach is illustrated with a 3D hyperelastic example with nonlinear behaviour arising from buckling uncertainty. Then, the GSFEM is specialised in the *A Posteriori* Finite Element Method (APFEM) where uniform distributions are taken by default to allow for parametric studies of the inputs of interest as a postprocessing step after the simulation. Doing so, APFEM only requires the knowledge of the vertices of the parameter space. In particular, one key advantage of APFEM is its use in the context of Bayesian inferences, where the random evaluations required by the Bayesian setting (usually done through Monte Carlo) can be done exactly without the need for further simulations. Finally, the APFEM is modified to obtain output's response under random geometric perturbations. This framework allows reliable mechanical outcome prediction for a set of geometries comprised between two given configurations.

The GSFEM has also been extended to a wide panel of constitutive models and has been modified to incorporate simple contact features leveraging the maturity of our stochastic algebra. Using the Monte Carlo (MC) method as a baseline, results show the excellent accuracy of the aforementioned stochastic method. The developed framework could potentially allow further enhancement of the design step in the engineering process as one simulation is enough to obtain all possible mechanical outcomes.

Dissemination

Peer-reviewed journal papers

D. Field, **Y. Ammouche**, J.M. Peña and A. Jérusalem. *Machine learning based multiscale calibration of mesoscopic constitutive models for composite materials: application to brain white matter*. Computational Mechanics 67 (6), 1629-1643, 2021. DOI: 10.1007/s00466-021-02009-1.

Y. Ammouche and A. Jérusalem. *A modular nonlinear stochastic finite element formulation for uncertainty estimation*. Computer Methods in Applied Mechanics and Engineering 396, 115044, 2022. DOI: 10.1016/j.cma.2022.115044.

Y. Ammouche and A. Jérusalem. *The a posteriori finite element method (APFEM), a framework for efficient parametric study and Bayesian inferences*. Computer Methods in Applied Mechanics and Engineering, **In Press**, 2023.

Y. Ammouche and A. Jérusalem. *Extension of APFEM to random topology, a framework for efficient geometric uncertainty quantification*. International Journal for Numerical Methods in Engineering, **Under Review**.

Conference presentations

Y. Ammouche and A. Jérusalem. *A modular nonlinear stochastic finite element formulation for uncertainty estimation*. 8th European Congress on Computational Methods in Applied Sciences and Engineering ECCOMAS Congress 2022, Oslo, Norway (2022)

Y. Ammouche and A. Jérusalem. *A modular nonlinear stochastic finite element formulation for uncertainty estimation*. 18th European Mechanics of Materials Conference EMMC18, Oxford, UK (2022).

Y. Ammouche and A. Jérusalem. *A modular nonlinear stochastic finite element formulation for uncertainty estimation*. XVI International Conference on Computational Plasticity. Fundamentals and Applications. COMPLAS 2021, Barcelona, Spain (2021).

Y. Ammouche and A. Jérusalem. *A modular nonlinear stochastic finite element formulation for uncertainty estimation*. X International Conference on Adaptive Modeling and Simulation ADMOS2021, Gothenburg, Sweden (2021).

~~**Y. Ammouche** and A. Jérusalem. *A modular nonlinear stochastic finite element formulation for uncertainty estimation*. Invited talk —IUTAM symposium~~

Computational Fracture Mechanics, Bad Honnef, Germany (2020) [Cancelled due to COVID-19.]

Contents

List of Abbreviations	xii
1 Introduction	1
2 Literature review	5
2.1 Uncertainty classification	6
2.1.1 Aleatoric uncertainties	6
2.1.2 Epistemic uncertainties	6
2.2 Non-intrusive methods	8
2.2.1 Monte Carlo method	8
2.2.2 Multilevel Monte Carlo method	13
2.2.3 Quadrature polynomial chaos	14
2.2.4 Regression-based method	18
2.3 Intrusive methods	22
2.3.1 Perturbation finite element method	22
2.3.2 Galerkin Stochastic Finite Element Method	25
2.4 To be intrusive or non-intrusive?	30
3 Theoretical framework and numerical implementation	32
3.1 Mathematical foundation of GSFEM	32
3.1.1 Stochastic space discretisation	33
3.1.2 Balance of linear momentum	34
3.1.3 Boundary conditions	34
3.1.4 Weak form of the balance of momentum	35
3.1.5 Numerical integration	35
3.1.6 Constitutive model	38
3.1.7 Expansion of the solution	46
3.1.8 Modularity of the code	50
3.1.9 Uncertainty of the inputs	51
3.2 APFEM and BI-APFEM	52
3.2.1 Legendre PCE	52
3.2.2 Specialisation of mixed Wavelet expansion to uniform variables	53

Contents

3.2.3	Bayesian inferences	54
3.3	Extension to topological uncertainties	56
3.3.1	Framework	56
3.4	Dissemination	59
4	Numerical applications	60
4.1	Stochastic buckling	60
4.1.1	Stochastic buckling: GSFEM approach	60
4.1.2	Multi-directional stochastic buckling using APFEM	65
4.1.3	Stochastic buckling: geometrical uncertainties	69
4.2	APFEM for parameter space exploration and optimisation	70
4.2.1	Estimation of a metamaterial's behaviour	71
4.2.2	Optimisation problem of a growing rod	73
4.3	APFEM for inverse problems	74
4.3.1	Contact mechanics: the Cattaneo-Mindlin problem	75
4.3.2	Theoretical framework	76
4.3.3	Results	78
4.3.4	Brain mechanics: a large scale problem	80
4.4	Dissemination	82
5	Conclusions, limitations and future directions	85
5.1	Summary and achievements	85
5.2	Limitations	88
5.3	Future directions	90
Appendices		
A	Operations in the stochastic space	92
A.1	Stochastic algebra	92
A.1.1	Linear combination of real numbers and stochastic variable	92
A.1.2	Product of two stochastic variables	93
A.1.3	Division of two stochastic variables	93
A.1.4	Product of a stochastic variable and a stochastic tensor	93
A.1.5	Product of two stochastic tensors	94
A.1.6	Trace of a stochastic tensor	94
A.1.7	Dyadic product of stochastic vectors	94
A.1.8	Inversion of a stochastic tensor	94
A.2	Expansions considering Gaussian stochastic variables	95

Contents

B	Nonlinear functions of random variables	96
B.1	Algorithm for computation of non-polynomial functions of random variables	96
B.2	Application to square root	98
B.3	Application to logarithm	99
C	Impact of remeshing strategy	101
C.1	Plate in tension with a single defect	101
	References	106

List of Abbreviations

APFEM	A Posteriori Finite Element Method
AM	Additive Manufacturing
BI	Bayesian Inferences
CFD	Computational Fluid Dynamics
EMWs	Electromagnetic Waves
FE	Finite Element
FRP	Fibre-Reinforced Polymers
GSFEM	Galerkin stochastic finite element method
MC	Monte Carlo
MLMC	Multilevel Monte Carlo
MPSM	Modified Perturbation Stochastic Method
PDEs	Partial Differential Equations
PFEM	Perturbation Finite Element Method
QPC	Quadrature Polynomial Chaos
UQ	Uncertainty Quantification

Chapter 1

Introduction

Flaws in engineering design process can severely jeopardise safety by contributing to early failures in construction projects. Such failures have important economic, environmental and social consequences [1]. Engineering failures account for as much as 10% of the total investment in new structures [2]. To prevent them, engineers have been typically using materials in excess of their requirements to ensure decent reliability in the functioning of their manufactured products. Generally, this excess material aims at addressing the various uncertainties envisaged during the design process including scenarios of overloading, accuracy of theoretical models, materials and manufacturing [3]. The extra raw materials going into a conservative design translate into higher energy consumption and the concomitant emission of green house gases. As optimising their production strategies has become a major concern for most companies [4], conservative designs are now increasingly challenged.

Engineering designs often rely on mathematical models to obtain predictions on the structural response. They mainly involve partial differential equations (PDEs) describing physical phenomena whose solutions are approximated by numerical calculations carried out by computers [5]. Among these numerical schemes, the finite element method (FEM) is widely used in mechanical engineering. Because this method is deterministic in nature (i.e., one output solution for one set of inputs),

researchers have coupled it with heuristic methods to explore the parameter space when aiming at achieving an optimal design, see, e.g., Ref. [6–8].

Paradoxically, relying on the deterministic nature of the FEM, and thus assuming that a given structure (i.e., its geometry, constitutive models and set of material parameters) is fully known at the onset of each simulation is at odds with the very nature of the mechanics of materials. As an illustration, the fabrication of composites, widely used in the aerospace and automotive industries for their superior properties, consists of a series of manufacturing steps (forming, consolidation/impregnation and curing) introducing variability to the subsequent manufacturing processes. As a result, strong interdependencies between the process parameters and their variability, and the resulting properties of the structure are expected [9]. Similarly, additive manufacturing (AM) allows the creation of more versatile designs compared to traditional manufacturing processes. However, because of the complex history dependent manufacturing process, structures generated using AM often exhibit strong geometrical deviations compared to the original target design [10]. Therefore, while widely adopted for all these applications, the use of deterministic simulation frameworks such as the FEM is not per se able to capture the real stochastic nature of structural deformation.

In the last few decades, some industries gathered an extensive amount of data about material and structural variabilities through a variety of experiments [11]. Probabilistic distributions of the material or structural uncertainties could then be documented by using inverse methods on these datasets [12, 13]. Alternatively, new advances in material characterisation (e.g, X-ray tomography) have also allowed to gather microstructural information not readily known a priori. This acquired wealth of information on material uncertainties can then be sampled in terms of material properties and used, e.g., in FEM frameworks, such as Monte Carlo (MC), with applications in failure and damage process prediction. While such approaches do not require a modification of the original deterministic simulator, i.e., non intrusive, they become inefficient for large-scale realistic problems due to the excessive computational cost arising from the sampling effort. To bypass

this limitation, other non-intrusive methods have been proposed. In particular, Qiu and Zang [14] proposed a novel efficient and accurate approach to crack propagation analysis in structures with random uncertainties based on polynomial chaos expansion (PCE) [15, 16]. The stochastic response is supposed to follow a prescribed shape where only the coefficients have to be determined. These methods are promising even if they suffer from the curse of dimensionality. They are, however, also sampling dependent, potentially decreasing their robustness.

Independently of this, in some industrial cases, inferring probability distributions requires a quantity of data that is either too costly or difficult to obtain. Hence, non-probabilistic approaches have been developed considering only the physical parameters bounds, a more accessible information. These approaches include interval methods [17, 18]. Interval methods infer the worst-case response of a given structure with only low computational cost, thus solving non-deterministic problems in solid mechanics with great efficiency. For example, Rao and coworkers [19] determined the crisp bounds of stress in beam structures with incomplete knowledge of the cross-sectional area and Young’s modulus. Afterwards, Long *et al.* [20] computed the life bounds of a turbine generator rotor where a crack was introduced. They managed to predict worst and best case scenarios for fatigue crack growth under uncertain knowledge of fracture toughness and initial crack length with satisfying accuracy. This method was enhanced to show its full potential in cases where the model response is monotonic with respect to the input parameters [18, 21]. Interval methods have now an increased level of maturity as they incorporate the possibility to model spatially random fields [22]. However, these methods can be over-conservative [18] potentially leading to suboptimal designs. In addition, if these methods provide the response’s extrema, no insights are given within the parameter space.

To this end, intrusive methods where both the physical and stochastic problems are solved altogether in one simulation have been proposed. Ghanem and Spanos have introduced the Galerkin stochastic finite element method (GSFEM) [23] as an extension of the deterministic FEM for solving boundary-valued problems with random material properties, for linear elasticity and in small deformation. Fifteen

years ago, Acharjee [24] extended this formulation to finite deformation and even considered uncertain initial geometry. Marzouk [25] proved the increased efficiency of intrusive methods compared to MC when carrying out a parameter identification on a diffusion problem. More recently, Rosic [26] developed a formulation to expand this method to elastoplasticity. Despite these recent advances, extending these intrusive methods to theories modelling phenomena such as fatigue, bifurcation, fracture or contact mechanics remains challenging. While some of these methods have been used to model problems where uncertainties are described as random fields with a given spatial correlation, they most often considered linear or weakly nonlinear problems, lacked modularity and an established unified mathematical formulation for a wider range of applications.

The aim of this thesis is thus to propose a modular nonlinear SFE formulation to circumvent these limitations. In the following, the relevant literature on non-deterministic methods is first reviewed in Chapter 2. New formulation of GSFEM able to simulate nonlinear problems involving bifurcation is then presented in Chapter 3. This chapter also contains the specialisation of GSFEM to inverse problems through the so-called *A posteriori* Finite Element Method (APFEM). The results of these methods are tested and evaluated in Chapter 4 to show the prospects of these methods for a wide panel of nonlinear and industry-relevant applications. Conclusions, limitations of the study and future perspectives are finally given in Chapter 5.

Chapter 2

Literature review

Over the past thirty years, researchers have proposed enhanced frameworks to make non-deterministic simulations tractable [27–33]. These methods fall into two types of categories. In the first category, any existing FE software can be used through an external script acting as a wrapper. These methods are called here and subsequently non-intrusive methods. The second category, termed called intrusive, requires modification of the governing equation and hence the solver. As a result, additional coding effort is required, hindering the possibilities of coupling these methods with commercial software.

In the following, we first present and classify uncertainties. Then, the most widely used methods for both non-intrusive and intrusive strategies are covered. In addition, an overview of applications proposed in the literature is given for each of these frameworks. Eventually, their main limitations and shortcomings are presented.

2.1 Uncertainty classification

Uncertainties traditionally encountered in any physical system are split into two main categories: aleatoric and epistemic.

2.1.1 Aleatoric uncertainties

Aleatoric uncertainties arise because of the unpredictable and random nature of the studied physical system. They encompass unknowns that differ each time an experiment is repeated. In the field of mechanics, these errors include assembly tolerance, randomness distribution of material microstructure and properties, among others. As aleatoric uncertainties describe the variability in the physical system, they can not be easily reduced. Traditionally, these uncertainties are represented using probability distributions, taking values within an established range, with a given probability of occurrence. Various distributions have been used to incorporate these randomnesses into a mathematical model [34, 35]. Following Soize [36], it is also possible to use non-parametric approaches to model uncertainties.

2.1.2 Epistemic uncertainties

Epistemic uncertainties, also called systematic uncertainties refer to the limited human knowledge of the system. Epistemic uncertainties are a major source of discrepancies when studying a wide range of systems, such as seismic activities [37] or flooding [38]. In the latter, for example, the unprecise assessment of how much and how often rainfall occurs (in past and future events) belong to epistemic uncertainties. Such uncertainties arise from the fact the numerical model incompletely describes the behaviour of the physical system. As opposed to aleatoric uncertainties, epistemic uncertainty can in principle be reduced with additional data. While some studies have described epistemic uncertainties using probability theory [39], it has been argued that such a representation is inappropriate [40]. For these reasons, quantification of epistemic uncertainties involves alternative strategies such as the fuzzy method [41, 42] or the possibility theory [43]. The most recent studies are able to model and quantify the impact of both aleatoric and

systemic uncertainties using mixed formulations [44, 45] where the probabilistic and possibilistic nature of aleatoric and epistemic randomness, respectively, are incorporated in a mathematical model.

2.2 Non-intrusive methods

Non-intrusive methods have been proposed for industrially relevant uncertainty quantification (UQ) in the 1950's by Ulam and Von Neumann. Due to their flexibility and smooth integration in existing frameworks, these approaches are still broadly used.

2.2.1 Monte Carlo method

The implementation of the MC method in this context is straightforward. Assuming that uncertain parameters of the simulation have a known probabilistic distribution, the values of these variables are sampled. These samples are then given as inputs to any FE software used as a 'black box'. Once enough inputs have been gathered, postprocessing the results allows for the acquisition of the statistics of mechanical outputs (displacement, stress, etc.). As shown in Figure 2.1, the

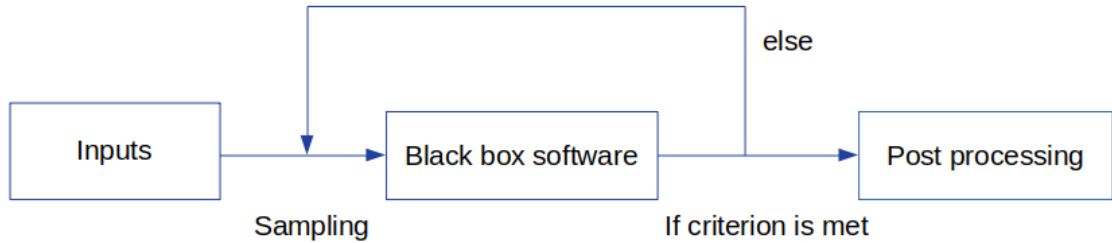


Figure 2.1: Scheme of the Monte Carlo method.

MC method solely requires a wrapper calling for repeated deterministic simulations. For its simplicity of use, researchers of various areas of computational mechanics use MC for UQ.

Unlike in computational solid mechanics, where the solvers, explicit or implicit, are relatively universal, in Computational Fluid Dynamics (CFD) each condition (e.g., transient or steady state, compressible or incompressible, low or high Reynolds number) requires a different solver. The intricacy of their deterministic form thus leaves only little room for further intrusive modification and implementation. As

a result, the MC method is extensively applied. Huilin *et al.* [46] carried out numerical studies to determine the behaviour of bubbles and particles in a bubbling fluidised bed. The collision of particles, a random process by nature, was simulated using MC. They found excellent agreement between computed particle velocities and experiments. Another group of researchers [47] examined the vapor-liquid equilibria of binary mixtures using MC to take into account uncertainties at the molecular level. The MC method is also widely used in the domain of aeroelasticity. He *et al.* [48] noted that frequency domain methods for predicting the dynamics of mistuned bladed disks are typically based on iterative aeroelastic calculations. Each iteration of that process requires a significant computation time. Consequently, the whole computational scheme would greatly benefit from a fast method predicting the number of iterations needed for converged results. To this end, this research group performed a parametric study using MC to show that the aerodynamic ratio and the aerodynamic gradient ratio are the two most important factors affecting the convergence history. More recently, Argentini *et al.* [49] quantified the effects of both mechanical and aerodynamic parameters variations on the aeroelastic stability of a slender suspended bridge. They narrowed down the sensitivity of critical flutter velocity and total damping trend to nine independent random aerodynamic and structural parameters. In addition, Murugan and coworkers [50] investigated the effects of spatially uncertain material properties on the aeroelastic response predictions (e.g., rotating frequencies, vibratory loads, etc.) of a composite helicopter rotor. Initially, the spatial uncertainty is modelled as discrete random variables along the blade span and UQ is performed with direct MC. Rodrigues and colleagues [51] used a coupling between Large Eddy Simulation and MC to analyse the radiative transfer in a turbulent sooting jet flame. The mean value of the flame radiative power field was computed using the MC method. The attractiveness of the MC method for UQ also reached the computational electromagnetism discipline.

While extensively studied, several real-world electromagnetic problems traditionally including electromagnetic radiation, modelling of waveguides [52, 53], scattering [54–56] have traditionally been solved using deterministic approximations. Recently,

progress has been made to incorporate uncertainties for more realistic simulations. Scattering describes a wide range of physical processes where moving particles or waves of any form, such as light or sound, are forced to deviate from a straight path by localised inhomogeneities (including particles) in the medium through which they travel. These particles can have random configurations and positions, limiting the accuracy of deterministic analyses. The study of electromagnetic waves (EMWs) in arid environments is highly challenging as sand-dust clusters of random positions alter their propagation. Li *et al.* reported reliable EMWs attenuation estimation through sand storms leveraging MC method and performing repeated deterministic simulations of EMWs propagation considering random positions of the scatterers. The MC method to study scattering problems was enhanced in Ref. [57]. Instead of solving for the propagation of EMWs in dielectric objects using Maxwell's equations, they relied on a Volume Integration Equation allowing them to propose an efficient MC parallelisation scheme where speed up increased linearly with respect to the number of nodes used.

Similarly, the field of computational solid mechanics contains a wide range of structural problems involving randomness. In the last decades, MC has been applied to simulations encompassing various disciplines such as fatigue crack growth and fracture, among others.

Stochastic studies are of particular interest as fatigue crack growth is a random process by nature [58]. Specimens cut from the same sheet, in a controlled environment under the same loading, show a wide range of lifetime scatter [59]. As there is a general consensus that this scatter on fatigue lives originates from material properties uncertainties [60] and random loadings [61], an increasing number of publications has modelled these disparities in reliability analysis under cycling loading. Liu *et al.* [62] based their stochastic reliability analyses on Paris' law. This law, derived phenomenologically, links the propagation rate using a stress intensity factor and material parameters. Assuming an unknown initial crack length and uncertain material constants, they solved for the random fatigue life of the coupon. The analytical solution for its distribution being impossible to obtain,

they resorted to MC and calculated the probabilistic fatigue-life distribution. For easier incorporation of random cycling loadings in probabilistic studies involving MC, the same group [63] used a rainflow counting algorithm [64] for proper cycle decomposition, aggregated the combined stochastic damage, using Miner’s rule [65]. In order to take into account multiaxial fatigue, Liu *et al.* [66] proposed a simulation-based calculation procedure combining MC with a response surface method. The proposed method included topological, structural and environmental uncertainties. The failure probability, defined when the accumulated damage exceeds an acceptable value, was obtained using MC. These numerical results, in addition to design experiments, allowed for the derivation of an empirical formula for the damage accumulation process, taking into account various kinds of uncertainties. Field failure data were in excellent agreement with numerical results. More recently, Low [67] used control variates, a variance reduction method in conjunction with MC. They reported an increase in computational efficiency compared to MC alone. For the study of long-term fatigue analysis of offshore structures in a random sea state.

The rupture of a structural component can also occur during static loading when the applied force exceeds a certain threshold. While hybrid materials such as composites are being increasingly used for their excellent mechanical properties, their highly complex manufacturing process introduce aleatoric uncertainties. Various experimental programmes have showed inevitable scatter in the measurement of fracture toughness for modes I, II, and mixed mode fracture [68, 69]. Consequently, MC drew the attention of researchers to fill the extensive knowledge gaps in stochastic analysis of fracture in composite materials. In the early 2000’s, Jeong *et al.* [70] performed a probabilistic strength analysis of T300 carbon/epoxy composite, a fibre-reinforced polymers (FRP) plate, with anti-symmetric stacking sequences. They modelled uncertain transverse lateral pressure load, elastic moduli, geometric and ultimate strength values of the laminates using normal and two-parameter Weibull probability distributions. First-ply probability failures of composites were

reported for six different failure criteria: maximum stress, maximum strain, Tsai-Hill, Hoffman, Tsai-Wu and Azzi-Tsai-Hill. In the same study, a sensitivity analysis was presented to show which aleatoric uncertainty had the largest impact for each limit state equation used. A decade later, Whiteside *et al.* [71] designed further sensitive analysis of FRP. They considered four physical-based rupture criteria for each failure mode: fibre tensile failure, matrix failure, fibre kinking and matrix splitting between the fibres, and performed stochastic analyses using MC. Considering random tensile and compressive strength informed by previous experiments [72], they reported that slight fibre misalignment ($<3^\circ$) was enough to cause considerable shear stresses and trigger a different failure mode compared to the nominal deterministic case. In a recent study [73], the Stochastic Numerical Analysis Architecture, based on a resampling method combined with MC, was developed to obtain the strength dispersion of a FRP. Using this framework, the authors showed an excellent agreement between experiments and *in silico* predictions.

The MC method is also used extensively in other domains of solid mechanics such as contact analysis [74, 75]. It is a major tool for UQ and even provides baseline results for the validation of new stochastic frameworks. Furthermore, MC is not affected by the curse of dimensionality. Indeed, its convergence rate scales as $\frac{\sigma}{\sqrt{N}}$, where N is the number of samples and σ the standard deviation. This slow rate [76] limits stochastic simulation efficiency when the deterministic problem is already time-consuming [74], which is the case when complex physical features are involved. To bypass these limitations, quasi MC methods have been proposed [31, 32, 76, 77]. In these methods, the parameter space is not sampled randomly but with a given pattern. The most common sampling method is the Latin hypercube sampling [78, 79]. The input space is separated in N equally probable subspaces, then each of these subspaces is sampled one time. The aim of this method is to fill the parameter space as efficiently as possible. Even if these sampling methods lead to faster convergence, they still underperform when compared to other non-deterministic approaches [77, 80].

2.2.2 Multilevel Monte Carlo method

The Multilevel Monte Carlo (MLMC) method [81, 82] is a variant of the MC method. The principle of the MLMC method is to perform a high number of simulations with less accuracy, and a low number of simulations with high accuracy [83]. For a system P discretised as P_h where the parameter $\frac{1}{h}$ is representative of the mesh size, when h tends towards infinity, the modelled problem P_h should accurately describe the problem P . The mean value of a quantity of interest Q_h , e.g., nodal displacements, can be rewritten as:

$$E(Q_h) = E(Q_0) + \sum_{j=1}^h (E(Q_j) - E(Q_{j-1})), \quad (2.1)$$

where E is the expectation operator. The purpose of rewriting this quantity is to introduce Q_j where j is an integer ranging from 0 to h . Obtaining these quantities requires computations on a coarser mesh than the original one. Consequently, instead of doing N costly simulations using a fine mesh, these simulations are distributed on various mesh sizes, thus decreasing the overall computational time.

This approach has been used in many engineering applications. For example, Rey and colleagues [84] quantified uncertainties related to contact mechanics of rough surfaces modeled by a Gaussian random field. They first determined the coarsest size so that the deterministic problem is solved with satisfying accuracy and created a succession of increasingly refined mesh was created. For each surface roughness realisation, the quantity $(Q_j - Q_{j-1})$ in Equation (2.1) was computed, where the quantity of interest Q is a surface contact area. They reported significant computational gains compared to the classical MC method. In 2022, this method was used for shape optimisation of flexoelectric structures. A broad class of energy-harvesting systems relies on the flexoelectricity phenomenon. Aiming to find the optimal shape maximising the conversion of mechanical to electric energy under material uncertainties, Hamdia *et al.* coupled a genetic algorithm [85] with MLMC. After different topologies were proposed, a set of meshes with different levels of refinement were created. Using Equation (2.1), the expected value of the energy

conversion factor was calculated in half of the computational time required using MC.

The rate of convergence of this method scales as $\mathcal{O}(N^{-1})$. For some specific problems, the convergence rate can even be enhanced up to $\mathcal{O}(N^{-2})$ using a Milstein Scheme [32]. However, the need to create multiple meshes often makes this method unsuitable for engineering problems. Other researchers have also proposed to modify the time-step instead [74], the MLMC method only gives an accurate estimation of the expectation, and this alone cannot be used for reliability analyses where more insights about higher-order statistics are required. For these reasons, MLMC has generally been overlooked for UQ in the field of computational mechanics.

2.2.3 Quadrature polynomial chaos

The principle of the quadrature polynomial chaos (QPC) is to avoid the time-consuming sampling strategies previously described by prescribing *a priori* the shape of the solution.

2.2.3.1 Polynomial chaos expansion

In 1938, Wiener [86] introduced a fast and attractive stochastic reduction technique based on polynomial chaos expansion (PCE). Wiener first defined PCE as Hermite polynomial of a Gaussian process. In 1944, the Cameron–Martin theorem [87] stated that the Fourier–Hermite series converge to any L_2 functional in the L_2 sense. This means that the Hermite-based PCE converges to any processes with finite second-order moments, thus further justifying Wiener’s claim. However, the rate of convergence of Hermite-based PCE is only optimal for modelling physical systems where the intrinsic uncertainties are following Gaussian distributions. When other distributions are involved, the convergence rate is slower.

In 1972, Ogura [88] introduced Charlier polynomials and presented possible applications to nonlinear problems involving Poisson process. Following this early work, Askey [89] and Xiu [90] proposed a scheme to represent stochastic processes with orthogonal polynomials taking into account the parameters probability

distribution while ensuring optimal convergence. The correspondance between probability distribution and class of orthogonal polynomials is presented in Table 2.1.

	Associated Polynomials
Gaussian distribution	Hermite
Gamma distribution	Laguerre
Beta distribution	Jacobi
Poisson distribution	Charlier
Negative binomial distribution	Meixner
Binomial distribution	Krawtchouk
Hypergeometric distribution	Hahn

Table 2.1: Example of probabilistic distribution and their associated PCE.

The procedure to define PCE was also extended to problems where arbitrary probability distributions are involved [91]. For sake of simplicity, we consider a univariate random variable θ , where $\theta: \Theta \rightarrow E$, here Θ is the sample space of a probability triple $(\Theta, \mathcal{A}, \mathbb{P})$ with a σ -algebra \mathcal{A} , probability measure \mathbb{P} , for a support E . We define \mathbb{P}_θ , the cumulative distribution function (CDF) of θ , as follows:

$$\mathbb{P}_\theta(w) = \mathbb{P}(v \in \Theta : \theta(v) \leq w), \quad (2.2)$$

where v belongs to the event space and w is a realisation of θ . Using a moment-based approach we briefly recall the methodology to obtain a set $\Psi = [\Psi_0, \dots, \Psi_p]$ of univariate PCE of order p for an arbitrary probability distribution. Orthonormality for polynomial Ψ_j and Ψ_k is enforced by verifying the following equality:

$$\int_E \Psi_j(w) \Psi_k(w) d\mathbb{P}_\theta(w) = \delta_{jk}, \quad (2.3)$$

where δ_{jk} is the Kronecker symbol. The uniqueness of the PCE-set is obtained by imposing that the leading coefficients of polynomials are equal to 1. A direct consequence of this condition is that $\Psi_0 = 1$. Assuming that Ψ_k can be written as:

$$\Psi_k(\theta) = \sum_{s=0}^k \Psi_{k,s} \theta^s, \quad (2.4)$$

the coefficients $\Psi_{k,s}$ are determined by imposing orthogonality of Ψ_k with all Ψ_j where $j \leq k$, akin to a Gram-Schmidt procedure. This condition leads to a system of k equations with $k+1$ unknowns. Taking into account the fact that the leading coefficient is set to 1, it is possible to derive the coefficient $\Psi_{k,s}$ by solving the following system:

$$\boldsymbol{\mu}\boldsymbol{\Psi} = \boldsymbol{R}, \quad (2.5)$$

where $\boldsymbol{\mu}$ is a matrix of size $(k+1) \times (k+1)$. The components of $\boldsymbol{\mu}$ only depend on the moments of the random variable θ . The right-hand side of Equation (2.5) is a vector of size $k+1$ containing k null-components, ensuring orthogonality, and a last component equal to 1, enforcing $\Psi_{k,0} = 1$.

Further mathematical details can be found for the extension to multivariate random variables in Ref. [92]. In the meantime, researchers have been trying to expand strongly non-Gaussian processes with realistic covariance function as a sum of uncorrelated random variables [93, 94]. In combination with PCE, such approaches allow for the creation of a workflow, pre-processing input data to express aleatoric uncertainties as a sum of random variables and propagating them to the output level using PCE.

2.2.3.2 Quadrature method

The main computational effort of QPC lies in determining the coordinates of the solution in the aforementioned PCE-basis. If the stochastic parameters are written as $\boldsymbol{\theta} = [\theta_1, \dots, \theta_M]$, a stochastic problem involving linear elasticity can be written as follows:

$$\boldsymbol{K}(\boldsymbol{\theta})\boldsymbol{u}(\boldsymbol{\theta}) = \boldsymbol{f}(\boldsymbol{\theta}) \quad (2.6)$$

where \boldsymbol{K} is the stiffness matrix, \boldsymbol{u} is the unknown nodal displacement vector and \boldsymbol{f} the force vector.

It is sometimes possible to obtain an analytical expression of \mathbf{K} and \mathbf{f} with respect to $\boldsymbol{\theta}$ but it is not the case for \mathbf{u} . It can be shown that it is possible to express the solution as [87, 92]:

$$\mathbf{u} = \mathbf{u}_0 + \sum_{j=1}^N \mathbf{u}_j \Psi_j(\boldsymbol{\theta}), \quad (2.7)$$

where $N + 1$ is the number of PCE terms. The number $N + 1$ is related to the degree p of the expansion by the relation: $N + 1 = \frac{(M+p)!}{p!M!}$ where M is the parameter space dimension. The expression of Ψ_j depends on the probabilistic function of $\boldsymbol{\theta}$. Following an Askey-Wiener scheme [90], Hermite polynomials are the most suited when Gaussian variables describe the randomness of the parameters. This is often the case as Gaussian uncertainties appear frequently due to the Central limit theorem [95]. In this case, and thanks to the orthogonality of this basis, the unknown coefficient \mathbf{u}_j can be expressed as:

$$\mathbf{u}_j = \frac{\langle \mathbf{u}, \Psi_j \rangle}{\langle \Psi_j, \Psi_j \rangle}. \quad (2.8)$$

Here, the symbol $\langle f, g \rangle$ represents the scalar product between two functions f and g such that:

$$\langle f, g \rangle = \int_{E_1} \int_{E_2} \dots \int_{E_M} f(\mathbf{w}) g(\mathbf{w}) d\mathbb{P}_{\boldsymbol{\theta}}(\mathbf{w}). \quad (2.9)$$

In Equation (2.8) the term $\langle \Psi_j, \Psi_j \rangle$ has an analytical solution in the case of PCE, and, only the computation of $\langle \mathbf{u}, \Psi_j \rangle$ remains. To do so, one can use quadrature methods [96, 97] and replace the continuous integral by a discrete sum. Choosing q points of quadrature for each dimension of the integral, Equation (2.9) becomes:

$$\langle f, g \rangle = \sum_{i=1}^q \sum_{j=1}^q \dots \sum_{k=1}^q f(w_1^i, w_2^j, \dots, w_M^k) g(w_1^i, w_2^j, \dots, w_M^k) d\mathbb{P}_{\boldsymbol{\theta}} W_{ij\dots k}, \quad (2.10)$$

where w_a^b is the a -th component of b -th quadrature point associated to $\boldsymbol{\theta}$ and $W_{ij\dots k}$ are the quadrature weights. Thus, the total number of deterministic simulations required scales as q^M where q is taken between 5 and 10 for accurate quadrature

[26]. In the late 2000's, Bruno and colleagues [98] studied an aeroelastic problem under uncertain flow conditions. Using PCE, combined with Gaussian quadrature rule, only a few deterministic simulations were required for a precise evaluation of Equation (2.8). They obtained an accurate and fast evaluation of the stochastic friction coefficient outperforming MC. More recently, a study [99] showed the feasibility of using the Smolyak quadrature, developed in 1963 [100], to evaluate Equation (2.8). Testing this method on a moderate-dimensional problem (11 random input variables), this work showed that Smolyak quadrature provided a correct estimation of PCE coefficients for a relatively low number of simulations (~ 1000).

Albeit affected by the curse of dimensionality, this method offers superior efficiency compared to MC and quasi MC method [16, 74] at low to moderate dimensions, by using a metamodel. Recently, researchers have developed frameworks to find the PCE coefficients with higher efficiency.

2.2.4 Regression-based method

Another class of method, the so-called regression-based method [101], a least mean square regression [102] is used in a collocation scheme. Expanding the solution with PCE, see Equation (2.7), the number of coefficients to determine is $N + 1 = \frac{(M+p)!}{p!M!}$. The procedure requires computing the deterministic outputs on collocation points and finding the coefficients that best fit the computed results. The vectors $\mathbf{x} = [\mathbf{u}_0, \dots, \mathbf{u}_N]$ and \mathbf{b} gathers the value of outputs at the collocation points. The least square regression method consists in finding \mathbf{x} that minimises:

$$\|\mathbf{Ax} - \mathbf{b}\|^2, \quad (2.11)$$

where \mathbf{A} is a matrix containing the value of PC at the collocation points. A trivial mathematical derivation shows that the solution \mathbf{x} can be expressed as:

$$\mathbf{x} = (\mathbf{A}^T \mathbf{A})^{-1} \mathbf{A}^T \mathbf{b}. \quad (2.12)$$

We emphasise the fact that \mathbf{A} is not a square matrix but of size $(N + 1) \times n_{col}$ where n_{col} is the number of collocation points. The number of deterministic simulations

n_{col} has to be greater than $N + 1$ (otherwise, the system is underdetermined). Thus, to solve the stochastic problem, at least $\frac{(M+p)!}{p!M!}$ deterministic runs are needed. The guidance to choose the collocation points, albeit varying from one publication to another, can be summarised as follows:

- The points containing maximum probability should be included [103] (the origin for the standard normal variable, for example);
- In priority, points that are the roots of the PCE should be selected;
- The sampling has to be as symmetric as possible [104].

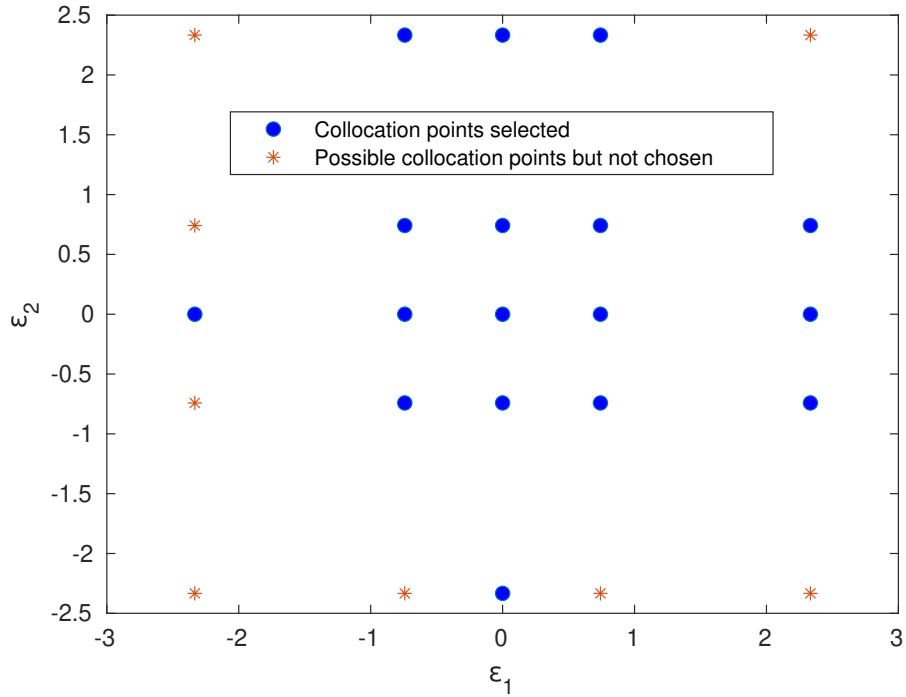


Figure 2.2: Collocation points selection adapted from Ref. [105]

In the middle of 2000's, Huang *et al.* studied a 1D rod with random Young's modulus exhibiting spatial covariance. After reducing the dimension of the problem to two Gaussian random variables, they performed the regression method, i.e. solving for Equation (2.12). With only 17 deterministic simulations at the collocation points defined in Figure 2.2, they reported similar accuracy compared to MC method ($\sim 10\,000$ simulations). One year later, Sudret [106] used the regression method to

perform a sensitivity analysis. Using one of the main advantages of PCE, which is to provide a polynomial metamodel of the stochastic response, the author derived analytically Sobol’s indices with a quick postprocessing step. After benchmarking the regression methods on study cases of moderate dimension (8 input parameters), the author observed that regression-based frameworks provide accurate sensitivity analyses at a computational cost which is 2–3 orders of magnitude smaller than the traditional MC method. Sepahvand and Marburg [107] studied a composite plate, at the interface of two domains, with Young’s and shear moduli following a normal distribution. In the first domain, an acoustic wave was sent to the composite that in turn transmits a wave in the other domain. The resulting pressure jump, frequency-dependent, was quantified through stochastic analysis. They claimed excellent agreement between the regression method and MC and reported a speed-up of 1000% for equivalent accuracy. Furthermore, they noted little dependence on the number of simulations required with respect to the PCE order. More recently, Peng *et al.* proposed a data-driven framework to perform stochastic analysis under insufficient input data [108]. Considering probabilistic and possibilistic uncertainties altogether, they extended PCE to create a data-driven metamodel of a composite laminated plate natural frequency. Using the regression method they reported a reduction of deterministic computations from 10^6 using MC to 1600 for a computed mean value relative error of 0.27%.

While being as flexible as the MC, regression-based strategies require much fewer simulations, reduced by 3 orders of magnitude in some studies, for similar accuracy. The FE model is run at specific points to inform a regression framework, typically based on a least-square algorithm, aiming to find the PCE metamodel coefficients that best minimises the error at those points. These methods, albeit efficient at moderate dimensions are yet again affected by the curse of dimensionality. Furthermore, the regression method is highly dependent on the collocation point choice, and a study [33] reported that increasing the number of points does not guarantee convergence of the regression-based methods. We now detail another

class of strategy aiming to find the PCE coefficients in Equation (2.7) without being dependent on a sampling process: the so-called intrusive methods.

2.3 Intrusive methods

As opposed to strategies developed in Section 2.2, intrusive methods require modifications of the governing equations where the stochastic problem is implemented. While they call for additional coding efforts, these methods are often more robust as they do not depend on any sampling process.

2.3.1 Perturbation finite element method

The perturbation method is one of the earliest developed approaches to the solution of nonlinear problems. It consists in linearising the governing equation, generally using Taylor Series expansions. In the early 1970's, this method was extended to stochastic problems for sensitivity analysis [109]. The perturbation finite element method (PFEM) approach assumes that input parameters of the structural problem are exhibiting small variations around their mean value. As a consequence, the stiffness matrix \mathbf{K} , the force vector \mathbf{F} and displacement vector \mathbf{u} in Equation (2.6) are expended using Taylor series:

$$\begin{aligned}\mathbf{K}(\boldsymbol{\theta}) &= \mathbf{K}_0 + \sum_{i=1}^M \mathbf{K}_i^I \theta_i + \frac{1}{2} \sum_{i=1}^M \sum_{j=1}^M \mathbf{K}_{ij}^{II} \theta_i \theta_j + \mathcal{O}(\|\boldsymbol{\theta}\|_2), \\ \mathbf{u}(\boldsymbol{\theta}) &= \mathbf{u}_0 + \sum_{i=1}^M \mathbf{u}_i^I \theta_i + \frac{1}{2} \sum_{i=1}^M \sum_{j=1}^M \mathbf{u}_{ij}^{II} \theta_i \theta_j + \mathcal{O}(\|\boldsymbol{\theta}\|_2), \\ \mathbf{F}(\boldsymbol{\theta}) &= \mathbf{F}_0 + \sum_{i=1}^M \mathbf{F}_i^I \theta_i + \frac{1}{2} \sum_{i=1}^M \sum_{j=1}^M \mathbf{F}_{ij}^{II} \theta_i \theta_j + \mathcal{O}(\|\boldsymbol{\theta}\|_2),\end{aligned}\tag{2.13}$$

where, for simplicity, we suppose that the mean value of each random variable θ_i is equal to zero without loss of generality. We define $\mathcal{O}(\|\boldsymbol{\theta}\|_2)$ as a third order truncated remainder. \mathbf{K}_0 , \mathbf{K}_i^I , \mathbf{K}_{ij}^{II} are respectively, the deterministic, first order partial derivative with respect to θ_i and second order partial derivative with respect to θ_i and θ_j of the stiffness matrix $\mathbf{K}(\boldsymbol{\theta})$. These quantities are defined as follows:

$$\begin{aligned}\mathbf{K}_0 &= \mathbf{K}(\boldsymbol{\theta})|_{\boldsymbol{\theta}=0}, \\ \mathbf{K}_i^I &= \frac{\partial \mathbf{K}(\boldsymbol{\theta})}{\partial \theta_i} |_{\boldsymbol{\theta}=0}, \\ \mathbf{K}_{ij}^{II} &= \frac{\partial^2 \mathbf{K}(\boldsymbol{\theta})}{\partial \theta_i \partial \theta_j} |_{\boldsymbol{\theta}=0}.\end{aligned}\tag{2.14}$$

The quantities \mathbf{u}_0 , \mathbf{u}_i^I , \mathbf{u}_{ij}^{II} , \mathbf{F}_0 , \mathbf{F}_i^I , \mathbf{F}_{ij}^{II} are defined similarly. To calculate the unknowns \mathbf{u}_0 , \mathbf{u}_i^I , \mathbf{u}_{ij}^{II} , (2.13) is first substituted in Equation (2.6). The deterministic displacement \mathbf{u}_0 and the higher order displacements \mathbf{u}_i^I and \mathbf{u}_{ij}^{II} can be expressed by order terms as:

$$\begin{aligned}\mathbf{u}_0 &= \mathbf{K}_0^{-1} \mathbf{F}_0, \\ \mathbf{u}_i^I &= \mathbf{K}_0^{-1} \left(\mathbf{F}_i^I - \mathbf{K}_i^I \mathbf{u}_0 \right), \\ \mathbf{u}_{ij}^{II} &= \mathbf{K}_0^{-1} \left(\mathbf{F}_{ij}^{II} - \mathbf{K}_i^I \mathbf{u}_j^I - \mathbf{K}_j^I \mathbf{u}_i^I - \mathbf{K}_{ij}^{II} \mathbf{u}_0 \right).\end{aligned}\tag{2.15}$$

Using this expression of \mathbf{u} , it is possible to extract the displacement statistics with a quick postprocessing step. An estimate of the mean component can be written as:

$$E(\mathbf{u}) = \mathbf{u}_0 + \frac{1}{2} \sum_{i=1}^M \sum_{j=1}^M \mathbf{u}_{ij}^{II} Cov(\theta_i, \theta_j),\tag{2.16}$$

where $Cov(\theta_i, \theta_j)$ denotes the covariance between the random variables θ_i and θ_j . The estimate of the displacement covariance matrix reads as:

$$Cov(\mathbf{u}, \mathbf{u}) = \sum_{i=1}^M \sum_{j=1}^M \mathbf{u}_i^I \left(\mathbf{u}_j^I \right)^T Cov(\theta_i, \theta_j),\tag{2.17}$$

The PFEM has been numerically implemented and used by many researchers. In 1981, Beacher *et al.* used the PFEM to obtain settlement statistics of a structure over an elastic soil mass. A few years later, Belytschko and colleagues [110] captured the displacement and stress statistics of a truss structure. Their framework included both material and geometrical uncertainties. They reported superior efficiency of PFEM compared to MC and satisfying performances when the coefficient of variation was moderate ($\sim 10\%$). In 2000, Kaminski [111] used PFEM to extract the first and second-order statistics of the homogenised elastic tensor components of a composite. Huang *et al.* [112] successfully extended the PFEM to structural analysis under fuzzy environments.

Though other studies reported good performances of PFEM over MC when studying structural problems [113, 114], the PFEM suffers from severe shortcomings:

- PFEM offers optimal performances for low-level uncertainties, i.e, when the coefficient of random variables does not exceed 10 to 15%;

- the computational cost of Equation (2.15) increases with the order of the Taylor expansion;
- information, such as the first and second-order derivatives of stiffness matrix and external effort is required.

To overcome these limitations, modifications to the PFEM have been proposed. Kaminski and colleagues made significant contributions to enhance the performance of PFEM and introduce it to different domains. In 1999 [115], they derived the perturbed heat transfer equation, extending PFEM to thermodynamic analysis. In 2005, Kaminski [116] broadened this methodology for fluid mechanics by studying the statistics of fluid pressure in Poiseuille and viscous Couette flow with randomly perturbed boundary conditions. In [117], a generalisation of PFEM to the n -th order for higher order statistics was proposed for linear elasticity. While a high efficiency of this method was claimed, the convergence of this methodology was highly dependent on the input parameters coefficient of variation. In the late 2000's, Kaminski [118] coupled the PFEM with response function method as a possible alternative. They successfully applied this method to the static analysis of elastic beams. With Solecka [119], they showed the potential of PFEM for design purposes, using this framework to optimise a tower structure under constraints.

Recently, Wu [120] modified the PFEM scheme to provide second-order estimates without the need to differentiate the stiffness matrices with respect to the random variables. There is still ongoing work to circumvent the drawbacks of the PFEM. In 2022, Shao and colleagues [121] proposed another enhancement of the PFEM involving algebraic manipulations. With this new framework, the so-called modified perturbation stochastic method (MPSM), it is possible to obtain the mean and standard deviation of the displacements without needing to know the partial derivatives of the stiffness matrix, akin to the work in Ref. [120], but with higher accuracy. They used MPSM for reliability analyses, performing stochastic simulations with random fields. However, they noted that their framework showed optimal efficiency in the case where random inputs were uncorrelated Gaussian

fields. As a result, they recommended an extension of MPSM to non-Gaussian random fields to widen its application to more realistic scenarios.

On top of its cumbersome formulation, the PFEM's applicability is limited to problems involving low-level uncertainties. In the following, we present an alternative method more suited to stochastic analysis where inputs can exhibit high-level uncertainties.

2.3.2 Galerkin Stochastic Finite Element Method

Ghanem and Spanos proposed the Galerkin Stochastic Finite Element Method (GSFEM) [23] in 1991. This method solves both spatial and stochastic problems at the same time.

2.3.2.1 Mathematical foundation

In the traditional FE method, the solution is searched on a Sobolev space. This Sobolev space being infinite, shape functions are used to create a finite basis approximating this space [122]. When the spatial mesh is refined, this basis becomes larger and can approximate the infinite Sobolev space. In the GSFEM, the solution has to be searched simultaneously in this space and the stochastic space. The PCE in Equation (2.7) can be seen as the shape functions in the stochastic space. The displacement field \mathbf{u} is separated in a mean component \mathbf{u}_0 and stochastic counterparts \mathbf{u}_j where j ranges from 1 to N as shown in Equation (2.7). This method assumed that the propagation of material uncertainties would lead to the following formulation of the stiffness matrix:

$$\mathbf{K} = \mathbf{K}_0 + \sum_{j=1}^N \mathbf{K}_j \Psi_j(\boldsymbol{\theta}). \quad (2.18)$$

An early strategy to find the displacement \mathbf{u} consists in using a Neumann series expansion of the inverse stochastic stiffness matrix. Instead, Ghanem *et al.* combined Equation (2.7) and Equation (2.18) in Equation (2.6) to obtain:

$$\left(\sum_{j=0}^N \mathbf{K}_j \Psi_j(\boldsymbol{\theta}) \right) \left(\sum_{j=0}^N \mathbf{u}_j \Psi_j(\boldsymbol{\theta}) \right) = \mathbf{F}. \quad (2.19)$$

This system of equations is underdetermined. Indeed, assuming the size of the deterministic problem is n , then Equation (2.19) provides n equations for $n \times (N + 1)$ unknowns. To close the system, a second projection, in the stochastic space is performed. First, a residual quantity $\mathbf{R}(\boldsymbol{\theta})$ is defined as:

$$\mathbf{R}(\boldsymbol{\theta}) = \left(\sum_{i=0}^N \mathbf{K}_i \Psi_i(\boldsymbol{\theta}) \right) \left(\sum_{j=0}^N \mathbf{u}_j \Psi_j(\boldsymbol{\theta}) \right) - \mathbf{F}. \quad (2.20)$$

Then, the coefficients \mathbf{u}_j are found by imposing:

$$\langle \mathbf{R}(\boldsymbol{\theta}), \Psi_k \rangle = 0, \quad \forall k \in [0, N]. \quad (2.21)$$

These constraints introduce a third order tensor \mathbf{C} , around which the whole GSFEM revolves:

$$C_{ijk} = \langle \Psi_i \Psi_j, \Psi_k \rangle. \quad (2.22)$$

Combining Equation (2.20) and Equation (2.19), the following system is obtained:

$$\sum_{i=0}^N \sum_{j=0}^N C_{ijk} \mathbf{K}_i \mathbf{u}_j = \mathbf{F}_k, \quad \forall k \in [0, N + 1] \quad (2.23)$$

where $\mathbf{F}_k = \langle \mathbf{F}, \Psi_k \rangle$. Taking into account the fact that each vector \mathbf{F}_k contains n components, the system in Equation (2.23) contains $(N + 1) \times n$ equations. It is then possible to write Equation (2.23) as:

$$\mathbb{K} \mathbf{u} = \mathbb{F}, \quad (2.24)$$

where $\mathbb{F} = [\mathbf{F}_k, k = 0, \dots, N]$ and \mathbb{K} is expressed in function of \mathbf{C} and the matrices \mathbf{K}_i . As both the physical and random problems are solved altogether, this system is larger than its deterministic counterpart, requiring more memory and computational resources to solve.

2.3.2.2 Extension to Spectral Stochastic Finite Element Method

To widen the scope of GSFEM, Ghanem extended the GSFEM formulation to incorporate random fields into their framework, the so-called Spectral Stochastic Finite Element Method (SSFEM), see Ref. [23]. While, the modelisation of aleatoric uncertainties, such as the amplitude of a concentrated load or applied displacement can be done by using random variables. However, when spatially varying quantities are involved, e.g., fracture toughness, using random fields is more appropriate [123, 124]. These random fields often exhibit spatial correlation, complicating their integration in numerical frameworks. To alleviate this limitation, the Karhunen-Loeve (K-L) theorem has been widely used in stochastic analyses [125, 126]. The K-L theorem states that any stochastic process can be extended as an infinite linear combination of orthogonal functions [127]. Assuming that $W(x)$ is a stochastic process, where $x \in D$ (D is the physical space) and θ is a random variable, with covariance $Cov(s, t) = \langle W(s), W(t) \rangle$. The theorem proves that $W(x)$ can be rewritten as:

$$W(x) = \bar{w}(x) + \sum_{i=1}^{\infty} \sqrt{\lambda_i} f_i(x) \theta_i, \quad (2.25)$$

where θ_i has a null mean and standard deviation of 1, λ_i and $f_i(x)$ are called eigenvalues and eigenfunctions or eigenvectors, respectively. The functions $f_i(x)$ are pairwise orthogonal in L_2 . Following Mercer's theorem [128], they must be the solution of the Fredholm equation [129]:

$$\int_D Cov(s, t) f_i(s) ds = \lambda_i f_i(t). \quad (2.26)$$

For numerical implementation, the K-L expansion in Equation (2.25) has to be truncated to a given order. If material properties, among other quantities, are described using K-L expansion, it is possible to rewrite the stiffness matrix as in Equation (2.18). Coupling the K-L expansion with the GSFEM for uncertainty propagation is the core strategy of SSFEM. Huang *et al.* used the SSFEM to obtain the tip displacement of a 1D cantilever beam where the Young's modulus

was a Gaussian random field with exponential covariance. A few years later, Ngah and colleagues [130] evaluated the performance of a 2D composite under uncertain material properties. They reported that SSFEM is applicable over a wide range of material variability where the standard variation reached 25% of the mean value and concluded that SSFEM is a potentially useful technique for application to reliability analyses. However, their framework did not include any nonlinearities with respect to the random variables. Soon after, SSFEM was extended to the study of 3D composites [131] to provide a reasonable probabilistic prediction with satisfactory computational efficiency while restricting their framework to linear operations with respect to random variables.

2.3.2.3 Recent development

The size of the system in Equation (2.24) can increase dramatically with the number of random variables and lead to prohibitive computational time. To alleviate this issue, researchers [132, 133] have coupled GSFEM with stochastic reduced basis methods (SRBMs). In contrast to the PCE, the response surface is represented using basis vectors spanning the preconditioned Krylov subspace. SRBMs constitute an efficient approach albeit limited to the analysis of random linear systems. In the early development of GSFEM, this method was solely used to model linear elastic problems.

In the middle of the 2000s, Debusschere [134] and coworkers introduced a range of nonlinear operations of random variables, ranging from multiplications to logarithms. The introduction of this algebra immediately led to further publications in CFD, where the Navier-Stokes equations were solved intrusively to study convection and diffusion phenomena induced by fluid flows [135–137], and in the study of chemical systems [138, 139].

Acharjee [24] was the first researcher to extend GSFEM to finite deformation with nonlinear constitutive laws. In this thesis, they also studied a 2D structure while incorporating geometrical uncertainties but without defining a precise mathematical formulation. In the early 2010s, Rosic *et al.* modified GSFEM to incorporate

plasticity in UQ. Severe limitations when introducing uncertainties in the yield stress were reported. Indeed, at every material point, a stochastic stress must be compared to a deterministic, or stochastic, threshold criterion. This comparison introduced an approximation of the convex set, altering the original problem. Consequently, the Monte Carlo solution could not be recovered even when using high-order PCE.

2.4 To be intrusive or non-intrusive?

All these methods aim to model the material properties variability and their impact on structural components. In the last decades, significant progress has been made to make calculations faster with increasingly more powerful processors. With parallel computing, simulations containing even higher levels of details [140] are now done regularly in the industry. However and despite these advances, traditional MC stochastic simulations remain intractable for large-scale problems [74].

Other methods, such as the ones presented in Sections 2.2.3 and 2.2.4, have proven to be efficient in cases where precise knowledge of the stochastic outputs can be acquired within less than a hundred simulations. However, they only perform better than MC-based methods because the number of stochastic inputs is moderate. In addition, the sampling process often varies from one research work to another, thus making the derivation of consistent guidelines difficult to establish.

The last reviewed method, presented in Section 2.3.2, requires the modification of the FE code. One simulation is enough to gather information on the output. Nevertheless, the problem solved is larger than its deterministic counterpart, as it is intended to answer both the spatial FE and the stochastic problem altogether. The stiffness matrix in Equation (2.19) is denser than the one in the deterministic problem [5], making the system inversion even more challenging. In addition, this framework has mainly been used for linear elasticity in small deformation. Any extension to realistic problems requires the use and development of a flexible and adaptive theoretical framework. For example, it is required to multiply or divide random variables during the computation. These operations, trivial in deterministic paradigms, require the introduction of a specialised algebra [134].

Both intrusive and non-intrusive methods offer advantages and shortcomings, with no clear current consensus [141]. In this thesis's defense, after careful comparisons, Acharjee stated that non-intrusive methods were more suited for

realistic FE analyses as they can be seamlessly integrated into any existing code, a relevant feature when simulations involving strong nonlinearities are needed. Furthermore, the convergence properties of this class of method are not affected when the problem involves discontinuities. Consequently, non-intrusive methods are mostly preferred for uncertainty quantification.

Although intrusive methods cannot be readily introduced in an existing FE solver, we argue that it is possible to incorporate them into an existing solver without excessive modifications. In addition, we prove here that intrusive methods can be used to simulate large-scale problems (> 1 million DoFs) with optimal programming. While GSFEM is not intrinsically suited for uncertainty quantification when the system exhibits sharp dependence with respect to parameters, it is possible to circumvent this limitation by using Wavelet expansion instead of PCE, a strategy used in CFD, but never employed in a FE framework. Furthermore, we show that it is possible to include constitutive models with highly nonlinear features in the GSFEM. The mathematical and numerical enhancement of GSFEM is first presented in Chapter 3. It is then validated in Chapter 4 for a wide range of applications, including bifurcation and Hertzian contact. The limitations of the work presented here and potential future directions for unlocking the full potential of intrusive methods are finally discussed in Chapter 5.

Chapter 3

Theoretical framework and numerical implementation

We propose here to combine GSFEM with Wavelet interpolants. This combination allows for the simulation of stochastic bifurcation problems. To broaden the range of applications, the formulation of three stochastic constitutive models and their subsequent discretisation is given. Then, the GSFEM is specialised into the APFEM by restricting the choice of polynomial interpolants to Legendre polynomials for efficient parameter space exploration and for application to Bayesian inferences. Finally, a methodology to extend GSFEM/APFEM for simulations encompassing geometrical uncertainties is proposed.

3.1 Mathematical foundation of GSFEM

This section provides the mathematical description of GSFEM and its modular architecture for seamless numerical implementation. After recalling the key features of PCE, the underlying theory of discontinuous expansion is introduced. The derivation of the stochastic tangent modulus is also provided for each constitutive model.

3.1.1 Stochastic space discretisation

The overarching principle of GSFEM is to decompose any given random quantity on a *a priori* known stochastic space generated by a set of interpolants Ψ_ϵ . Accordingly, displacements are characterised by nodal and stochastic components, and the finite element displacement function \mathbf{u} is written as follows:

$$\mathbf{u}(\mathbf{x}, \boldsymbol{\theta}) = \sum_a N_a(\mathbf{x}) \mathbf{u}^a = \sum_a N_a(\mathbf{x}) \sum_\epsilon \Psi_\epsilon(\boldsymbol{\theta}) \mathbf{u}^{a\epsilon}, \quad (3.1)$$

where the functions N_a are the usual finite element shape functions, Ψ_ϵ the shape functions associated with the stochastic space and $\mathbf{u}^{a\epsilon}$ the displacement of node a with stochastic direction ϵ^1 . The dependence on $\boldsymbol{\theta}$ denotes a function on the probability space. Consequently, at a given node, both spatial and stochastic components of the displacement have to be determined. The choice of the shape functions depends on the probabilistic distribution of the inputs as explained in Section 2.2.3.1. The deformation gradient tensor \mathbf{F} in this stochastic finite element space follows then from the following expression:

$$\mathbf{F} = \sum_\epsilon \Psi_\epsilon \mathbf{F}^\epsilon \quad (3.2)$$

where, in the indicial notation, with $\boldsymbol{\delta}$ being the Kronecker delta,

$$F_{iJ}^\epsilon = \delta_{\epsilon 0} \delta_{iJ} + \sum_a N_{a,J} u_i^{a\epsilon} \quad (3.3)$$

is the stochastic component of \mathbf{F} associated to the polynomial Ψ_ϵ . Note that the presence of the identity tensor (δ_{iJ}) existing only when $\epsilon = 0$ arises from the fact that this tensor is deterministic, and that, it thus only appears in the first term of the stochastic polynomial interpolation. Similarly, the usual finite element tensors such as the Green-Lagrange strain tensor \mathbf{E} , the first and second Piola-Kirchhoff stress tensors \mathbf{P} and \mathbf{S} , among others, are all defined in the stochastic space.

¹Here and subsequently, indices noted with Greek letters relate to the stochastic space.

3.1.2 Balance of linear momentum

In GSFEM, the equation of the balance of linear momentum with respect to the reference (or undeformed) configuration follows the same equation as in its deterministic counterpart, but with stochastic tensors, i.e.,

$$\text{Div } \mathbf{P} + \rho_0 \mathbf{b} = \rho_0 \ddot{\mathbf{u}}, \quad \forall \mathbf{X} \in \Omega_0 \text{ almost surely.} \quad (3.4)$$

where \mathbf{P} , \mathbf{b} and ρ_0 are the stochastic first Piola-Kirchhoff stress tensor, the stochastic body force vector per unit reference mass and the stochastic reference material density.

3.1.3 Boundary conditions

Similarly, the Neumann and Dirichlet boundary conditions, $\bar{\mathbf{T}}$ on $\partial\Omega_n$ and $\bar{\mathbf{u}}$ on $\partial\Omega_d$, respectively (both potentially stochastic in nature), are imposed in the reference configuration with:

$$\begin{cases} \mathbf{P} \cdot \mathbf{N} = \bar{\mathbf{T}}, \quad \forall \mathbf{X} \in \partial\Omega_n \text{ almost surely} \\ \mathbf{u} = \bar{\mathbf{u}}, \quad \forall \mathbf{X} \in \partial\Omega_d \text{ almost surely,} \end{cases} \quad (3.5)$$

where \mathbf{N} is the normal to the boundary in the reference configuration, and where the subscript “0” (indicating the reference configuration) of $\partial\Omega_n$ and $\partial\Omega_d$ was dropped for clarity. The geometry of the body Ω_0 is discretised into elements Ω_{0h}^e such that $\Omega_{0h} = \bigcup_e \Omega_{0h}^e$, see Figure 3.1.

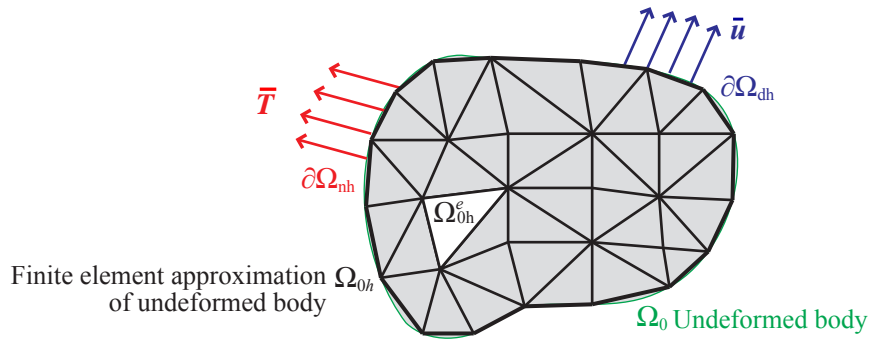


Figure 3.1: Finite element discretisation of the undeformed body Ω_0 into elements Ω_{0h}^e .

3.1.4 Weak form of the balance of momentum

We consider a multivariate random variable $\boldsymbol{\theta} = [\theta_1, \dots, \theta_N]$. Without loss of generality we define $\theta_i: \Theta \rightarrow E, \forall i \in [1, N]$, where Θ is a sample space of a probability triple $(\Theta, \mathcal{A}, \mathbb{P})$ with a σ -algebra \mathcal{A} , probability measure \mathbb{P} , and a support E . For algebraic convenience, we suppose that the support E is the same for each variable θ_i . We define $\mathbb{P}_{\boldsymbol{\theta}}$, the cumulative distribution function (CDF) of $\boldsymbol{\theta}$, as follows:

$$\mathbb{P}_{\boldsymbol{\theta}}(\mathbf{w}) = \mathbb{P}(v_1 \in \Theta_1, \dots, v_N \in \Theta_N : \theta(v_1) \leq w_1, \dots, \theta(v_N) \leq w_N), \quad (3.6)$$

where $\mathbf{w} = [w_1, \dots, w_N]$ is a vector of realisations. The weak form of the balance of linear momentum described in Equation (3.4) can be formulated as follows: for all arbitrary admissible virtual stochastic displacement $\boldsymbol{\eta}$, with $\boldsymbol{\eta}(\mathbf{X}, \theta) = \mathbf{0}$ almost surely for all $\mathbf{X} \in \partial\Omega_d$,

$$\int_{E^N} \int_{\Omega_0} \text{Div } \mathbf{P} \cdot \boldsymbol{\eta} dV d\mathbb{P}_{\boldsymbol{\theta}} + \int_{E^N} \int_{\Omega_0} \rho_0 \mathbf{b} \cdot \boldsymbol{\eta} dV d\mathbb{P}_{\boldsymbol{\theta}} = \int_{E^N} \int_{\Omega_0} \rho_0 \ddot{\mathbf{u}} \cdot \boldsymbol{\eta} dV d\mathbb{P}_{\boldsymbol{\theta}}. \quad (3.7)$$

Note the second integral over the support space E^N . Integrating by parts and using Green's theorem, the above expression can be rewritten as

$$\begin{aligned} & \int_{E^N} \int_{\partial\Omega_0} (\mathbf{P} \cdot \mathbf{N}) \cdot \boldsymbol{\eta} dS d\mathbb{P}_{\boldsymbol{\theta}} + \int_{E^N} \int_{\Omega_0} \rho_0 \mathbf{b} \cdot \boldsymbol{\eta} dV d\mathbb{P}_{\boldsymbol{\theta}} \\ &= \int_{E^N} \int_{\Omega_0} \mathbf{P} : \text{Grad } \boldsymbol{\eta} dV d\mathbb{P}_{\boldsymbol{\theta}} + \int_{E^N} \int_{\Omega_0} \rho_0 \ddot{\mathbf{u}} \cdot \boldsymbol{\eta} dV d\mathbb{P}_{\boldsymbol{\theta}}, \end{aligned} \quad (3.8)$$

which, noting that $\boldsymbol{\eta} = \mathbf{0}$ almost surely for all $\mathbf{X} \in \partial\Omega_d$ and using Equation (3.5), leads to

$$\begin{aligned} & \int_{E^N} \int_{\partial\Omega_n} \bar{\mathbf{T}} \cdot \boldsymbol{\eta} dS d\mathbb{P}_{\boldsymbol{\theta}} + \int_{E^N} \int_{\Omega_0} \rho_0 \mathbf{b} \cdot \boldsymbol{\eta} dV d\mathbb{P}_{\boldsymbol{\theta}} \\ &= \int_{E^N} \int_{\Omega_0} \mathbf{P} : \text{Grad } \boldsymbol{\eta} dV d\mathbb{P}_{\boldsymbol{\theta}} + \int_{E^N} \int_{\Omega_0} \rho_0 \ddot{\mathbf{u}} \cdot \boldsymbol{\eta} dV d\mathbb{P}_{\boldsymbol{\theta}}. \end{aligned} \quad (3.9)$$

The relation between \mathbf{P} and \mathbf{F} is defined by the material constitutive law $\mathbf{P} = \tilde{\mathbf{P}}(\mathbf{F})$.

3.1.5 Numerical integration

Both displacements (real and virtual) and stresses are now stochastic quantities. The same decomposition as in Equation (3.1) applies for all other stochastic

quantities with the stochastic shape functions Ψ_ϵ being space independent.

GSFEM problem: Find all $\mathbf{u}^a \in \mathbb{R}^3 \times \mathbb{R}^N$ such that for all admissible virtual displacement $\boldsymbol{\eta}^b \in \mathbb{R}^3 \times \mathbb{R}^N$:

$$\begin{aligned} \sum_e \int_{E^N} \int_{\Omega_0^e} \rho_0^\kappa N_a^e N_b^e \ddot{\mathbf{u}}^{ae} \cdot \boldsymbol{\eta}^{b\iota} \Psi_\kappa \Psi_\epsilon \Psi_\iota dV d\mathbb{P}_\theta + \sum_e \int_{E^N} \int_{\Omega_0^e} \left(\tilde{\mathbf{P}}(\mathbf{F}) \cdot \nabla_0 N_b^e \right) \cdot \boldsymbol{\eta}^{b\iota} \Psi_\iota dV d\mathbb{P}_\theta \\ = \sum_e \int_{E^N} \int_{\partial\Omega_n^e} N_b^e \bar{\mathbf{T}} \cdot \boldsymbol{\eta}^{b\iota} \Psi_\iota dS d\mathbb{P}_\theta + \sum_e \int_{E^N} \int_{\Omega_0^e} \rho_0^\kappa N_b^e \mathbf{b} \cdot \boldsymbol{\eta}^{b\iota} \Psi_\kappa \Psi_\iota dV d\mathbb{P}_\theta. \end{aligned} \quad (3.10)$$

Since the above equation must be valid for all admissible $\boldsymbol{\eta}^b$, the finite element problem now reads: Find \mathbf{u}^a such that, for all b ,

$$\sum_e \mathbf{M}_{\epsilon b \iota a}^e \ddot{\mathbf{u}}^{ae} + \sum_e \mathbf{f}_{\iota b}^{e \text{ int}} = \sum_e \mathbf{f}_{\iota b}^{e \text{ ext}}, \quad (3.11)$$

where the stochastic mass tensor \mathbf{M}^e , the stochastic element internal force vector $\mathbf{f}^{e \text{ int}}$ and the stochastic external force vector $\mathbf{f}^{e \text{ ext}}$ are

$$\mathbf{M}_{\epsilon b \iota a}^e = \int_{E^N} \int_{\Omega_0^e} \rho_0^\kappa N_a^e N_b^e \Psi_\kappa \Psi_\epsilon \Psi_\iota dV d\mathbb{P}_\theta, \quad (3.12)$$

$$\mathbf{f}_{\iota b}^{e \text{ int}} = \int_{E^N} \int_{\Omega_0^e} \tilde{\mathbf{P}}(\mathbf{F}) \cdot \nabla_0 N_b^e \Psi_\iota dV d\mathbb{P}_\theta, \quad (3.13)$$

$$\mathbf{f}_{\iota b}^{e \text{ ext}} = \int_{E^N} \int_{\partial\Omega_n^e} N_b^e \bar{\mathbf{T}} \Psi_\iota dS d\mathbb{P}_\theta + \int_{E^N} \int_{\Omega_0^e} \rho_0^\kappa N_b^e \mathbf{b} \Psi_\kappa \Psi_\iota dV d\mathbb{P}_\theta. \quad (3.14)$$

After expanding $\tilde{\mathbf{P}}$ as $\tilde{\mathbf{P}}^\tau \Psi_\tau$, $\bar{\mathbf{T}}$ and \mathbf{b} in the same manner, the internal and external forces vectors become:

$$\mathbf{f}_{\iota b}^{e \text{ int}} = \int_{E^N} \int_{\Omega_0^e} \tilde{\mathbf{P}}^\tau \cdot \nabla_0 N_b^e \Psi_\iota \Psi_\tau dV d\mathbb{P}_\theta, \quad (3.15)$$

$$\mathbf{f}_{\iota b}^{e \text{ ext}} = \int_{E^N} \int_{\partial\Omega_n^e} N_b^e \bar{\mathbf{T}}^\tau \Psi_\iota \Psi_\tau dS d\theta + \int_{E^N} \int_{\Omega_0^e} \rho_0^\kappa N_b^e \mathbf{b}^\tau \Psi_\kappa \Psi_\iota \Psi_\tau dV d\mathbb{P}_\theta. \quad (3.16)$$

To ease the notation, the scalar product $\int_{E^N} f(\mathbf{w})g(\mathbf{w})d\mathbb{P}_\theta$ is noted $\langle f, g \rangle$ where f and g are two stochastic functions. As, by virtue of orthogonality, $\langle \Psi_\iota, \Psi_\tau \rangle$ is different from zero only when $\iota = \tau$, the force vectors can be further simplified by:

$$\mathbf{f}_{\iota b}^{e \text{ int}} = \int_{\Omega_0^e} \tilde{\mathbf{P}}^\iota \cdot \nabla_0 N_b^e \langle \Psi_\iota, \Psi_\iota \rangle dV \quad (3.17)$$

$$\mathbf{f}_{ib}^{e \text{ ext}} = \int_{\partial\Omega_n^e} N_b^e \bar{\mathbf{T}}_\tau < \Psi_\iota, \Psi_\iota > \, dS + \int_{\Omega_0^e} \rho_0^\kappa N_b^e \mathbf{b}_\iota < \Psi_\kappa \Psi_\iota, \Psi_\tau > \, dV. \quad (3.18)$$

Using Gauss quadrature, one then has:

$$f_{ia}^{e \text{ int}} = \sum_q W_q P_{iJ}^\iota(\boldsymbol{\xi}_q) N_{a,J}^e(\boldsymbol{\xi}_q) J_0(\boldsymbol{\xi}_q) < \Psi_\iota, \Psi_\iota >, \quad (3.19)$$

$$f_{ia}^{e \text{ ext}} = \sum_p W_p T_i^\iota(\boldsymbol{\xi}_p) N_a^e(\boldsymbol{\xi}_p) J_0(\boldsymbol{\xi}_p) < \Psi_\iota, \Psi_\iota > + \sum_q W_q \rho_0^\kappa b_{i\iota}(\boldsymbol{\xi}_q) N_a^e(\boldsymbol{\xi}_q) J_0(\boldsymbol{\xi}_q) < \Psi_\kappa \Psi_\iota, \Psi_\iota >. \quad (3.20)$$

where $\boldsymbol{\xi}_q$ is the coordinate vector of Gauss point q of element e in its isoparametric coordinate system, W_q is its corresponding weight, and J_0 is the Jacobian between the isoparametric coordinate system and the reference configuration. The term with the sum in p (first term of Equation (3.20)) is on the surface elements belonging to $\partial\Omega_{nh}^e$ mapped onto the corresponding faces of the volume elements. Note that this quadrature only concerns the physical space as all integrals on the stochastic space can be computed without any numerical approximations.

As the internal force vector $\mathbf{f}^{e \text{ int}}$ is not necessarily linear, a Newton-Raphson procedure can be used to enforce Equation (3.11). In this case, the stochastic element stiffness matrix \mathbf{K}^e is needed:

$$Res_{ia}^e = f_{ia}^{e \text{ int}} - f_{ia}^{e \text{ ext}}, \quad (3.21)$$

$$K_{ia\epsilon kb}^e = \frac{\partial Res_{ia}^e}{\partial u_{\epsilon kb}} = \frac{\partial f_{ia}^{e \text{ int}}}{\partial u_{\epsilon kb}} = \sum_q W_q \frac{\partial P_{iJ}^\iota}{\partial F_{qM}^\omega}(\boldsymbol{\xi}_q) N_{a,J}^e(\boldsymbol{\xi}_q) J_0(\boldsymbol{\xi}_q), \quad (3.22)$$

where \mathbf{Res} is the stochastic residual vector and where

$$\frac{\partial F_{qM}^\omega}{\partial u_{\epsilon kb}} = \delta_{qk} N_{b,M} \delta_{\epsilon\omega}. \quad (3.23)$$

Note that the external force vector is assumed here to be deformation independent for simplicity, but this term could be added straightforwardly if needed (e.g., when a pressure on the deformed surface is imposed or gravity is accounted for). Here, we assume that the problem is inertialess. Solving Equation (3.11) is finally done with the usual Newmark scheme, whose deterministic formulation can be used

as such with the new definition of the mass matrix, see Equation (3.12). In the case of explicit, the lumping of the mass matrix is done in the same manner as its deterministic counterpart.

3.1.6 Constitutive model

The function $\mathbf{P} = \tilde{\mathbf{P}}(\mathbf{F})$ and its derivative (the stochastic tangent modulus) are provided by the constitutive law. When using GSFEM, their numerical expressions are not straightforward as differentiation of stochastic quantities are involved. They can, however, be facilitated by the use of stochastic operators mirroring their deterministic counterparts, see Appendix A. We detail here the three stochastic constitutive models used in Chapter 4: the Saint Venant-Kirchhoff model, the Neo-Hookean and area growth model.

3.1.6.1 Saint Venant-Kirchhoff constitutive model

Starting with the case of the hyperelastic Saint Venant-Kirchhoff model used in Section 4, the formulation of the stochastic second Piola-Kirchhoff stress tensor \mathbf{S} can be linked to the stochastic Green-Lagrange strain tensor \mathbf{E} by:

$$\mathbf{S} = 2\mu \hat{\times} \mathbf{E} \hat{+} \lambda \hat{\times} \hat{tr}(\mathbf{E}), \quad (3.24)$$

where $\mathbf{P} = \mathbf{F} \hat{\times} \mathbf{S}$ and $\mathbf{E} = 1/2(\mathbf{F}^T \hat{\times} \mathbf{F} \hat{+} \mathbf{I})$. See Appendix A for the definition of the operators $\hat{\times}$, $\hat{+}$, $\hat{-}$, \hat{tr} and $\hat{\cdot}$. Here, λ and μ are stochastic Lamé constants.

This subsection presents the complete derivation of the partial derivative terms in Equation (3.22) when using a Saint Venant-Kirchhoff constitutive model with stochastic material properties.

3.1.6.1.1 Derivation of $\frac{\partial P_{iJ}^\iota}{\partial F_{qM}^\omega}$

The term P_{iJ}^ι can be written as:

$$P_{iJ}^\iota = C_{\alpha\beta\iota} F_{iK}^\alpha S_{KJ}^\beta \quad (3.25)$$

Consequently, the term $\frac{\partial P_{iJ}^\iota}{\partial F_{qM}^\omega}$ can be written as follows:

$$\frac{\partial P_{iJ}^\iota}{\partial F_{qM}^\omega} = C_{\alpha\beta\iota} \left(\frac{\partial F_{iK}^\alpha}{\partial F_{qM}^\omega} S_{KJ}^\beta + F_{iK}^\alpha \frac{\partial S_{KJ}^\beta}{\partial F_{qM}^\omega} \right) \quad (3.26)$$

3.1.6.1.2 Derivation of $\frac{\partial S_{KJ}^\beta}{\partial F_{qM}^\omega}$

Making use of the operators defined in Appendix A, Equation (3.24) can be written as follows:

$$S_{KJ}^\beta = C_{\gamma\zeta\beta} (2\mu^\gamma E_{KJ}^\zeta + \lambda^\gamma E_{XX}^\zeta \delta_{KJ}) \quad (3.27)$$

The term $\frac{\partial S_{KJ}^\beta}{\partial F_{qM}^\omega}$ can be written as:

$$\frac{\partial S_{KJ}^\beta}{\partial F_{qM}^\omega} = \frac{\partial S_{KJ}^\beta}{\partial E_{RS}^\psi} \frac{\partial E_{RS}^\psi}{\partial F_{qM}^\omega} \quad (3.28)$$

Using the symmetry of the spatial indices of the tensor \mathbf{E} , the term $\frac{\partial S_{KJ}^\beta}{\partial E_{RS}^\psi}$ can be written as:

$$\frac{\partial S_{KJ}^\beta}{\partial E_{RS}^\psi} = C_{\gamma\zeta\beta} (\mu^\gamma \delta_{\zeta\psi} (\delta_{KR} \delta_{JS} + \delta_{SK} \delta_{JR}) + \lambda^\gamma \delta_{\zeta\psi} \delta_{RS} \delta_{KJ}) \quad (3.29)$$

This equation can further be simplified as:

$$\frac{\partial S_{KJ}^\beta}{\partial E_{RS}^\psi} = C_{\gamma\psi\beta} (\mu^\gamma (\delta_{KR} \delta_{JS} + \delta_{SK} \delta_{JR}) + \lambda^\gamma \delta_{RS} \delta_{KJ}) \quad (3.30)$$

The last term to determine is $\frac{\partial E_{RS}^\psi}{\partial F_{qM}^\omega}$. The expression of E_{RS}^ψ is:

$$E_{RS}^\psi = \frac{1}{2} C_{\chi\varphi\psi} (F_{nR}^\chi F_{nS}^\varphi - \delta_{RS} \delta_{0\psi}) \quad (3.31)$$

Consequently, the term $\frac{\partial E_{RS}^\psi}{\partial F_{qM}^\omega}$ can be written as:

$$\frac{\partial E_{RS}^\psi}{\partial F_{qM}^\omega} = \frac{1}{2} C_{\chi\varphi\psi} (\delta_{nq} \delta_{\chi\omega} \delta_{RM} F_{nS}^\varphi + \delta_{nq} \delta_{\varphi\omega} \delta_{SM} F_{nR}^\chi) \quad (3.32)$$

and eventually as:

$$\frac{\partial E_{RS}^\psi}{\partial F_{qM}^\omega} = \frac{1}{2}(C_{\omega\varphi\psi}\delta_{RM}F_{qS}^\varphi + C_{\chi\omega\psi}\delta_{SM}F_{qR}^\chi) \quad (3.33)$$

As a result, the term $\frac{\partial S_{KJ}^\beta}{\partial F_{qM}^\omega}$ can finally be expressed as:

$$\frac{\partial S_{KJ}^\beta}{\partial F_{qM}^\omega} = \frac{1}{2}C_{\gamma\psi\beta}(\mu^\gamma(\delta_{KR}\delta_{JS} + \delta_{SK}\delta_{JR}) + \lambda^\gamma\delta_{RS}\delta_{KJ})(C_{\omega\varphi\psi}\delta_{RM}F_{qS}^\varphi + C_{\chi\omega\psi}\delta_{SM}F_{qR}^\chi) \quad (3.34)$$

3.1.6.1.3 Derivation of $\frac{\partial P_{iJ}^\iota}{\partial F_{qM}^\omega} \frac{\partial F_{qM}^\omega}{\partial u_{kb}^\epsilon}$

Using Equation (3.23), the term $\frac{\partial P_{iJ}^\iota}{\partial F_{qM}^\omega} \frac{\partial F_{qM}^\omega}{\partial u_{kb}^\epsilon}$ can be written as:

$$\frac{\partial P_{iJ}^\iota}{\partial F_{qM}^\omega} \frac{\partial F_{qM}^\omega}{\partial u_{kb}^\epsilon} = \frac{\partial P_{iJ}^\iota}{\partial F_{qM}^\omega} \delta_{qk} N_{b,M} \delta_{\epsilon\omega} = \frac{\partial P_{iJ}^\iota}{\partial F_{kM}^\epsilon} N_{b,M} \quad (3.35)$$

which, noting that

$$\frac{\partial F_{iK}^\alpha}{\partial F_{kM}^\epsilon} = \delta_{ik}\delta_{\alpha\epsilon}\delta_{KM}, \quad (3.36)$$

can then be further expanded into:

$$\begin{aligned} \frac{\partial P_{iJ}^\iota}{\partial F_{kM}^\epsilon} N_{b,M} &= C_{\alpha\beta\iota} \left(\frac{\partial F_{iK}^\alpha}{\partial F_{kM}^\epsilon} S_{KJ}^\beta + F_{iK}^\alpha \frac{\partial S_{KJ}^\beta}{\partial F_{kM}^\epsilon} \right) N_{b,M} = \\ C_{\alpha\beta\iota} \left(\delta_{ik}\delta_{\alpha\epsilon} S_{MJ}^\beta + F_{iK}^\alpha \frac{1}{2} C_{\gamma\psi\beta} (\mu^\gamma(\delta_{KR}\delta_{JS} + \delta_{SK}\delta_{JR}) + \lambda^\gamma\delta_{RS}\delta_{KJ}) (C_{\epsilon\varphi\psi}\delta_{RM}F_{kS}^\varphi + C_{\chi\epsilon\psi}\delta_{SM}F_{kR}^\chi) \right) & \\ = C_{\alpha\beta\iota} (\delta_{ik}\delta_{\alpha\epsilon} S_{MJ}^\beta + F_{iK}^\alpha \frac{1}{2} C_{\gamma\psi\beta} \mu^\gamma \delta_{KR}\delta_{JS} C_{\epsilon\varphi\psi} \delta_{RM} F_{kS}^\varphi + & \\ F_{iK}^\alpha \frac{1}{2} C_{\gamma\psi\beta} \mu^\gamma \delta_{KR}\delta_{JS} C_{\chi\epsilon\psi} \delta_{SM} F_{kR}^\chi + & \\ F_{iK}^\alpha \frac{1}{2} C_{\gamma\psi\beta} \mu^\gamma \delta_{SK}\delta_{JR} C_{\epsilon\varphi\psi} \delta_{RM} F_{kS}^\varphi + & \\ F_{iK}^\alpha \frac{1}{2} C_{\gamma\psi\beta} \mu^\gamma \delta_{SK}\delta_{JR} C_{\chi\epsilon\psi} \delta_{SM} F_{kR}^\chi + F_{iK}^\alpha \frac{1}{2} C_{\gamma\psi\beta} \lambda^\gamma \delta_{RS}\delta_{KJ} C_{\epsilon\varphi\psi} \delta_{RM} F_{kS}^\varphi + & \\ F_{iK}^\alpha \frac{1}{2} C_{\gamma\psi\beta} \lambda^\gamma \delta_{RS}\delta_{KJ} C_{\chi\epsilon\psi} \delta_{SM} F_{kR}^\chi) & \end{aligned} \quad (3.37)$$

Simplifying the Kronecker indices, Equation (3.37) becomes:

$$\begin{aligned}
\frac{\partial P_{iJ}^\iota}{\partial F_{kM}^\epsilon} N_{b,M} = & C_{\alpha\beta\iota} (\delta_{ik} \delta_{\alpha\epsilon} S_{MJ}^\beta + F_{iM}^\alpha \frac{1}{2} C_{\gamma\psi\beta} \mu^\gamma C_{\epsilon\varphi\psi} F_{kJ}^\varphi + F_{iK}^\alpha \frac{1}{2} C_{\gamma\psi\beta} \mu^\gamma \delta_{JM} C_{\chi\epsilon\psi} F_{kK}^\chi + \\
& F_{iK}^\alpha \frac{1}{2} C_{\gamma\psi\beta} \mu^\gamma \delta_{JM} C_{\epsilon\varphi\psi} F_{kK}^\varphi + \\
& F_{iM}^\alpha \frac{1}{2} C_{\gamma\psi\beta} \mu^\gamma C_{\chi\epsilon\psi} F_{kJ}^\chi + F_{iJ}^\alpha \frac{1}{2} C_{\gamma\psi\beta} \lambda^\gamma C_{\epsilon\varphi\psi} F_{kM}^\varphi + \\
& F_{iJ}^\alpha \frac{1}{2} C_{\gamma\psi\beta} \lambda^\gamma C_{\chi\epsilon\psi} F_{kM}^\chi) N_{b,M}.
\end{aligned} \tag{3.38}$$

Using the symmetry of the third-order tensor \mathbf{C} finally leads to:

$$\begin{aligned}
\frac{\partial P_{iJ}^\iota}{\partial F_{kM}^\epsilon} N_{b,M} = & C_{\alpha\beta\iota} (\delta_{ik} \delta_{\alpha\epsilon} S_{MJ}^\beta + F_{iM}^\alpha C_{\gamma\psi\beta} \mu^\gamma C_{\epsilon\varphi\psi} F_{kJ}^\varphi + F_{iK}^\alpha C_{\gamma\psi\beta} \mu^\gamma \delta_{JM} C_{\epsilon\varphi\psi} F_{kK}^\varphi + \\
& F_{iJ}^\alpha C_{\gamma\psi\beta} \lambda^\gamma C_{\epsilon\varphi\psi} F_{kM}^\varphi) N_{b,M}.
\end{aligned} \tag{3.39}$$

3.1.6.2 Neo-Hookean constitutive model

The hyperelastic Neo-Hookean material, first proposed by Ronald Rivlin in 1948, can be used for predicting the nonlinear stress-strain behaviour of materials undergoing large deformations. The formulation of the stochastic second Piola-Kirchhoff stress tensor \mathbf{S} is linked to the stochastic right Green-Cauchy strain tensor \mathbf{C} following the same form as its deterministic counterpart:

$$\mathbf{S} = \mu \hat{\times} \left(\mathbf{I} - \mathbf{C}^{-1} \right) \hat{+} \lambda \hat{\times} \hat{\log}(J) \mathbf{C}^{-1}, \tag{3.40}$$

where $\mathbf{C} = 1/2(\mathbf{F}^T \hat{\cdot} \mathbf{F})$. The extension of inverse $\widehat{-1}$ and logarithm $\hat{\log}$ operators to stochastic variables and tensors are respectively detailed in Appendix A and Appendix B.

3.1.6.2.1 Derivation of $\frac{\partial P_{iJ}^\iota}{\partial F_{qM}^\omega}$

The first Piola-Kirchhoff tensor \mathbf{P} can be written as:

$$\mathbf{P} = \mu \hat{\times} \left(\mathbf{F} - \mathbf{F}^{-T} \right) \hat{+} \lambda \hat{\times} \hat{\log}(J) \mathbf{F}^{-T}. \tag{3.41}$$

Consequently, the term $\frac{\partial P_{iJ}^\iota}{\partial F_{qM}^\omega}$ can be written as follows:

$$\begin{aligned} \frac{\partial P_{iJ}^\iota}{\partial F_{qM}^\omega} &= C_{\alpha\beta\iota} \mu^\alpha \left(\frac{\partial F_{iJ}^\beta}{\partial F_{qM}^\omega} - \frac{\partial (F^{-1})_{Ji}^\beta}{\partial F_{qM}^\omega} \right) \\ &+ C_{\alpha\beta\iota} \left((\lambda \log(J))^\alpha \frac{\partial (F^{-1})_{Ji}^\beta}{\partial F_{qM}^\omega} + \frac{\partial (\lambda \log(J))^\alpha}{\partial F_{qM}^\omega} (F^{-1})_{Ji}^\beta \right), \end{aligned} \quad (3.42)$$

where the stochastic operator $\hat{\cdot}$ is dropped for clarity.

3.1.6.2.2 Derivation of $\frac{\partial (\lambda \log(J))^\alpha}{\partial F_{qM}^\omega}$

Taking into account the fact that λ is independent of the deformation tensor, we can rewrite $\frac{\partial \lambda \log(J)^\alpha}{\partial F_{qM}^\omega}$ as:

$$\frac{\partial (\lambda \log(J))^\alpha}{\partial F_{qM}^\omega} = C_{\gamma\delta\alpha} \lambda^\gamma \frac{\partial \log(J)^\delta}{\partial F_{qM}^\omega}. \quad (3.43)$$

The difficulty lies in determining the expression of $\frac{\partial \log(J)^\delta}{\partial F_{qM}^\omega}$.

3.1.6.2.3 Derivation of $\frac{\partial \log(J)^\delta}{\partial F_{qM}^\omega}$

Recalling that J depends on \mathbf{F} , the term $\frac{\partial \log(J)^\delta}{\partial F_{qM}^\omega}$ can be rewritten as:

$$\frac{\partial \log(J)^\delta}{\partial F_{qM}^\omega} = C_{\xi\phi\delta} \frac{\partial J^\xi}{\partial F_{qM}^\omega} \left(\frac{1}{J} \right)^\phi. \quad (3.44)$$

While the term $\frac{1}{J}$ can be computed using the division operator detailed in Appendix A, the calculation of $\frac{\partial J^\xi}{\partial F_{qM}^\omega}$ is less trivial.

3.1.6.2.4 Derivation of $\frac{\partial J^\xi}{\partial F_{qM}^\omega}$

The stochastic Jacobian J has a polynomial expression with respect to the components of \mathbf{F} . Therefore, it is possible to derive an analytic expression of $\frac{\partial J^\xi}{\partial F_{qM}^\omega}$. However, for simplicity, we compute here this term, using a perturbation approach:

$$\frac{\partial J^\xi}{\partial F_{qM}^\omega} = \frac{(J(\mathbf{F}_{perturbed}) - J(\mathbf{F}))^\xi}{\tau}. \quad (3.45)$$

We define the components of $\mathbf{F}_{perturbed}$ in Equation (3.45) as follows:

$$(F_{perturbed})_{iJ}^\alpha = F_{iJ}^\alpha + \tau \delta_{\alpha\omega} \delta_{iq} \delta_{JM}. \quad (3.46)$$

The constant τ is a user-defined quantity, supposed to be small enough so that the approximation in Equation (3.45) is valid. This approximation of $\frac{\partial J^\xi}{\partial F_{qM}^\omega}$ has to be computed at every iteration of the Newton-Raphson algorithm.

3.1.6.2.5 Derivation of $\frac{\partial F_{iJ}^\beta}{\partial F_{qM}^\omega}$

The derivation of $\frac{\partial F_{iJ}^\beta}{\partial F_{qM}^\omega}$ can be computed and stored at the beginning of the simulation for higher efficiency. This term can be trivially expressed as:

$$\frac{\partial F_{iJ}^\beta}{\partial F_{qM}^\omega} = \delta_{\beta\omega} \delta_{iq} \delta_{JM}. \quad (3.47)$$

3.1.6.2.6 Derivation of $\frac{\partial (F^{-1})_{Ji}^\beta}{\partial F_{qM}^\omega}$

The derivation of $\frac{\partial (F^{-1})_{Ji}^\beta}{\partial F_{qM}^\omega}$ requires recalling the definition of \mathbf{F}^{-1} :

$$\mathbf{F} \cdot \mathbf{F}^{-1} = \mathbf{I}. \quad (3.48)$$

Differentiating Equation (3.48) with respect to \mathbf{F} leads to:

$$\frac{\partial \mathbf{F}}{\partial \mathbf{F}} \mathbf{F}^{-1} + \mathbf{F} \frac{\partial \mathbf{F}^{-1}}{\partial \mathbf{F}} = \mathbf{0}. \quad (3.49)$$

After rearranging Equation (3.48), we can write:

$$\frac{\partial \mathbf{F}^{-1}}{\partial \mathbf{F}} = -\mathbf{F}^{-1} \cdot \frac{\partial \mathbf{F}}{\partial \mathbf{F}} \cdot \mathbf{F}^{-1}. \quad (3.50)$$

The computation of the right-hand side of Equation (3.50) requires stochastic manipulations. We first express the term $\frac{\partial (F^{-1})_{Ji}^\beta}{\partial F_{qM}^\omega}$ as follows:

$$\frac{\partial(F^{-1})_{Ji}^\beta}{\partial F_{qM}^\omega} = -C_{\gamma\delta\beta} \left(\mathbf{F}^{-1} \cdot \frac{\partial \mathbf{F}}{\partial \mathbf{F}} \right)_{JKqM}^{\gamma\omega} (F^{-1})_{Ki}^\delta. \quad (3.51)$$

The term $\left(\mathbf{F}^{-1} \cdot \frac{\partial \mathbf{F}}{\partial \mathbf{F}} \right)_{JKqM}^{\gamma\omega}$ can be written as:

$$\left(\mathbf{F}^{-1} \cdot \frac{\partial \mathbf{F}}{\partial \mathbf{F}} \right)_{JKqM}^{\gamma\omega} = C_{\psi\phi\gamma} (F^{-1})_{Jn}^\psi \frac{\partial F_{nK}^\phi}{\partial F_{qM}^\omega}. \quad (3.52)$$

After combining Equation (3.36) and Equation (3.52), we obtain the following form of $\left(\mathbf{F}^{-1} \cdot \frac{\partial \mathbf{F}}{\partial \mathbf{F}} \right)_{JKqM}^{\gamma\omega}$:

$$\left(\mathbf{F}^{-1} \cdot \frac{\partial \mathbf{F}}{\partial \mathbf{F}} \right)_{JKqM}^{\gamma\omega} = C_{\psi\phi\gamma} (F^{-1})_{Jn}^\psi \delta_{\phi\omega} \delta_{nq} \delta_{KM}. \quad (3.53)$$

This equation can be finally simplified as:

$$\left(\mathbf{F}^{-1} \cdot \frac{\partial \mathbf{F}}{\partial \mathbf{F}} \right)_{JKqM}^{\gamma\omega} = C_{\psi\omega\gamma} (F^{-1})_{Jq}^\psi \delta_{KM}. \quad (3.54)$$

3.1.6.3 Area growth constitutive model

This constitutive model describes the special case of transversely isotropic growth, present for example in growing mucous membranes [142]. Such a model can potentially be useful for *in silico* diagnosis of certain diseases. The main feature of this model is to separate multiplicative the deformation gradient \mathbf{F} into a growth part \mathbf{F}_g and an elastic part \mathbf{F}_e :

$$\mathbf{F} = \mathbf{F}_e \cdot \mathbf{F}_g. \quad (3.55)$$

In the case of isotropic growth, the model is characterised by a growth multiplier ζ^g . The first Piola-Kirchhoff tensor \mathbf{P} is described as follows:

$$\mathbf{P} = \mathbf{P}_e \cdot \widehat{\mathbf{F}_g^{-T}}. \quad (3.56)$$

The tensor \mathbf{P}_e follows a similar form as in Equation (3.41):

$$\mathbf{P}_e = \mu \hat{\times} \left(\mathbf{F}_e \hat{-} \widehat{\mathbf{F}_e^{-T}} \right) \hat{+} \lambda \hat{\times} \log(J_e) \widehat{\mathbf{F}_e^{-T}}, \quad (3.57)$$

where the elastic part of the deformation gradient \mathbf{F}_e has the following expression:

$$\mathbf{F}_e = \frac{1}{\sqrt{\zeta^g}} \mathbf{F} \hat{+} \left(1 - \frac{1}{\sqrt{\zeta^g}}\right) \mathbf{n} \hat{\otimes} \mathbf{n}_0, \quad (3.58)$$

where $\hat{\otimes}$ is the stochastic extension of the dyadic product, defined in Appendix A, \mathbf{n}_0 is the initial growth direction, \mathbf{n} is the growth direction in the deformed configuration and ζ^g is the growth factor.

We now present the derivation of the partial derivative terms in Equation (3.22) when using area growth constitutive model with stochastic material properties.

3.1.6.3.1 Derivation of $\frac{\partial P_{iJ}^\iota}{\partial F_{qM}^\omega}$

The term $\frac{\partial P_{iJ}^\iota}{\partial F_{qM}^\omega}$ can be written as follows:

$$\frac{\partial P_{iJ}^\iota}{\partial F_{qM}^\omega} = C_{\alpha\beta\iota} \frac{\partial (P_e)_{ik}^\alpha}{\partial F_{qM}^\omega} (F_g^{-1})_{Jk}^\beta. \quad (3.59)$$

3.1.6.3.2 Derivation of $\frac{\partial (P_e)_{iJ}^\iota}{\partial F_{qM}^\omega}$

The derivation of $\frac{\partial (P_e)_{iJ}^\iota}{\partial F_{qM}^\omega}$ is similar to the one performed in Section 3.1.6.2.1. Instead of using the total deformation tensor \mathbf{F} in Equation (3.55), solely its elastic component \mathbf{F}_e is used. Then, the main difficulty lies in finding the expression of $\frac{\partial \mathbf{F}_e}{\partial \mathbf{F}}$.

3.1.6.3.3 Derivation of $\frac{\partial \mathbf{F}_e}{\partial \mathbf{F}}$

Assuming ζ^g deterministic, differentiating Equation (3.58) with respect to \mathbf{F} allows us to write:

$$\frac{\partial \mathbf{F}_e}{\partial \mathbf{F}} = \frac{1}{\sqrt{\zeta^g}} \frac{\partial \mathbf{F}}{\partial \mathbf{F}} \hat{+} \left(1 - \frac{1}{\sqrt{\zeta^g}}\right) \frac{\partial \mathbf{n} \hat{\otimes} \mathbf{n}_0}{\partial \mathbf{F}}, \quad (3.60)$$

where $\mathbf{n} = \mathbf{F} \hat{+} \mathbf{n}_0$. While the derivation of $\frac{\partial \mathbf{F}}{\partial \mathbf{F}}$ has already been provided in Equation (3.36), the derivation of $\frac{\partial \mathbf{n} \hat{\otimes} \mathbf{n}_0}{\partial \mathbf{F}}$ is less straightforward.

3.1.6.3.4 Derivation of $\frac{\partial n \hat{\otimes} n_0}{\partial \mathbf{F}}$

Noting that $\mathbf{n} = \mathbf{F} \hat{\otimes} \mathbf{n}_0$, we can write its components as follows:

$$n_i^\gamma = C_{\alpha\beta\gamma} F_{iK}^\alpha (n_0)_K^\beta. \quad (3.61)$$

Therefore, the components of $\frac{\partial n \hat{\otimes} n_0}{\partial \mathbf{F}}$ can be written as follows:

$$(n \hat{\otimes} n_0)_{iJ}^\epsilon = C_{\gamma\kappa\epsilon} C_{\alpha\beta\gamma} F_{iK}^\alpha (n_0)_K^\beta (n_0)_J^\kappa. \quad (3.62)$$

Consequently, the terms of $\frac{\partial n \hat{\otimes} n_0}{\partial \mathbf{F}}$ have the following expression:

$$\frac{\partial (n \hat{\otimes} n_0)_{iJ}^\epsilon}{\partial F_{qM}^\omega} = C_{\gamma\kappa\epsilon} C_{\alpha\beta\gamma} (n_0)_K^\beta (n_0)_J^\kappa \delta_{\omega\alpha} \delta_{iq} \delta_{KM}. \quad (3.63)$$

This expression can be further simplified as:

$$\frac{\partial (n \hat{\otimes} n_0)_{iJ}^\epsilon}{\partial F_{qM}^\omega} = C_{\gamma\kappa\epsilon} C_{\omega\beta\gamma} (n_0)_M^\beta (n_0)_J^\kappa \delta_{iq}. \quad (3.64)$$

This term, independent of \mathbf{F} can be computed and stored at the beginning of the calculation.

3.1.7 Expansion of the solution

This section details the three expansions used in this work: PCE, Haar and a mixed Wavelet approach.

3.1.7.1 Polynomial chaos expansion

The PCE, introduced for the first time by Wiener in 1938 [86], was aimed at creating a metamodel that determines the evolution of uncertainty in a dynamical system. This metamodel is dependent on the probabilistic distribution of input parameters. According to the Cameron-Martin theorem [87], such an expansion converges in the L_2 sense for a stochastic process with finite variance depending on Gaussian stochastic variables. Xiu [90] extended these results to various probabilistic

distributions of the inputs. The PCE interpolant univariate polynomials $\psi_\lambda(\theta)$, where λ is the degree of the polynomial, must verify this integral:

$$\int_E \psi_\lambda(w) \psi_{\lambda'}(w) f_\theta(w) dw = 0 \text{ if } \lambda \neq \lambda', \quad (3.65)$$

where the function $f_\theta(w)$ is the probability distribution of the stochastic variable θ . The polynomials ψ 's are determined recursively. The uniqueness of these polynomials is imposed by setting the coefficient of the highest degree to 1, see Section 2.2.3.1.

We now consider $\boldsymbol{\theta} = [\theta_1, \dots, \theta_N]$, the vector of input random variables. For simplicity, the stochastic variables are supposed to be uncorrelated so that the joint probabilistic distribution is the product of each probabilistic distribution function. The M multivariate polynomials Ψ of the PCE are defined as follows:

$$\Psi = \left\{ \prod_{i=1}^N \psi_{\lambda_i}(\theta_i) : \sum_{i=1}^N \lambda_i \leq n \right\}, \quad (3.66)$$

where λ_i refers to the order of the univariate polynomial associated to θ_i and where n indicates the degree of the expansion. The number of multivariate polynomials in a PCE expansion of order n is $M = \binom{n+N}{n}$. These expansions are suitable when the quantity of interest exhibits a smooth dependence on the input parameters.

3.1.7.2 Haar expansion

The use of PCE can sometimes lead to instabilities such as the Gibbs phenomenon, see Chapter 4. To overcome this limitation of the PCE expansion, the stochastic inputs and the solution can instead be decomposed using Haar expansion [143]. Given a realisation w of a random variable θ , we note $\mathbb{P}_\theta(x)$ the probability that $w < x$, where x is a real number. The function \mathbb{P}_θ is assumed to be a continuous strictly increasing function of x . Based on these assumptions, there is one unique solution x such that $\mathbb{P}_\theta(x) = y$, where $0 \leq y \leq 1$. We note $F = \mathbb{P}_\theta^{-1}$ and we introduce the Haar function ψ^h :

$$\psi^h(y) = \begin{cases} 1, & \text{if } 0 \leq y \leq 0.5 \\ -1, & \text{if } 0.5 \leq y \leq 1 \\ 0, & \text{otherwise.} \end{cases}$$

The Haar function is the mother Wavelet that generates the Wavelet family:

$$\psi_{j,k}(y) = 2^{\frac{j}{2}} \psi^h(2^j y - k), \quad (3.67)$$

where $j = 0, \dots, n$ is the scale index and $k = 0, \dots, 2^j - 1$ is the space index, with n being a user-defined index indicating the resolution of the expansion. Any stochastic process X function of the random variable θ with finite variance can be approximated arbitrarily well by the following expression:

$$X = \bar{X} + \sum_{j=0}^n \sum_{k=0}^{2^j-1} X_{j,k} \psi_{j,k}. \quad (3.68)$$

The values of $X_{j,k}$ are determined by a scalar projection of X on the functions $\Psi_{j,k}$:

$$X_{j,k} = \int_0^1 X(F(y)) \psi_{j,k}(y) dy. \quad (3.69)$$

For simplicity, we concatenate the two indices j and k using an integer $\lambda = 2^k + j$. We note ∇ the set of integers λ , $\nabla \equiv \{\lambda : j = 0, \dots, n, k = 2^j - 1\}$. Noting $\psi_0 = 1$, and $\nabla_0 = \nabla \cup \{0\}$, Equation (3.68) can be rewritten as:

$$X = \sum_{\lambda \in \nabla_0} X_\lambda \psi_\lambda. \quad (3.70)$$

Considering now a multi-dimensional stochastic process, with multi-dimensional index $\boldsymbol{\lambda} = [\lambda_1, \dots, \lambda_N]$ the univariate sequence defined by Equation (3.67) is used to create the multivariate family Ψ^H :

$$\Psi^H = \left\{ \prod_{k=1}^N \psi_{\lambda_k}(\theta_k) : \sum_{k=1}^N |\lambda_k| \leq n \right\}, \quad (3.71)$$

where n is the level of resolution.

3.1.7.3 Wavelet expansion

The Haar expansion, while allowing to capture discontinuous behaviours, can require a high level of resolution to capture continuous distributions, see Chapter 4. To overcome this issue, we propose here to use a mixed Wavelet expansion. This expansion uses both continuous and discontinuous functions. Here, a space V^R , containing polynomials of order equal or smaller than R is constructed with a cardinality of $R + 1$. Typically, the scaled Legendre polynomials $[\phi_0, \dots, \phi_R]$ are used as a basis of V^R . Discontinuous orthonormal functions $[\psi_0, \dots, \psi_R]$ are then built as follows [144]:

- (i) Two sets of polynomials $p_i(y)$ and $q_i(y)$ are defined:

$$\begin{cases} p_i(y) = y^i \\ q_i(y) = \begin{cases} p_i(y), & \text{if } 0 \leq y \leq 0.5 \\ -p_i(y), & \text{if } 0.5 < y \leq 1. \end{cases} \end{cases}$$

- (ii) Each polynomial q_i is orthogonalised with respect to all the function p_i to obtain a new set of polynomials $[\tilde{q}_0, \dots, \tilde{q}_R]$;
- (iii) Using a Gram-Schmidt scheme, the set of polynomials $[\tilde{q}_0, \dots, \tilde{q}_R]$ are orthogonalised with respect to each other to give a set of polynomials $[r_0, \dots, r_R]$;
- (iv) The set of polynomials $[r_0, \dots, r_R]$ is normalised to obtain the functions $[\psi_0, \dots, \psi_R]$.

By construction, the functions ψ_i and ϕ_j are orthogonal. We define the functions ψ_{ik}^j as:

$$\psi_{ik}^j(y) = 2^{\frac{j}{2}} \psi_i(2^j y - k). \quad (3.72)$$

Similarly to Equation (3.68), a given stochastic process is finally expanded using the Wavelet expansion:

$$X(y) = \sum_{i=0}^R X_i \phi_i(y) + \sum_{i=0}^R \sum_{j=0}^n \sum_{k=0}^{2^j-1} X_{i+(R+1)(2^j+k)} \psi_{ik}^j(y). \quad (3.73)$$

The coordinates X_i , where $i = 0, \dots, 2^{n+1}(R+1) - 1$, are obtained by projection of X on the functions ψ_i and ϕ_i . More information can be found about the underlying mathematical theory of these expansions in Ref. [144] and [145].

3.1.8 Modularity of the code

In GSFEM, solving both the stochastic and spatial FE problem at the same time requires the modification of the governing equations. Therefore, using a commercial solver is impractical. However, with appropriate changes, an in-house FE code can be modified intrusively to perform simulations of stochastic problems. The general framework of any FE software can be summarised as shown in Figure 3.2.

At first, an input file gathering all the information about the geometry, connectivity, type of simulation, constitutive model, value of parameters, among other usual inputs, has to be read. Afterwards, at each iteration, the displacements are updated either explicitly or implicitly to satisfy the mechanical equilibrium up to a threshold value. Then, the time of the simulation is advanced and the process is repeated, until the end time is reached. Finally, the outputs are postprocessed (or once in a while during the course of the simulation).

In Figure 3.2, the parts of the solver that require modifications are specified in lighter green. The writing and reading of the input file has to be done so that the probabilistic distributions of each stochastic variable (geometry, constitutive parameters, initial conditions) are specified. Before the computation of internal/external forces, key mathematical quantities, such as the third order tensor \mathbf{C} , see Appendix A, are computed once and stored to gain computational time. Afterwards, the computation of the internal, external inertial forces and stiffness matrices are modified accordingly. These modifications can be done in a modular way using a stochastic algebra library. This algebra allows for the computation of basic operations such as addition/multiplication/division of stochastic variables that have been detailed in the literature [24, 134] but also more sophisticated operations, including stochastic dyadic product.

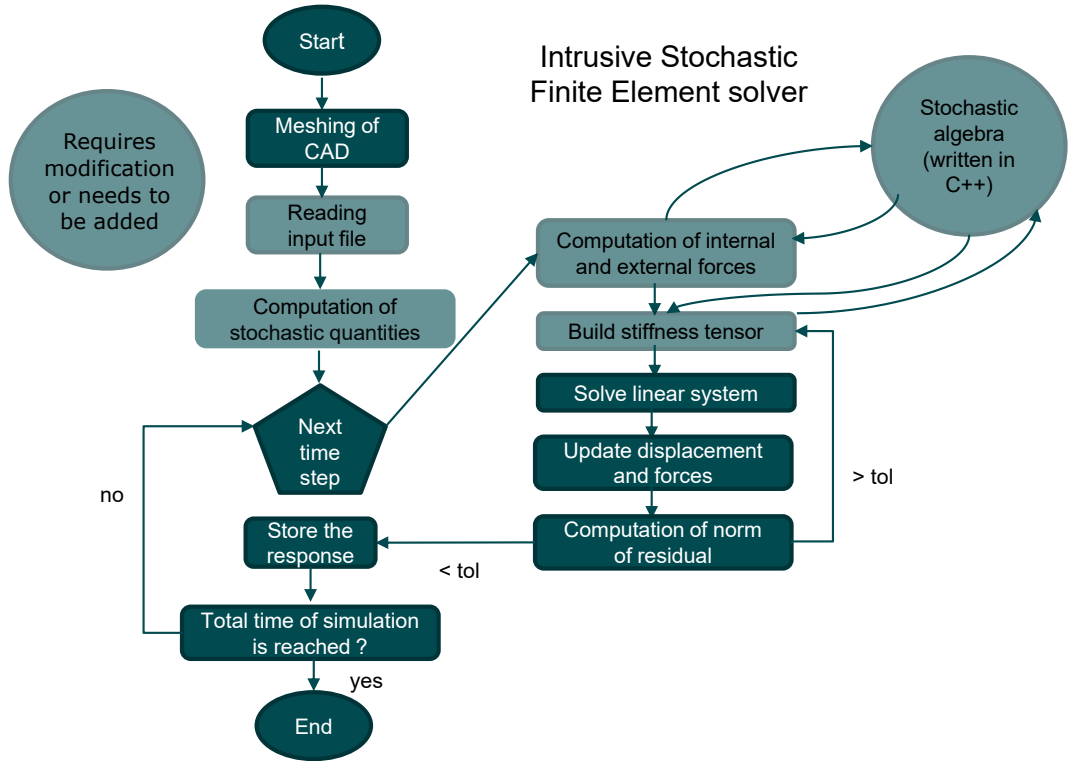


Figure 3.2: Scheme of the stochastic in-house code. The differences with the deterministic solver are indicated in lighter colour.

3.1.9 Uncertainty of the inputs

The GSFEM and its underlying mathematical theory suppose perfect knowledge of the probability distribution of the input variables. These distributions are often idealised by researchers for ease of manipulation or when data are not available. While doing so allows for more flexibility, e.g., the computation of the univariate polynomial chaos with closed forms, more realistic distributions can be found using experimental data, potentially capturing better the uncertainties. For any probabilistic distribution, the corresponding PCE can be determined using a second-moment approach, detailed in Section 2.2.3.1. This approach only requires the knowledge of the distribution moments. For user-defined distributions, these quantities can be obtained using numerical integration.

While the mathematical formulation of the GSFEM can readily incorporate random fields, the following work only presents the propagation of space-independent

uncertainties. Any random fields, with known space-dependent covariance, can be decomposed into a spatial and stochastic basis that are independent, using the K-L theorem, see Equation (2.25). Using this decomposition, these space-dependent uncertainties can be included in this framework.

In mechanics, some variables exhibit strong interdependence. As an example, the Young’s modulus and the porosity of a structure are likely to be correlated. Manipulating correlated random variables can be impractical as their joint distribution is no longer the combination of each variable distribution, making the obtention of PCE more tedious to obtain. To overcome this issue, it is possible to use the Rosenblatt transformation [146] to map a vector of correlated random variables into a vector of uncorrelated random variables for smoother integration in the GSFEM.

3.2 APFEM and BI-APFEM

Here, we propose an extension of the GSFEM—termed the *A posteriori* Finite Element Method or APFEM—where uniform distributions are considered to allow for parametric studies of the inputs of interest as a postprocessing step *after* the simulation. As a result, APFEM only requires the knowledge of the vertices of the parameter space. In addition, the uniform distribution weights the error equally over the whole parameter space, as opposed to Gaussian distributions penalising the error near the mean of the parameter space. One key advantage of APFEM is its use in the context of Bayesian inferences, where the random evaluations required by the Bayesian setting (and usually done through MC) can be done exactly without the need for further simulations.

First, the specialisation of PCE and mixed Wavelet to uniform random variables is addressed, then the extension of APFEM to the Bayesian setting is detailed.

3.2.1 Legendre PCE

The main feature of APFEM is to specialise GSFEM to uniform random variables. Ref. [90] established the optimal expansions for various probabilistic distributions of

the inputs, including the uniform one. Following this, we use Legendre polynomials for the PCE. Accordingly, the order n Legendre polynomial is given by:

$$P_n(\theta) = \frac{1}{2^n} \sum_{k=0}^n \binom{n}{k}^2 (\theta - 1)^{n-k} (\theta + 1)^k. \quad (3.74)$$

The univariate polynomials ψ 's are taken as proportional to the Legendre polynomials P_n . The multiplication factor is found by imposing the coefficient of the highest degree to 1 for each of the univariate polynomials. The first five polynomials are shown in Figure 3.3.

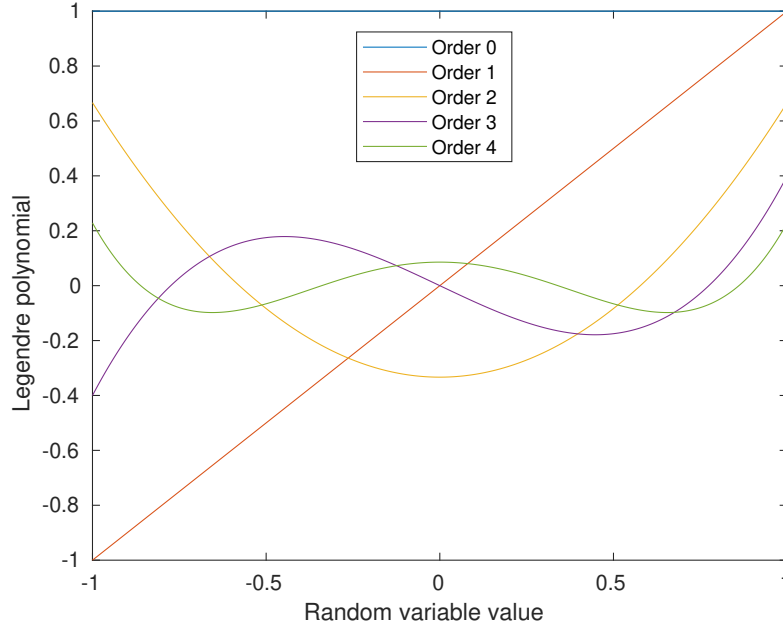


Figure 3.3: Legendre polynomials. The first five polynomials are shown.

3.2.2 Specialisation of mixed Wavelet expansion to uniform variables

We recall that any given stochastic process can be expanded using the Wavelet expansion:

$$X(y) = \sum_{i=0}^R X_i \phi_i(y) + \sum_{i=0}^R \sum_{j=0}^n \sum_{k=0}^{2^j-1} X_{i+(N+1)(2^j+k)} \psi_{il}^k(y). \quad (3.75)$$

The variable y represents the cumulative distribution (CDF) of the input parameters. For most probabilistic distributions, e.g., Gaussian distributions, the variable y does not have a closed form, which introduces inaccuracies in the numerical implementation of Equation (3.75). This is not the case for uniform distribution, that are used, and the CDF can be written as follows:

$$y(w) = \frac{w + 1}{2} \quad (3.76)$$

where w is comprised between -1 and 1 and belongs to the support space of the uniform random variable. The extension to multivariate uniform distributions follows naturally.

3.2.3 Bayesian inferences

The principle of the Bayesian method is to deduce some parameters of a model by using observable quantities. While regression methods return a single value for each parameter using optimisation principles, BI estimates the probability distribution of inputs.

Let us assume a forward model describing the relationship between two multivariate random variables $\mathbf{X} = [X_1, \dots, X_{n_i}]$ and $\widetilde{\mathbf{Y}} = [\widetilde{Y}_1, \dots, \widetilde{Y}_{n_o}]$. We introduce n_i and n_o as respectively the number of unknown parameters and the number of observable outputs. We define $X_i: \Theta \rightarrow E$ and $\widetilde{Y}_j: \Theta \rightarrow \mathbb{R}$, $\forall i \in [1, n_i]$ and $\forall j \in [1, n_o]$, where the support E is $[-1, 1]$. We then write:

$$\widetilde{\mathbf{Y}} = \mathbf{f}(\mathbf{X}). \quad (3.77)$$

We emphasise the fact that the realisation $\widetilde{\mathbf{y}}$ and \mathbf{x} of $\widetilde{\mathbf{Y}}$ and \mathbf{X} , respectively, are considered to be in a Bayesian setting. The starting point of this framework is to use Bayes' theorem to evaluate the probability of \mathbf{x} knowing \mathbf{y} :

$$p(\mathbf{x}|\mathbf{y}) = \frac{p(\mathbf{y}|\mathbf{x})p_{prior}(\mathbf{x})}{\int_{E^{n_i}} p(\mathbf{y}|\mathbf{x}')p_{prior}(\mathbf{x}')d\mathbf{x}'}, \quad (3.78)$$

where \mathbf{y} represents the measurements of the outputs, $p_{prior}(\mathbf{x})$ is the supposed distribution of \mathbf{x} -values. In this formulation, the data are taken into account in

the term $p(\mathbf{y}|\mathbf{x})$, the so-called likelihood, which represents the degree of belief of measurement \mathbf{y} for a given set \mathbf{x} -values. These measurements deviate from the theoretical outputs obtained from realisations of Equation (3.77). When assuming that the theoretical model is perfectly accurate and that the discrepancies only come from measurement errors, e.g., sensor noises, \mathbf{y} can be written as follows:

$$\mathbf{y} = \tilde{\mathbf{y}} + \boldsymbol{\eta}, \quad (3.79)$$

where the components of $\boldsymbol{\eta}$ are supposed to be independent random variables, i.e, the measurement noise of two different outputs have no correlation. Subsequently, we assume that each component η_i of $\boldsymbol{\eta}$ follows a Gaussian distribution p_η of zero-mean and σ -standard deviation. Consequently, the likelihood $p(\mathbf{y}|\mathbf{x})$ has the following expression:

$$p(\mathbf{y}|\mathbf{x}) = \prod_i p_\eta(y_i - \tilde{y}_i(\mathbf{x})). \quad (3.80)$$

Combining Equations (3.78) and (3.80), the posterior distribution of the parameters $p(\mathbf{x}|\mathbf{y})$ is obtained by making use of the Markov Chain MC Method [147, 148]. This step requires to evaluate Equation (3.77) over the parameter space. Instead of using sampling methods like MC or latin-hypercube sampling, we replace here Equation (3.77) with a surrogate:

$$\tilde{\mathbf{Y}} = \sum_{\epsilon=0}^N \tilde{\mathbf{Y}}_\epsilon \Psi_\epsilon(\boldsymbol{\theta}), \quad (3.81)$$

where all the sampled uncertainties of \mathbf{x} are gathered in a vector of random variables $\boldsymbol{\theta}$, and the Ψ_ϵ 's are the interpolants detailed in Section 3.1.7. In APFEM, the coefficients $\tilde{\mathbf{Y}}_\epsilon$ are straightforwardly determined by solving Equation (3.9) over the stochastic and physical space. By using APFEM instead of MC and derivatives, one can accelerate the computation of the likelihood and consequently the derivation of the posterior distribution. Furthermore, by assuming here that the prior distribution is described by uniform random variables, no knowledge is required on the parameter space, except its vertices.

3.3 Extension to topological uncertainties

Geometrical imperfections are ubiquitous in structural components. Mainly introduced during the manufacturing process, these deviations from nominal geometry can have a strong impact on the mechanical behaviour [149]. To quantify this impact, researchers have been mainly relying on MC, where the mechanical response is obtained for various geometries. While being highly flexible, this method requires remeshing for each sampled geometry. In addition, when modelling systems with high-fidelity, each simulation can require a great amount of computational resources. Hence, using MC method with a high number of deterministic simulations is highly ineffective. To address this issue, researchers have been focusing on fictitious domain methods. This class of methods aims at solving the PDE on a single fictitious domain. This fictitious domain encompasses all possible geometrical configurations the structure can exhibit. Albeit accurate, this method can require significant mathematical efforts to reformulate the PDE. Building on this approach, Nouy *et al.* developed the X-SFEM [150], an intrusive stochastic finite element method. They used random level-set functions to model the uncertain geometrical configurations. Similarly, Pivovarov *et al.* derived the homogenised behaviour of a composite [151]. The geometrical uncertainties were introduced through a jump in the mechanical properties. The shear modulus and Poisson's ratio value were supposed to be space dependent random quantities, varying from their matrix nominal value to the inclusion counterpart. While being applicable to a wide range of inclusion shapes, this method is dependent on a user-defined smoothness parameter. The extension of GSFEM to the simulation of geometric uncertainties has been largely ignored, barring a few exceptions [24]. There, we use our newly developed framework to this end.

3.3.1 Framework

This framework revolves around the creation of an intermediate stochastic configuration Ω_{int} . This intermediate configuration is supposed to represent all possible geometries of the structural component. The deformation gradient tensor is then

decomposed into two parts, the first one, \mathbf{F}_{Map} , mapping the original configuration Ω_0 to Ω_{int} . The second part of the decomposition, \mathbf{F}_{Mech} , transforms Ω_{int} to the final deformed configuration Ω :

$$\mathbf{F} = \mathbf{F}_{Mech} \cdot \mathbf{F}_{Map}. \quad (3.82)$$

Assuming that these geometric deviations can be expressed using a transformation function of one or more parameters, we perform a first computation where the governing equations are solved. In this computation, solely Dirichlet boundary conditions introducing geometrical discrepancies are applied. At the end of this step, the stochastic coordinates of each node of the deterministic configuration are obtained. Once the mapping tensor \mathbf{F}_{Map} is obtained, the mechanical loadings can be included. The second computation assumes that the intermediate configuration Ω_{int} is stress-free. As Equation (3.9) is solved in the original configuration, all mechanical quantities have to be pushed back into the reference configuration. As an example, the effective second Piola-Kirchhoff \mathbf{S}_{eff} tensor reads as:

$$\mathbf{S}_{eff} = J_{Map} \mathbf{F}_{Map}^{-1} \cdot \mathbf{S} \cdot \mathbf{F}_{Map}^{-T}, \quad (3.83)$$

where J_{Map} is the determinant of \mathbf{F}_{Map} . The tensor \mathbf{S} is the derivative of the Helmholtz free energy with respect to the Green strain tensor. Once this second boundary-valued problem is solved, the results can finally be postprocessed. Note that this framework can be used for both GSFEM and APFEM. The overall procedure is detailed in Algorithm 1.

Algorithm 1 Computation procedure for topological uncertainties incorporation

- 1: Find appropriate stochastic Dirichlet boundary conditions to represent the set of possible defects.
 - 2: Perform an offline PCE projection of these boundary conditions.
 - 3: Solve the governing equation with these stochastic boundary conditions to find the mapping tensor \mathbf{F}_{Map} .
 - 4: Solve the second governing equation with the mechanical loading. The second Piola-Kirchhoff tensor has to be pushed back to the original configuration.
 - 5: Postprocess the results.
-

The second step in Algorithm 1 is a limitation to this framework. The PCE projection introduces discrepancies when the function to project grows in complexity. While our proposed algebra reached a certain degree of maturity, it is expected that highly nonlinear functions, e.g., negative power functions, could require high-order PCE for accurate projection and consequently more computational time. Finally the mapping \mathbf{F}_{Map} can take many forms. One solution is that it only contains the stochastic displacements of the boundary nodes to be considered (in which case $\mathbf{F}_{Map} = \mathbf{I}$ elsewhere). This solution becomes problematic when the nodal displacements degenerate the elements connected to it. The solution used here is to leverage an elastic law between the reference and the intermediation configuration. Doing so moves stochastically all the mesh nodes to minimise the overall energy. As the mechanical solver mapping the intermediate configuration to the final deformed configuration is solely concerned with $\mathbf{F}_{mech} = \mathbf{F} \cdot \mathbf{F}_{Map}^{-1}$, it is in fact agnostic to this remeshing.

3.4 Dissemination

The mathematical formulations of GSFEM and APFEM presented in this chapter were published in Computational Methods in Applied Mechanical Engineering as manuscripts titled “A modular nonlinear stochastic finite element formulation for uncertainty estimation”, DOI:10.1016/j.cma.2022.115044 and “The a posteriori finite element method (APFEM), a framework for efficient parametric study and Bayesian inferences”, In Press. The extension to topological uncertainties has also been submitted.

Chapter 4

Numerical applications

The final step of this work is to illustrate the flexibility of the proposed methods to a wide range of examples. We first focus on a buckling problem of increasing complexity where material parameters, boundary conditions and/or body geometry are stochastically defined and solved with GSFEM and APFEM. The APFEM is then used in the context of metamaterial optimisation where parameter exploration is required. A direct corollary of that feature is the possibility to use APFEM for BI for two final applications: first in contact mechanics for the determination of a friction coefficient in the Cattaneo-Mindlin problem, and then for inferring the stiffness of brain cancer using midline shift measurements arising during cardiac cycle tissue deformation. In all the following examples uncertainties are assumed to be time-independent.

4.1 Stochastic buckling

4.1.1 Stochastic buckling: GSFEM approach

Bifurcation problems are a common challenge in structural mechanics problems. In such cases, a slight variation in an input parameter can dramatically change the output values. Consequently, the distribution of outputs may exhibit discontinuous and/or sharp behaviours. Here, we illustrate the ability of GSFEM to capture

bifurcation problems by considering a 3D beam clamped at its left extremity and submitted to an axial displacement on its right extremity, see Figure 4.1a. If this displacement is compressive the structure above a certain threshold, the beam buckles and experiences large lateral displacements at the tip (either up or down in Figure 4.1a). If the displacement is tensile, then the lateral displacement of the tip should be null. Here, we prescribe a stochastic axial displacement following a Gaussian distribution centred on zero displacement, see Figure 4.1b. Boundary conditions are prescribed such that the lateral surfaces cannot move in the z -direction. To provoke an upward buckling, we impose a negligible deterministic displacement positive in the y -direction at the tip. Finally, the beam is arbitrarily made of a Saint Venant-Kirchhoff material. The geometrical features of the beam, the FE discretisation and the material properties are given in Table 4.1. While the proposed scheme can also account for stochastic constitutive parameters, we restrict the stochasticity of our model to the boundary conditions described above and retain deterministic material parameters.

Parameters	Value
Geometrical features	Length = 25 m, width = depth = 1 m
Number of nodes	1,336
Type of elements	quadratic tetrahedron
Number of elements	703
Mean value of axial displacement	0 m
Standard deviation of axial displacement	1 m
Young's modulus and Poisson's ratio	1×10^7 Pa, 0.4

Table 4.1: FE discretisation, material parameters and geometric features of the beam.

Here, we provide a comparison between the non-intrusive approach (MC) and intrusive approach with continuous (PCE) and discontinuous expansions (Haar and Wavelet). All simulations are performed in our in-house code software, MuPhiSim. The results using MC provide a baseline for comparisons as this framework ensures that, given enough simulations, the output's probabilistic distribution is accurately captured. The distribution of the lateral tip displacement is shown in Figure 4.2. Two regimes can be observed. When the displacement is negative enough

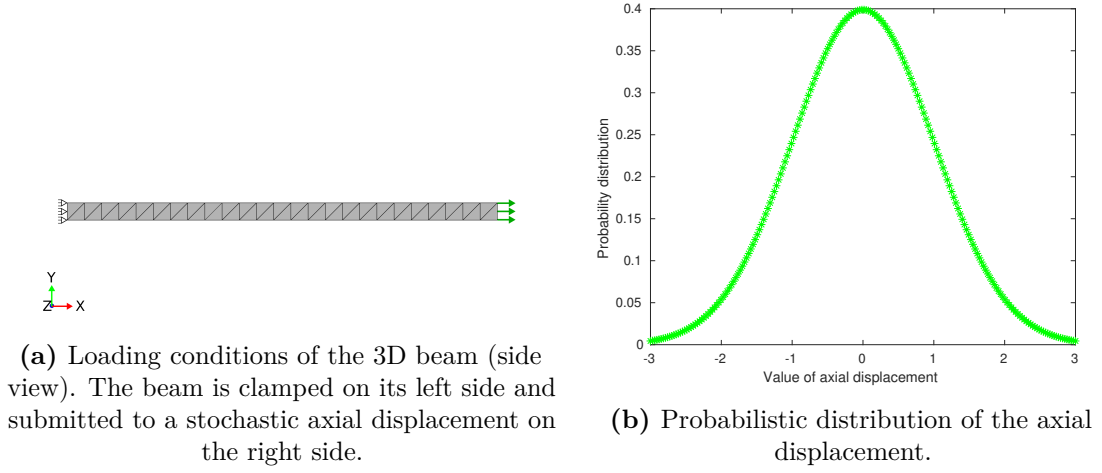


Figure 4.1: A 3D beam is submitted to stochastic boundary conditions triggering buckling in the case of a sufficiently large compression.

(compressive), the lateral displacement varies quickly with the axial displacement. When the displacement is positive (tensile), the displacement does not vary with the axial displacement.

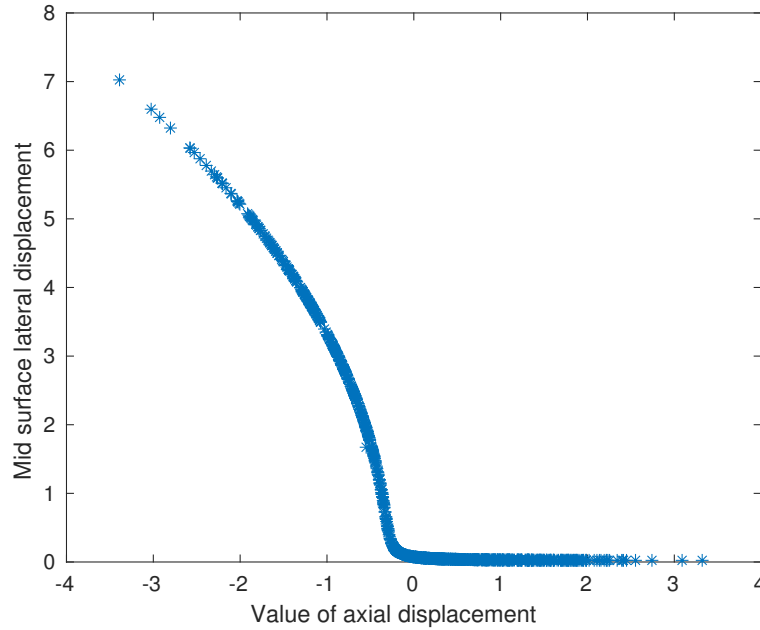
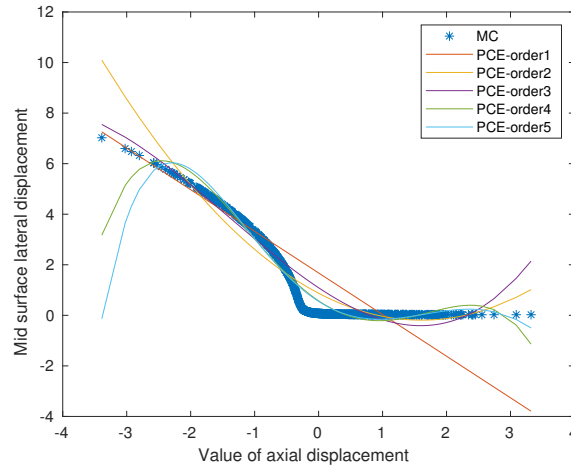


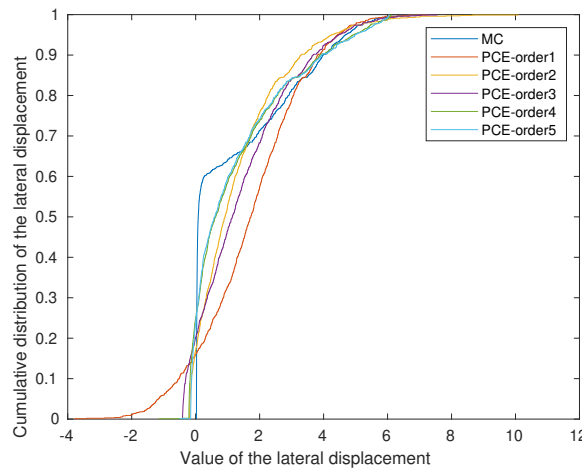
Figure 4.2: Distribution of the tip displacement using MC method.

The model presented in this section is used with PCE, Haar and mixed Wavelet. All three are compared in the following. While capturing the MC

results, approaching the distribution of the lateral tip displacement using PCE is ineffective, see Figure 4.3a. Indeed, increasing the order of the expansion only results in greater oscillations and does not guarantee convergence. This is predictable as using smooth functions to approximate a non-smooth function is expected to lead to such issue: the Gibbs phenomenon. The inaccuracy of the PCE approach is even more striking when comparing the CDF of the lateral displacement, see Figure 4.3b. Even if there seems to be a convergence pattern, the PCE is not able to model the sharp increase in the CDF.



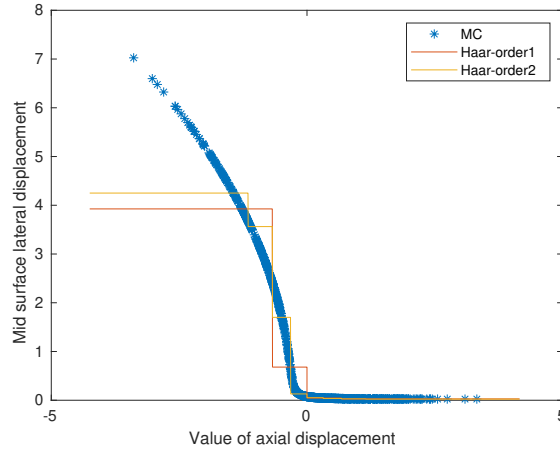
(a) Comparison of the distribution of the tip displacement using PCE and MC.



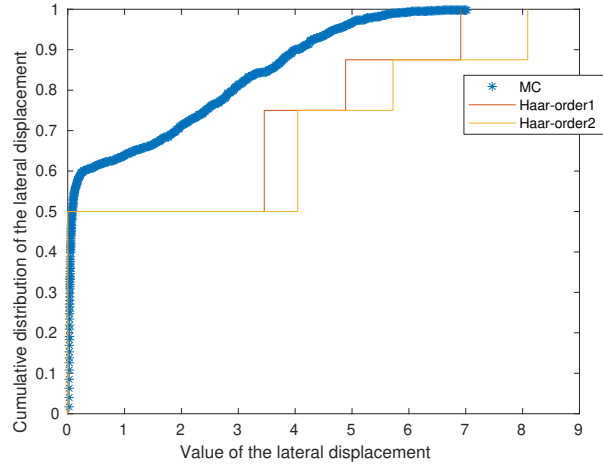
(b) Comparison of the CDF of the tip displacement using PCE and MC.

Figure 4.3: Performance of the PCE in capturing discontinuous behaviour.

Figure 4.4a shows that Haar expansions are able to capture accurately the transition between the plateau and the smooth part of the tip displacement distribution. This is expected as Haar expansions are intrinsically discontinuous. However, the convergence of these expansions is slow, see Figure 4.4b, and would require too much computational time as increasing the order by one increases the number of degree of freedom by two.



(a) Comparison of the distribution of the tip displacement using Haar expansion and MC.



(b) Comparison of the CDF of the tip displacement using Haar expansion and MC.

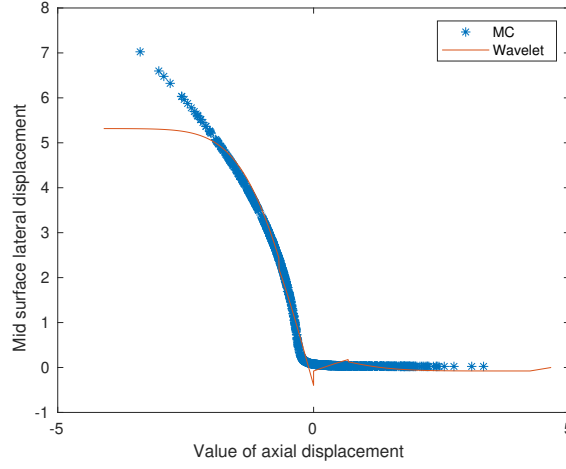
Figure 4.4: Performance of the Haar polynomials in capturing discontinuous behaviour.

Finally, the expansion mixing smooth and discontinuous expansions provides the most accurate results with minimal numbers of degree of freedoms, and with a simulation time an order of magnitude faster compared to the MC approach.

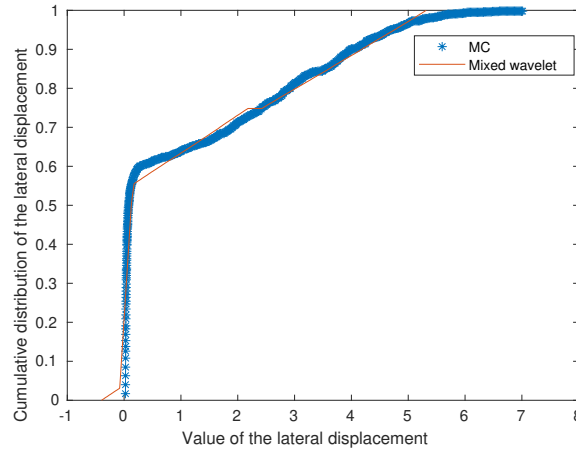
We here choose the values $n = R = 1$ in Equation (3.73). As shown in Figure 4.5a, both the smooth regions and the plateau of the distribution are captured with precision. It can be noted that the extreme negative part of the curve is not properly captured, in line with the fact that this region belongs to the tail of the Gaussian distribution: 96 % of the Gaussian distribution lies in the range $[-2, 2]$. As confirmed in Figure 4.5b showing that the discrepancy in the left tail is negligible as the CDF of both GSFEM and MC are close when the CDF approaches unity. Overall, the information contained in approximately $\sim 1,000$ MC simulations can be obtained with only one simulation at the cost of 8 times more degrees of freedoms. Negative values are predicted with the mixed Wavelet method. This can hamper the efficiency of this method as non-physical values can thus be computed. The only way to alleviate this issue is to either increase the order of the polynomial expansion (the term R in Equation (3.73)) or the number of discontinuities (the term n in Equation (3.73)). Increasing the order of the expansion results in a more accurate solution, at the cost of increased the computational time.

4.1.2 Multi-directional stochastic buckling using APFEM

Mechanical structures with high slenderness ratio can suddenly collapse under compressive loading. This phenomenon (known as buckling) often needs to be modelled accurately to evaluate precisely the reliability of a structural component. While all critical buckling loads and theoretical buckling modes can often be predicted by analytical theories [152], experimental instability often starts with a single local buckle [153]. In this section, we focus on the stochastic buckling problem of a slender beam. In Ref. [154], imperfections are introduced by a small deterministic lateral displacement, slightly distorting the beam to ensure buckling mode in one direction. A stochastic axial displacement is then applied spanning both compression and tension, demonstrating that the sharp variation of the lateral tip displacement with respect to axial displacement (increasing suddenly in compression due to buckling and remaining null in tension) is efficiently captured with the GSFEM [154].



(a) Comparison of the distribution of the tip displacement using mixed Wavelet expansion and MC.



(b) Comparison of the CDF of the tip displacement using mixed Wavelet expansion and MC.

Figure 4.5: Performance of the mixed Wavelet expansion in capturing discontinuous behaviour.

Here, we revisit this problem with APFEM by simultaneously considering a range of lateral displacement (both positive and negative) in the x -direction at the extremity of the beam (see Figure 4.6a) along with an additional range of displacement (both positive and negative) in the z -direction at the same extremity (see Figure 4.6b), while clamping the other extremity. The latter replaces the negligible deterministic displacement of the previous problem. The lateral loading is first solved for, followed by the axial loading during which the lateral displacement constraints are released and measured. Note that both resolutions are done statically,

meaning that the aim of the first loading is to introduce a bias for the second loading (similarly to the earlier deterministic displacement). The mechanical behaviour of the beam is modelled with a Saint Venant-Kirchhoff model. Three regimes are expected. When the axial displacement is tensile: no tip-displacement; when the axial displacement is compressive enough, beam buckling either in the $+x$ or $-x$ -direction depending on the introduced lateral displacement in the first load.

The aim of this study is to demonstrate that the APFEM can provide an accurate surrogate of the lateral displacement of the midpoint—a non- C^1 quantity of interest—with respect to a range of boundary conditions. To do so, we use the mixed Wavelet interpolants, following Section 3.1.7.3 with $n = R = 1$, thus leading to a dimension of the stochastic space of 36. The FE discretisation and the geometry are detailed in Table 4.2. The baseline comparison results are done by running 2,500 MC simulations with deterministic displacement inputs spanning the same ranges as the APFEM.

Table 4.2: Geometrical features, FE discretisation, boundary conditions and material parameters of the simulated beam buckling.

Parameters	Value
Geometrical features	length = 25 m, width = depth = 1 m
Number of nodes	1,336
Type of elements	quadratic tetrahedron
Number of elements	703
Range of lateral displacement	-0.1 m to 0.1 m
Range of axial displacement	-0.2 m to 0.2 m
Young’s modulus and Poisson’s ratio	1×10^7 Pa, 0.4

The APFEM results and MC simulations are shown in Figure 4.7. This example displays the capability of our method to capture pitchfork bifurcations in parametric studies. The mixed Wavelet interpolants capture with excellent accuracy the bifurcation point occurring near the transition between tensile and compressive displacement and the jump in tip displacement on both sides of the singularity. The fidelity of our surrogate could be further enhanced by adding more terms to the expansion, i.e, increasing the value of n and N in Equation (3.73), though at a

trade-off with computational time. Overall, the results show a very good ability for APFEM to capture singular problems by making use of PCE to mixed Wavelet interpolants. Note that the results shown here were done with 36 times more degrees of freedom (for the first order interpolants as $n = N = 1$) than a deterministic simulation. While this number might seem large (with important implications on computing memory required by the solver), it also needs to be compared to the potentially large number of MC simulations one might require to capture the full spectrum of variation. Overall, APFEM is capable to capture complex bifurcation problems such as the ones pertaining to material failure (e.g., buckling, fracture).

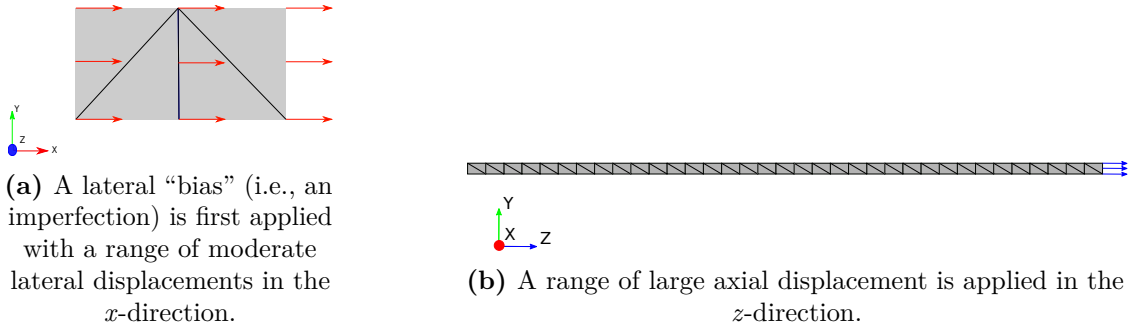


Figure 4.6: Multi-directionally loaded beam problem.

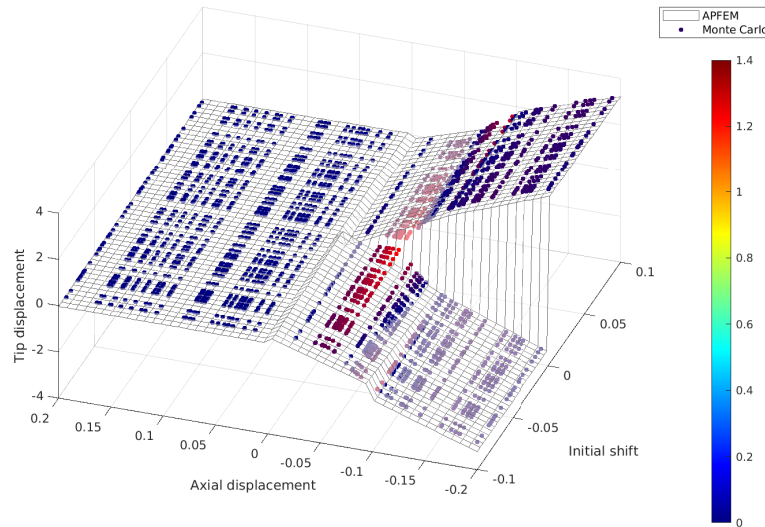


Figure 4.7: Comparison of tip displacement values between MC and APFEM using mixed Wavelet interpolants; the colour legend corresponds to the absolute error between APFEM and baseline MC simulations.

4.1.3 Stochastic buckling: geometrical uncertainties

Taking into account that buckling often occurs because of geometrical imperfections, we use the method detailed in Section 3.3 to introduce geometrical deviation in a perfectly straight beam. Here, we used a two-step process to study the buckling behaviour of a beam. In the first step, we map a perfectly straight beam to beams with geometrical defects within a certain range, see Figure 4.8a. The angle ω is a random variable ranging between 45° and 135° . In the second step, we apply a mechanical loading to the resulting beam with stochastic shape. The beam is clamped on its left side and submitted to a deterministic compressive displacement, see Figure 4.8b.

The first step is done by using the same constitutive model as the second step, essentially corresponding to a remeshing exercise by minimising the Neo-Hookean energy after a stochastic change of w . Appendix C demonstrates how the choice of constitutive model in this first step does not influence the second step.

Here, the imposed displacement in the mechanical loading is deterministic. The mechanical behaviour of the beam is modelled with a Neo-Hookean model. Both steps of the framework are solved statically. Two regimes are expected; for $\omega \leq 90^\circ$, the beam will buckle in the $-y$ -direction, for $\omega \geq 90^\circ$, the beam will buckle in the $+y$ -direction.

The aim of the study is twofold. First, we aim to show the successful incorporation of geometrical perturbation on the APFEM. Second, we want to report that introducing geometrical defects in a realistic fashion is a promising strategy for buckling studies. To do so, we use mixed Wavelet interpolants, with $n = R = 1$, thus leading to a dimension of the stochastic space of 8. The FE discretisation and the geometry are detailed in Table 4.3. The baseline comparison results are done by running 11 MC simulations with deterministic geometrical configuration spanning the same ranges as the APFEM.

The APFEM results and MC simulations are shown in Figure 4.9. This example illustrates the capability of our method to capture pitchfork bifurcations arising from geometric imperfections. The mixed Wavelet interpolants capture with good

accuracy the bifurcation point occurring at the angle $\omega = 90^\circ$, where no buckling occurs. As expected, the PCE fails to capture this jump between upward and downward buckling. However, there is only a small mismatch between the MC results and the mixed Wavelet response surface arising from the first step remeshing leading to meshed slightly different from the ones done by direct deterministic mesh when using MC.

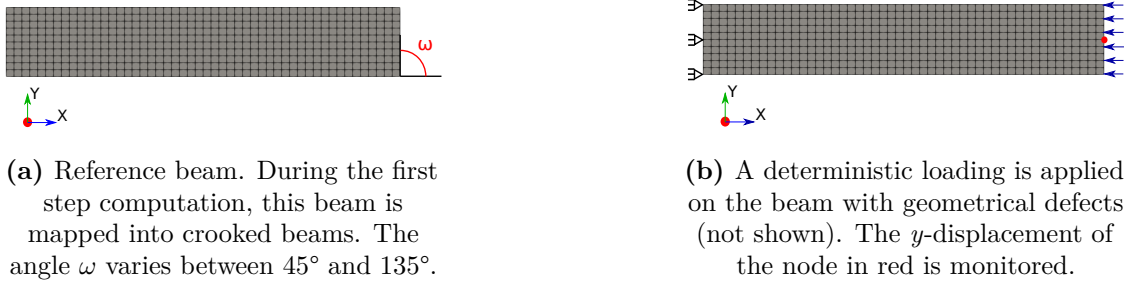


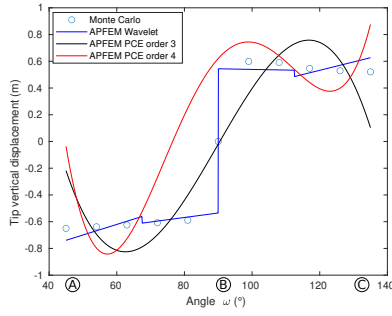
Figure 4.8: Loaded beam with geometrical uncertainties.

Table 4.3: Geometrical features, FE discretisation, boundary conditions and material parameters of the simulated beam buckling.

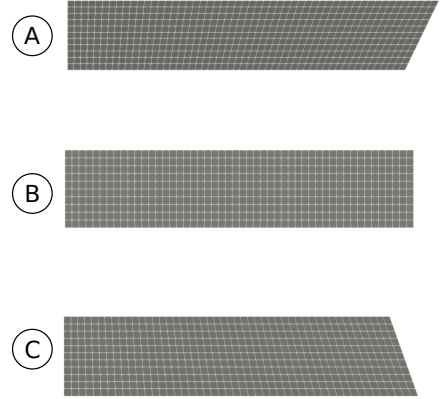
Parameters	Value
Geometrical features	length = 5 m, height = 1 m
Number of nodes	561
Type of elements	linear squares
Number of elements	500
Range of ω angle	45° to 135°
Axial displacement	-0.2 m
Young's modulus and Poisson's ratio	1×10^6 Pa, 0.3

4.2 APFEM for parameter space exploration and optimisation

Here, the APFEM potential for contemporary for engineering optimisation is highlighted with two examples. First, the mechanical response of a metamaterial actuator to a parametric input is studied. Second, the growing behaviour of a 3D beam, a highly non-linear and discontinuous problem is solved.



(a) Comparison of vertical tip displacement using mixed Wavelet, PCE with MC. The geometries *A*, *B* and *C* corresponds respectively to angles $\omega = 45^\circ, 90^\circ, 135^\circ$.



(b) Geometrical configuration *A*, *B* and *C*.

Figure 4.9: Tip displacement results for different geometric configurations.

4.2.1 Estimation of a metamaterial's behaviour

Metamaterials are a new class of materials showing superior performances—or at least “non-mainstream” properties—compared to traditional materials [155]. In particular, they have been the focus of an increased interest in the solid mechanics community due to their potential tunable high stiffness and strength-to-weight ratio [156]. These excellent properties arise from their designed geometry, consisting in units arranged in periodic patterns. Their manufacturing has become possible on an industrial scale thanks to the development of AM. Metamaterials have been extensively studied in virtually all fields of engineering applications [157, 158]. Here, we build on the work of Bonfanti *et al.* [159] to highlight the potential for APFEM to provide optimisation support for this class of metamaterials. In this work, a geometric optimisation of a lattice structure was proposed by making use of a machine learning layer framework. The target goal of the optimisation was the efficiency of the structure, defined as the ratio of the output displacement of a region of the structure to the input displacement of another region, see Figure 4.10. This efficiency varies nonlinearly with respect to the input displacement. Instead of obtaining the output-input displacement curve by running repeated deterministic simulations with different values of input values, we apply here the APFEM for a given range of displacement, ranging from 0 to -10 (approximately 30% strain), see

red arrow in Figure 4.10. The metamaterial is modelled by a Saint Venant-Kirchhoff model with deterministic Young’s modulus and Poisson’s ratio. We expect the problem to be smooth enough for a PCE of order 3 to give accurate results. The parameters of the APFEM static plane stress simulation are given in Table 4.4.

Table 4.4: FE discretisation, boundary conditions and material parameters of the simulated metamaterial.

Parameters	Value
Number of nodes	8,805
Type of elements	linear triangle
Number of elements	14,688
Range of displacement	0 to 10
Young’s modulus and Poisson’s ratio	1×10^7 Pa, 0.3

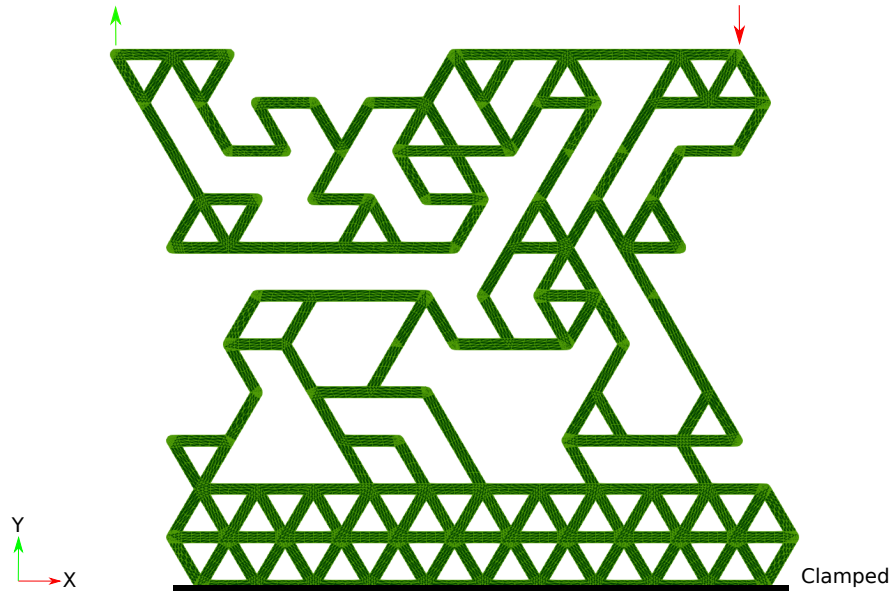


Figure 4.10: Geometry of the metamaterial, taken from Ref. [159]. The bottom of the structure is clamped while a vertical displacement (red arrow) is imposed and a vertical output displacement (green arrow) is measured.

Baseline results are gathered using a single deterministic static FE analysis with 10 time steps over which the input displacement of -10 is reached (i.e., by increment of -1). The simulation being static—as opposed to dynamic—the output at step n corresponds to a loading of $-n$. The distribution of the output displacement

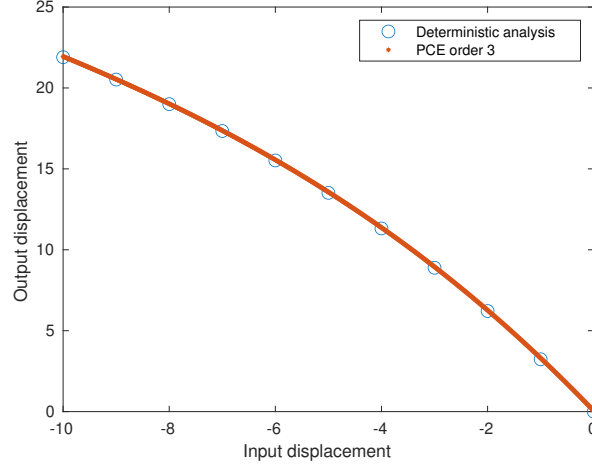


Figure 4.11: Output displacement distribution using APFEM and deterministic analysis.

is shown in Figure 4.11 for both the baseline result (11 points) and the APFEM (continuous function of the displacement). For the latter, the displacements were calculated by extracting from the stochastic nodal unknowns solved for (i.e., the $\mathbf{u}^{a\epsilon}$) the ones for the node of interest and reconstructing the function of the input parameter θ (here ramping from 0 to -10) through Equation (3.1).

As expected, the output displacement is a nonlinear function of the input displacement, increasing with the absolute value of the input displacement. The APFEM continuous output matches perfectly the control points provided by the deterministic analysis. Remarkably, though no other information than the bounds of the input displacement are provided to the APFEM simulation, the framework is able to capture accurately all the intermediary loading conditions, i.e., the entire parameter space is explored with only one simulation.

4.2.2 Optimisation problem of a growing rod

Here, we revisit an optimisation problem performed by Peña *et al.* [8]. A 3D rod is described with a Neo-Hookean constitutive model coupled to a growth model detailed in Chapter 3. In this formulation, $\zeta^g = G_c t$, where G_c is the growth factor and t is the time. The rod is clamped at its base and pulled with a constant velocity for 1s. If the rod is pulled too fast, the pulled area will decrease. Conversely, if the rod is

pulled too slowly, the pulled area will increase. Consequently, there should be an optimal value of G_c so that the pulled area remains the same after 1s, see Figure 4.12.

To obtain a baseline, we use the MC method by running 200 simulations with different values of G_c and gathering the change ΔA_0 . We compared this framework with the APFEM, where only one simulation is needed to obtain the distribution of ΔA_0 for a range of G_c values. The parameters of the simulations and the order of PCE expansion are detailed in Table 4.5. The results in Figure 4.13 show a good agreement between MC and APFEM. The APFEM predicts the optimum value of G_c with almost perfect accuracy ($<0.05\%$ difference with MC). Note that APFEM shows a slight deviation with MC when $G_c > 0.5s^{-1}$.

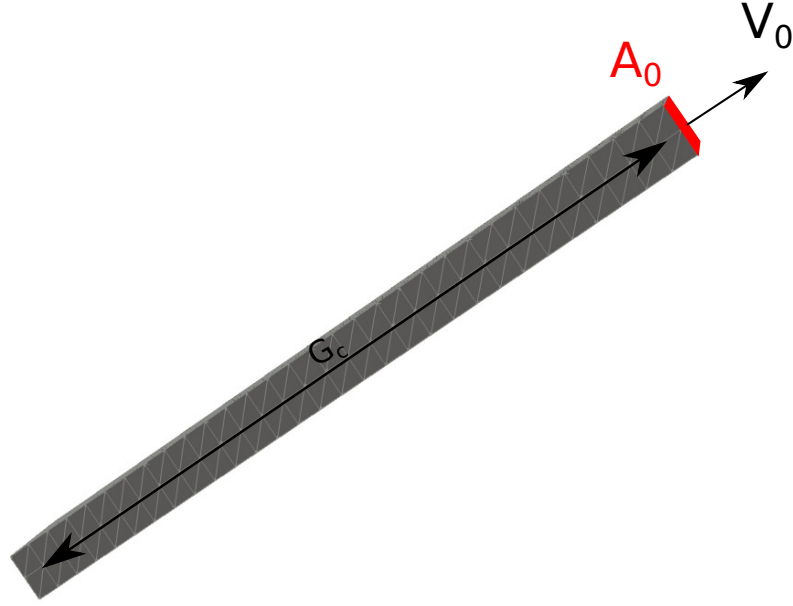


Figure 4.12: Clamped rod submitted to a pull at constant velocity V_0 . The aim of the problem is to find the value of G_c such that A_0 remains the same after 1s.

4.3 APFEM for inverse problems

In this section, we demonstrate how APFEM is particularly suitable for inverse problems such as inferences. We focus particularly on the identification of constitutive properties of mechanical components from the knowledge of a set

Table 4.5: FE discretisation, boundary conditions and material parameters of the simulated growing rod.

Parameters	Value
Number of nodes	612
Type of elements	linear tetrahedron
Number of elements	2,324
Range of G_c	1 to 2 s^{-1}
Geometrical features	length = 600 m, height = 80 m, width = 40 m
PCE order	2
Young's modulus and Poisson's ratio	1.58×10^9 Pa, 0.3
Time step	$3.93 \cdot 10^{-5}$ s

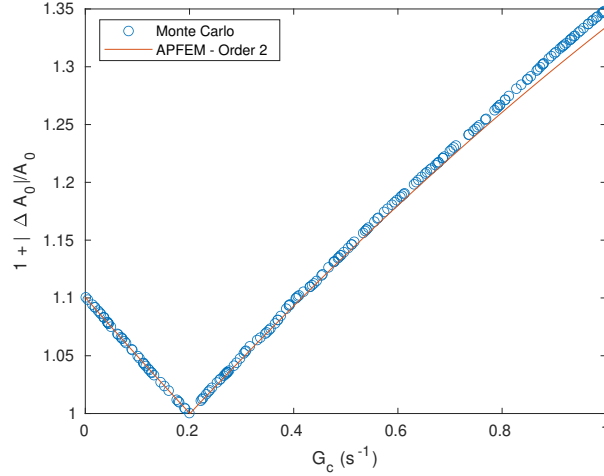


Figure 4.13: Comparison of $1 + \frac{|\Delta A_0|}{A_0}$ with MC and APFEM.

of measurements (e.g., experimental). We first apply APFEM to contact mechanics for the determination of a friction coefficient in the Cattaneo-Mindlin problem, and then infer the stiffness of brain cancer from midline shift measurements arising during cardiac cycle tissue deformation.

4.3.1 Contact mechanics: the Cattaneo-Mindlin problem

Virtually all engineering structures with moving parts do involve contacts. These contacts can result in nucleation of cracks and eventually failure. The problem, in addition to being complex from a theoretical standpoint, is also constrained

in its experimental monitoring, relying on external observations when potential issues arise within the (inaccessible) contact area. We propose here to use BI in conjunction with APFEM to approach this challenge.

4.3.2 Theoretical framework

In most FE frameworks, solving contact mechanics problems requires the discretisation of one or all bodies in contact and the computation of the distance between the nodes or the element faces of the surfaces in contact. Coupling these algorithms with APFEM is outside the scope of our study. Instead, we simulate contact between a spherical object and a plane by making use of the analytical approaches developed by Cattaneo and Mindlin [160, 161] for partial slip Hertzian contact, see Figure 4.14a. This approach has been used for fretting analysis in roller bearings [162] in turbines but also in biomechanics for prosthetic hip bearings [163]. Cattaneo and Mindlin independently derived the distribution of normal and tangential loading distributions when a sphere is pressed into a half space. In the case where the total normal and tangential forces applied in the half space are P and Q , respectively, their spatial distribution p and q can be written as:

$$p(r) = p_0 \sqrt{1 - \frac{r^2}{a^2}} \text{ if } 0 \leq r \leq a, \quad (4.1)$$

$$q(r) = \begin{cases} \mu p_0 \left(\sqrt{1 - \frac{r^2}{a^2}} - \frac{c}{a} \sqrt{1 - \frac{r^2}{c^2}} \right) & \text{if } 0 \leq r \leq c \\ \mu p(r) & \text{if } c \leq r \leq a, \end{cases} \quad (4.2)$$

where a is the radius of contact, c the length of the stick zone, μ the friction coefficient, r the radial coordinate of the material point and p_0 a normalised pressure at the centre of the contact surface ($r = 0$), see Figure 4.14a. The stick zone radius c depends nonlinearly on the friction coefficient and the external forces:

$$c = a \left(1 - \frac{Q}{\mu P} \right)^{\frac{1}{3}}. \quad (4.3)$$

Here, our aim is to evaluate the value of the unknown friction coefficient through the sole observation of the contact's outer boundary. In the APFEM framework,

the friction coefficient is taken to be an unknown parameter. Because Equation (4.3) is a power function of μ , the evaluation of the stick zone size's distribution is not straightforward. One can however do so by solving a differential equation through a method proposed in Ref. [134]; see Appendix B for more details on its use for Equation (4.3). In our approach, the uncertainty of the contact is modelled by an uncertainty on the Neumann boundary conditions. Indeed, while the normal pressure p is applied deterministically, it is not the case for the tangential pressure as its treatment differs whether the material point at a radius r is inside the stick zone or in the slip zone, see Equation (4.3). Similarly, a direct evaluation of the term $\sqrt{1 - \frac{r^2}{c^2}}$ is also impractical as the content of the square root can have non-zero probability of being negative, and the condition $c \leq r$ is not uniquely defined as r is a deterministic quantity while c is a probability distribution. Here, we approximate the inequality of Equation (4.2) as follows:

$$q(r) = \begin{cases} \mu p_0 \left(\sqrt{1 - \frac{r^2}{a^2}} - \frac{c}{a} \sqrt{1 - \frac{r^2}{c^2}} \right) & \text{if } 0 \leq r \leq c_{inf} \\ \mu p_0 \left(\sqrt{1 - \frac{r^2}{a^2}} - \frac{c}{a} \tilde{f}\left(\frac{r}{c}\right) \right) & \text{if } c_{inf} \leq r \leq c_{sup} \\ \mu p(r) & \text{if } c_{sup} \leq r \leq a, \end{cases} \quad (4.4)$$

where c_{inf} and c_{sup} are respectively the inferior and superior bounds of c . The second term of the first line of the equation is calculated making use of Appendix B. In the second line, however, the square root is replaced by the function $\tilde{f}(x) = -52 + 162.6x - 114.93x^2 - 92.1x^3 + 141.47x^4 - 44.96x^5$, which is a polynomial approximation of $\sqrt{1 - x^2}$ in $[0.763, 1.31]$, corresponding to $[\frac{c_{inf}}{c_{sup}}, \frac{c_{sup}}{c_{inf}}]$ with the values used in this example. This change in Equation (4.2) is required as the probability of $1 - \frac{r^2}{c^2}$ of being negative is non-zero when $r \in [c_{inf}, c_{sup}]$. While this is in fact not strictly an issue when using the algorithm in Appendix B to compute square root of stochastic quantities, it introduces errors that can be avoided by use of the proposed polynomial approximation along with the usual stochastic operations for polynomials. We emphasise that Equation (4.4) introduces irreversible modifications on Equation (4.2). Hence, the MC solution cannot be recovered, even with high order PCE, as the problem solved in the deterministic and stochastic framework

are not completely equivalent, similarly to what Rosic *et al.* noted when extending intrusive stochastic methods to plasticity [26].

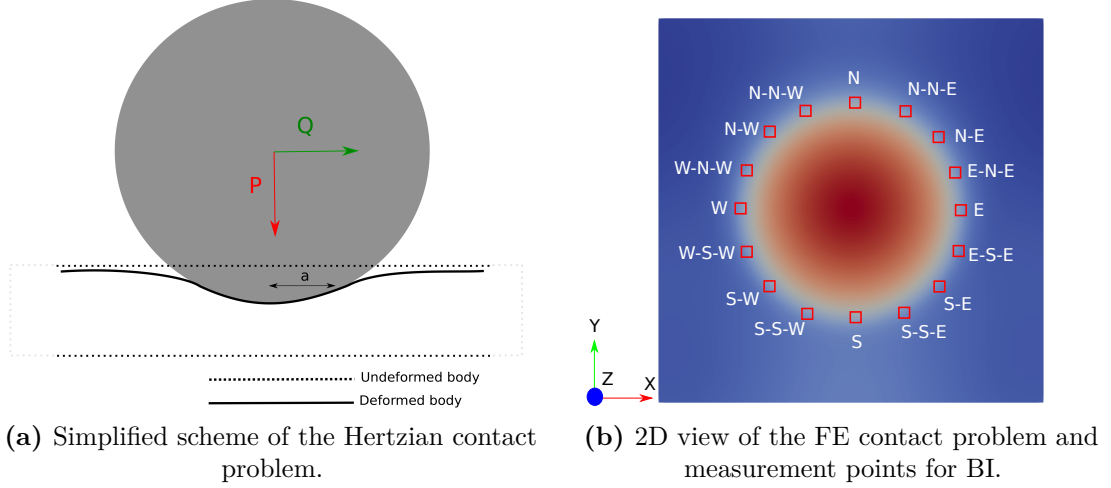


Figure 4.14: Cattaneo-Mindlin problem.

4.3.3 Results

Here, the contact problem is idealised by pressing normally a spherical object into a hyperrectangle, and dragging it over its surface. By only modelling the half-plane where the contact is taken into account through boundary conditions, we aim to determine the friction coefficient using measurements of the x -displacement of material points located at the edge of the contact surface, see Figure 4.14b. The material behaviour of the half-plane is modelled by a Saint Venant-Kirchhoff constitutive model. The geometrical features, FE discretisation and constitutive model material parameters are given in Table 4.6. Finally, we assume that the prior distribution of the friction coefficient is a uniform distribution between 0.3 and 0.4.

We use *in silico* data to simulate an external set of measurements (e.g., of experimental nature). This is done by performing a deterministic simulation with a friction coefficient equal to 0.35, gathering the x -displacements of the cardinal points (see Figure 4.14b), and artificially “polluting” these measurements (as could be expected from experimental measurements) with a Gaussian noise centered in 0 with a standard deviation of $5 \cdot 10^{-5}$ to generate the vector of measurements \mathbf{y} , see Equation (3.79). Taking the prior distribution of friction coefficient to be uniform

between 0.3 and 0.4, the likelihood of Equation (3.80) can then be computed, eventually leading to the posterior distribution of the friction coefficient through Equation (3.78) using APFEM with order 4 PCE.

Figure 4.15 shows the comparison between the true value of the friction coefficient and the posterior distribution after BI with various levels of measurement knowledge defined by a) two measurement points (W and E), b) four measurement points (W, N, E and S), c) eight measurement points (W, N-W, N, N-E, E, S-E, S, S-W) and d) sixteen measurements (W, W-N-W, N-W, N-N-W, N, N-N-E, N-E, E-N-E, E, E-S-E, S-E, S-S-E, S, S-S-W, S-W, W-S-W). As expected, the greater the number of measurements, the narrower the posterior distribution is. However, the maximum value of the posterior distribution is converging towards approximately 0.355, i.e., an absolute error $e = 0.005$ with respect to the original deterministic model defined with $\mu = 0.35$ (a 1.4% relative error). Again, this discrepancy was expected, as Equation (4.2) had to be approximated for our stochastic framework to be leveraged. While this theoretical approximation hampers the accuracy of our framework for complex relationships between parameters and boundary conditions, the predicted distribution of the friction coefficient remains remarkably close to the original values with a relatively low number of measurements: four measurements of the outer boundary of the contact area are enough to estimate the friction coefficient within $\sim 2\%$ of error.

Table 4.6: Geometrical features, FE discretisation, boundary conditions and material parameters of the contact simulation.

Parameters	Value
Geometrical features	Length = width = 10 m, depth = 2 m
Number of nodes	59,049
Type of elements	quadratic tetrahedron
Number of elements	52,000
Total normal force P	8×10^5 N
Total friction force Q	2×10^5 N
Young's modulus and Poisson's ratio	1×10^6 Pa, 0.3

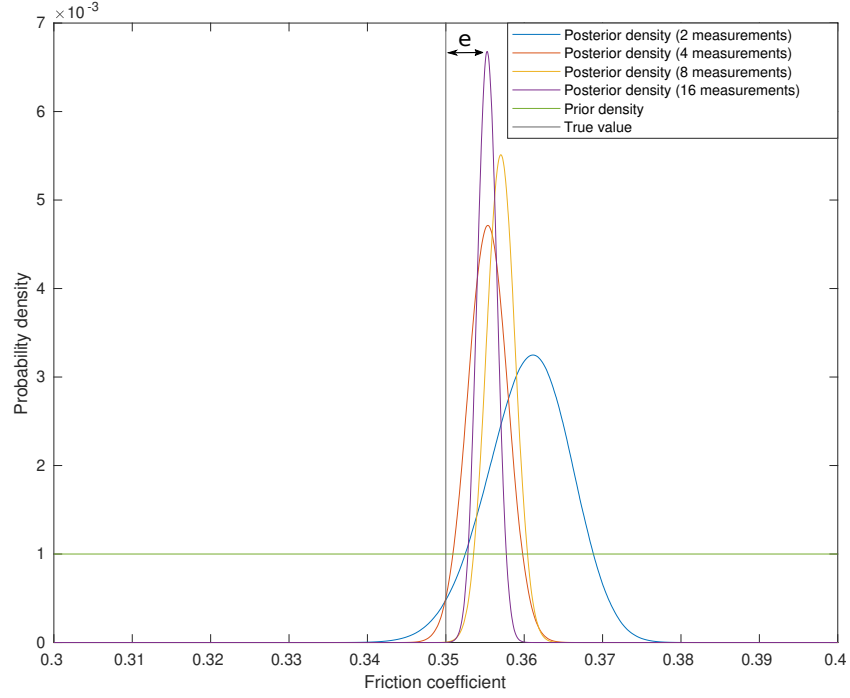


Figure 4.15: Prior and posterior distributions of the friction coefficient.

4.3.4 Brain mechanics: a large scale problem

This section illustrates the flexibility of the BI-APFEM framework for large scale simulations (>1 million degrees of freedom) with an application involving brain mechanics modelling.

Clinicians have traditionally been using the measurement of midline shift (MLS)—the topological line separating left and right hemispheres, readily observable through common imaging techniques—as an indicator of structural movement and tool for surgical decision-making, in particular in the context of stroke. Here, we borrow the simulation framework of Ref. [164] to infer from MLS measurements the stiffness of a brain tumour creating an asymmetrical brain deformation during a pressure rise in the arteries. In this work, a FE human head was created using MRI and magnetic resonance angiography, see Ref. [164] for more details. The model includes vasculature, brain organs and skulls. We use a Saint Venant-Kirchoff model to simulate the mechanical behaviour of the brain components as a first approximation.

The parameters of the constitutive model are detailed in Table 4.7 while the details of the FE discretisation are given in Table 4.8. Here, we arbitrarily assume that a tumour in the temporo-parietal region of the left hemisphere has an increased stiffness, and that an arbitrary increase of blood pressure of 100 Pa, a fraction of the physiological blood pressure, (applied on the inside of the vasculature) coupled to the presence of this mass leads to a small MLS, see Figure 4.16. Note that, while theoretically possible, the clinical relevance of this hypothetical method is by no means demonstrated here; it is merely used here as an illustrative example of BI-APFEM in large scale problems.

Similarly to the contact mechanics problem, we use an *in silico* experiment to generate “experimental” measurement data of the MLS by: i) gathering MLS-values through a deterministic simulation with a arbitrary tumour’s Young’s modulus of 13021 Pa, see Figures 4.16a and 4.16c; and ii) “polluting” these values with a Gaussian noise of null mean value and standard deviation of $4 \cdot 10^{-10}$, supposed to be independent for each measurement. Making use of BI-APFEM with second order PCE with a Young’s modulus ranging from 12.37 kPa to 13.67 kPa, the measurements allow the computation of the likelihood of the Young’s modulus of the tumour, see Equation (3.80), and eventually its posterior distribution. As shown on Figure 4.17, the posterior distribution converges to the true value with a good accuracy from five experimental MLS measurements onwards.

Table 4.7: Material parameters of the brain.

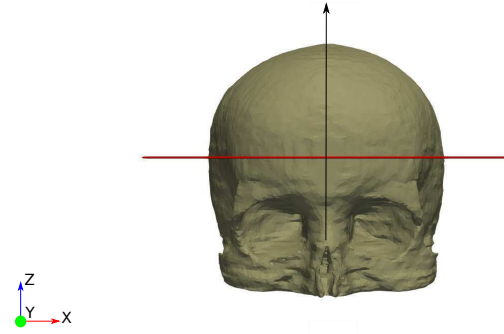
Brain components	Young’s modulus	Poisson’s ratio
White matter/Brainstem	1.302×10^4 Pa	0.45
Grey matter/Cerebellum	2.958×10^3 Pa	0.45
Falx	3.15×10^7 Pa	0.45
Ventricle/CSF	2.90×10^2 Pa	0.45
Edema	To be determined	0.45

Table 4.8: FE discretisation parameters of the brain mechanics simulation.

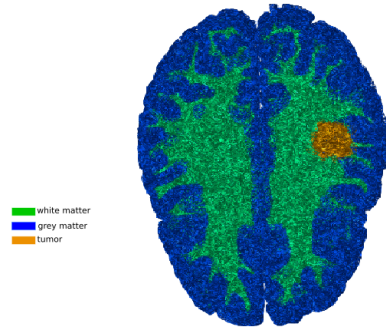
Parameters	Value
Number of nodes	344,872
Type of elements	linear tetrahedron
Number of elements	1,952,523
Pressure	100 Pa

4.4 Dissemination

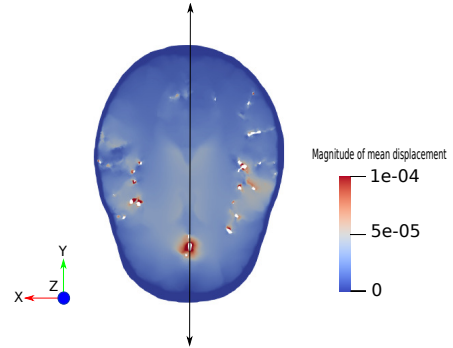
The results presented in this chapter were published in Computational Methods in Applied Mechanical Engineering as manuscripts titled “A modular nonlinear stochastic finite element formulation for uncertainty estimation”, DOI:10.1016/j.cma.2022.115044 and “The a posteriori finite element method (APFEM), a framework for efficient parametric study and Bayesian inferences”, In Press. The extension to topological uncertainties has also been submitted.



(a) 3D Head model. In red, the plane where the MLS values are acquired.



(b) Horizontal meshed section of the brain showing tumour in the temporo-parietal region of the left hemisphere.



(c) Horizontal section for one deterministic simulation. The black line indicates the midline. The displacement field is provided as an illustration for the case of an edema's Young's modulus of 1.97×10^6 Pa.

Figure 4.16: 3D head model and section used for gathering of MLS data.

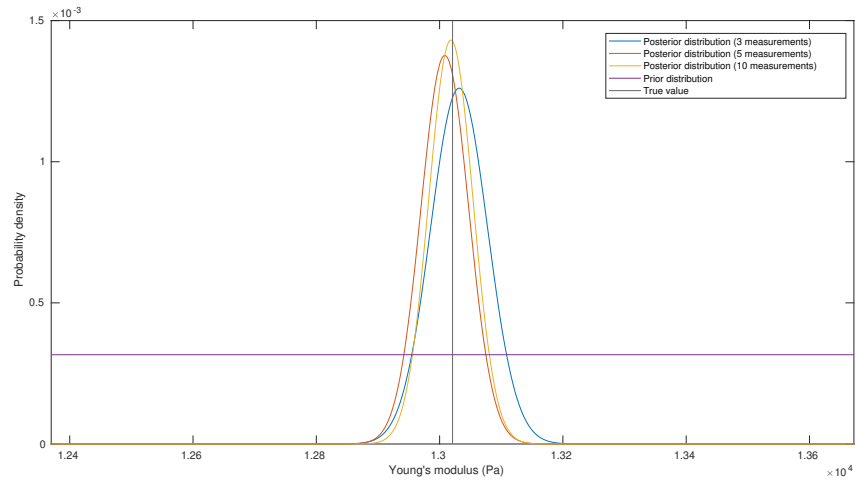


Figure 4.17: Prior and posterior distributions of the edema's Young's modulus.

Chapter 5

Conclusions, limitations and future directions

5.1 Summary and achievements

Uncertainties are ubiquitous in virtually all engineering applications. They include variability in the material properties and topology randomness, and can lead to unpredictable mechanical responses, eventually leading to failure. Due to the difficulty to do so, their precise quantification tends to be avoided by engineers, relying instead on highly conservative approaches for safe design. After categorising uncertainties, Chapter 1 identified the current methodologies aimed at propagating them. Intrusive methods-requiring a formulation of the governing equations-have been traditionally ignored in favour of simpler but more expensive stochastic frameworks requiring multiple deterministic simulations. This thesis aims to address this by providing a new framework, GSFEM, implemented in a modular manner and extended to a vast range of nonlinear applications in the solid mechanics field.

The mathematical formulations of GSFEM for finite deformation, its extension to APFEM and Bayesian inferences are defined in Chapter 3. The numerical validation of these formulations is demonstrated in Chapter 4 where the surface response of a bifurcation problem was studied using GSFEM with discontinuous expansion. The APFEM was tested and shown to be an efficient tool for parameter space

exploration and fast Bayesian inferences. In particular, the proposed methodology was used to characterise the stochastic efficiency of a metamaterial and the inference of the friction coefficient in the case of a Hertzian contact with partial slip. Finally, the extension of APFEM to geometric uncertainties was employed to describe the stress concentration in a 2D plate. In all these numerical examples, the prospects of the proposed framework was demonstrated for design purposes.

The first and main contribution of this thesis was the versatile and modular framework proposed to implement the intrusive FE method in any existing code. This method relies on the development of a stochastic algebra. This algebra can be used as an external library to compute the random internal and external forces and tangent modulus. While the traditional FE operators had to be modified in order to process the input file so that the type of uncertainties, their amplitude and the choice of expansion could be extracted, the backbone of the FE solver was left untouched.

As the original GSFEM was shown to be unfit for the study of problems involving sharp discontinuities [24], another type of expansion, involving Wavelets [144] was introduced. Excellent agreement with MC method was observed to capture the bifurcation of a tip displacement when studying the stochastic buckling of a beam. This method still provided excellent results when introducing another bifurcation point in the mechanical problem showing the robustness of the enhanced GSFEM.

Following the pioneering work done by Marzouk *et al.* [25], we restricted the GSFEM to uniform continuous distributions. This allows an even weight of the metamodel error on the whole parameter space. The resulting method, termed here APFEM, allows for efficient exploration of the parameter space with only a single simulation. As a direct corollary, the APFEM was proposed as an alternative to mainstream methods [147, 148] for parameter identification. The BI-APFEM showed excellent results when inferring the Young’s modulus of a brain tumor for potential surgical planning. While promising, APFEM showed some inaccuracies when extended to contact mechanics. As the problem introduced comparisons of distances, the mathematical formulation had to be slightly adapted, introducing

unrecoverable deviations from the baseline solution acquired using MC. Despite this limitation, the results showed satisfying accuracy.

Finally, the formulation of APFEM was adjusted to simulate the effect of geometric uncertainties. Using a two-step scheme, the kinematic transformation mapping a deterministic configuration to a random intermediate topological configuration is obtained. Then, assuming this configuration stress-free, the mechanical problem can be solved. This method integrates material parameters' deviation from their nominal values and topological uncertainties altogether. However, the analytical expression of the topology shape alteration is needed. Finally, this expression is projected in the PCE space.

While key milestones have been reached to extend the GSFEM for realistic industrial applications including large-scale problems (>1 Million DoFs), bifurcation problems and uncertain topology, among others, some development both from the mathematical and implementation perspective are still required to unlock the full potential of the GSFEM.

5.2 Limitations

In the following, the limitations of the thesis are presented. First, the restrictions of the current GSFEM/APFEM are listed. Second, suggestions to overcome these shortcomings, as well as future directions, are proposed.

Although our proposed framework shows prospects for efficient uncertainty quantification, it has several limitations. While this list is non-exhaustive, we enumerate the main identified key shortcomings of the presented work:

- Some material parameters exhibit variation across the physical space. Consequently, their random counterpart requires the introduction of random fields. While the mathematical formulation shown in Chapter 3 can be readily adjusted to integrate random fields with spatial correlation, the current implementation can only take random variables as input parameters.
- Similarly to the regression and quadrature-based non-intrusive frameworks presented in Chapter 2, the GSFEM is affected by the curse of dimension. Indeed, the number of terms in the PCE increases as a power law with respect to the number of random inputs.
- While the GSFEM has been extended to a wide range of constitutive models, some further developments are required to broaden the scope of GSFEM. Indeed, enhanced realistic modelling of structural components involving sophisticated features, such as impact or fracture mechanics, remains challenging at best. Indeed, during contact between structural components, evaluation of distances between surfaces has to be performed to ensure nonpenetration. The nonpenetration condition generally requires a comparison operation. Such operation introduces a modification, polluting the obtained results. Moreover, deterministic contact mechanics algorithms are prone to convergence instabilities.

- The stochastic algebra presented in this thesis, allows for complex nonlinear operations, such as square root or exponential. However, this algebra is incomplete and requires additional development. Indeed, at the moment, it is impossible to perform PCE projection of operations such as cosine or sine, who could be useful for various domains ranging from vibration analysis to ultrasound neuromodulation.

5.3 Future directions

The introduction of random fields to the work could be included seamlessly in the mathematical formulation detailed in Chapter 3, by using the K-L theorem [165, 166]. As of now, our in-house code does not allow for the storage or evaluation of random parameters at a given material point. Consequently, structural modification has to be provided to the current FE solver to take into account inhomogeneous parameters. Moreover, the actual framework would benefit from the implementation and resolution of the Fredholm equation.

Realistic constitutive models often require complex mathematical operations. As an example, the widely used Ogden hyperelastic model [167] involves obtaining the deformation gradient's eigenvalues. The mathematical extension of the eigenvalue concept to random tensor would greatly benefit the GSFEM as this would potentially allow for the implementation of stochastic Ogden models and perform uncertainty quantification on rubber polymers or biological tissues.

Fluid-structure interactions (FSI) are now increasingly used in solid mechanics but also in biological applications. Drug delivery strategies or stunts design require FSI simulations to ensure optimal performance and mechanical integrity. Our in-house software already allows for deterministic FSI using an external fluid solver. Assuming irrotational flow, the Navier-Stokes equation reduces to the linear Euler equations. Using an intrusive framework on these equations would result in uncoupled deterministic systems. Consequently, without any additional coding effort required in the fluid solver, stochastic FSI for non-viscous fluid could potentially be performed making use of the CFD solver for solving the deterministic systems.

Finally, it is possible to reduce the power increase of terms in the PCE by using a hyperbolic set of indices in Equations (3.66) and (3.71) following the work of Sudret *et al.* [33]. For an equivalent precision, they found that it is possible to divide the number of terms in PCE by an order of magnitude, making large-scale stochastic analyses more tractable.

Appendices

Appendix A

Operations in the stochastic space

This appendix details i) the algebra used to perform operations on stochastic quantities, ii) the derivation of the tangent modulus for the stochastic Saint Venant-Kirchhoff model, iii) the closed form of the PCE with Gaussian distributed uncertainties.

A.1 Stochastic algebra

While this distinction was not made in the manuscript for readability, here, the stochastic variables are defined with the $\hat{\cdot}$ symbol, while their deterministic counterparts are not.

A.1.1 Linear combination of real numbers and stochastic variable

Let us consider a stochastic variable \hat{A} with coordinates $[a_0, \dots, a_\zeta]$ in the stochastic space $\mathbf{H} = [\Psi_0, \dots, \Psi_\zeta]$, and two real numbers f and g . $\hat{B} = f\hat{A} + g$ can be expressed as follows:

$$\hat{B} = \sum_{\alpha=0}^{\zeta} f a_{\alpha} \Psi_{\alpha} + g. \quad (\text{A.1})$$

As $\Psi_0 = 1$, the coordinates of \hat{B} in the stochastic space thus are $[fa_0 + g, fa_1, \dots, fa_\zeta]$. The definition of $\hat{-}$ follows trivially. Note also that the extension of $\hat{+}$ and $\hat{-}$ to the linear combination of two stochastic variables is trivial.

A.1.2 Product of two stochastic variables

As the direct product of two stochastic variables belonging to H does not necessarily belong to the stochastic space H , we define here the stochastic product $\hat{\times}$ by projection on H . As such, for a stochastic variable \hat{A} of coordinates $[a_0, \dots, a_\zeta]$ and \hat{B} of coordinates $[b_0, \dots, b_\zeta]$, the stochastic product $\hat{D} = \hat{A} \hat{\times} \hat{B}$ with $\hat{D} = [d_1, \dots, d_\zeta]$ in H is defined by Galerkin projection of the quantity $(\sum_{\alpha=0}^{\zeta} a_\alpha \Psi_\alpha) \times (\sum_{\beta=0}^{\zeta} b_\beta \Psi_\beta)$, i.e.,

$$d_\gamma < \Psi_\gamma, \Psi_\gamma > = \sum_{\alpha=0}^{\zeta} \sum_{\beta=0}^{\zeta} a_\alpha b_\beta < \Psi_\alpha \Psi_\beta, \Psi_\gamma >, \quad \forall \gamma \in [0, \zeta]. \quad (\text{A.2})$$

Noting that $C_{\alpha\beta\gamma} = \frac{< \Psi_\alpha \Psi_\beta, \Psi_\gamma >}{< \Psi_\gamma, \Psi_\gamma >}$, Equation (A.2) becomes:

$$d_\gamma = \sum_{\alpha=0}^{\zeta} \sum_{\beta=0}^{\zeta} C_{\alpha\beta\gamma} a_\alpha b_\beta, \quad \forall \gamma \in [0, \zeta]. \quad (\text{A.3})$$

The tensor \mathbf{C} is a key element of the stochastic algebra and is unique to each interpolation basis. It only needs to be computed once.

A.1.3 Division of two stochastic variables

The division of \hat{A} by \hat{B} , noted here as $\hat{D} = \hat{A} \hat{\div} \hat{B}$, can be recast as $\hat{A} = \hat{D} \hat{\times} \hat{B}$ where the coordinates of \hat{D} in H have to be determined. This is thus equivalent to solving the linear system $\mathbf{C} \cdot \hat{D} = \hat{A}$, where the coefficient of \mathbf{C} are defined as follow:

$$\mathbf{C}_{\beta\gamma} = \sum_{\alpha=0}^{\zeta} b_\alpha C_{\alpha\beta\gamma}. \quad (\text{A.4})$$

A.1.4 Product of a stochastic variable and a stochastic tensor

Using the same approach, the coordinates $[d_0, \dots, d_\zeta]$ of the product $\hat{D} = \hat{A} \hat{\times} \hat{B}$ between a stochastic tensor \hat{A} of coordinates $[a_0, \dots, a_\zeta]$ and a stochastic scalar \hat{B} of coordinates $[b_0, \dots, b_\zeta]$ are straightforwardly defined by:

$$\mathbf{d}_\gamma = \sum_{\alpha=0}^{\zeta} C_{\alpha\beta\gamma} \mathbf{A}_\alpha b_\beta, \quad \forall \gamma \in [0, \zeta]. \quad (\text{A.5})$$

Note that this product is commutative as \mathbf{C} is symmetric on its two first indices.

A.1.5 Product of two stochastic tensors

Similarly, the coordinates $[\mathbf{d}_0, \dots, \mathbf{d}_\zeta]$ of the product $\hat{\mathbf{D}} = \hat{\mathbf{A}} \hat{\mathbf{B}}$ between two stochastic tensors $\hat{\mathbf{A}}$ and $\hat{\mathbf{B}}$ of coordinates $[\mathbf{a}_0, \dots, \mathbf{a}_\zeta]$ and $[\mathbf{b}_0, \dots, \mathbf{b}_\zeta]$ are defined by:

$$\mathbf{d}_\gamma = \sum_{\alpha=0}^{\zeta} C_{\alpha\beta\gamma} \mathbf{a}_\alpha \cdot \mathbf{b}_\beta, \quad \forall \gamma \in [1, \zeta]. \quad (\text{A.6})$$

Again, this product is commutative.

A.1.6 Trace of a stochastic tensor

The coordinates $[b_0, \dots, b_\zeta]$ of the trace $\hat{B} = \hat{tr}(\hat{\mathbf{A}})$ of a stochastic tensor $\hat{\mathbf{A}}$ of coordinates $[\mathbf{a}_0, \dots, \mathbf{a}_\zeta]$ are defined by:

$$b_\beta = \text{tr}(\mathbf{A}_\beta), \quad \forall \beta \in [0, \zeta]. \quad (\text{A.7})$$

A.1.7 Dyadic product of stochastic vectors

The coordinates $[\mathbf{d}_0, \dots, \mathbf{d}_\zeta]$ of the dyadic product $\hat{\otimes}$ of stochastic tensors $\hat{\mathbf{A}}$ and $\hat{\mathbf{B}}$ of coordinates $[\mathbf{a}_0, \dots, \mathbf{a}_\zeta]$ and $[\mathbf{b}_0, \dots, \mathbf{b}_\zeta]$ are defined by:

$$\mathbf{d}_\gamma = \sum_{\alpha=0}^{\zeta} \sum_{\beta=0}^{\zeta} C_{\alpha\beta\gamma} \mathbf{a}_\alpha \otimes \mathbf{b}_\beta, \quad \forall \gamma \in [0, \zeta]. \quad (\text{A.8})$$

A.1.8 Inversion of a stochastic tensor

The coordinates $[\mathbf{B}_0, \dots, \mathbf{B}_\zeta]$ of the inverse of a stochastic tensor $\hat{\mathbf{A}}$ of coordinates $[\mathbf{A}_0, \dots, \mathbf{A}_\zeta]$ must verify:

$$\sum_{\alpha=0}^{\zeta} \sum_{\beta=0}^{\zeta} C_{\alpha\beta\gamma} \mathbf{A}_\alpha \mathbf{B}_\beta = \mathbf{I}_\gamma, \quad \forall \gamma \in [0, \zeta], \quad (\text{A.9})$$

where $\mathbf{I}_\gamma = 0$ for $k \neq 0$ and \mathbf{I}_0 is the identity tensor. The above equation can be solved for \mathbf{B}_β to obtain the inverse of the stochastic tensor \mathbf{A} .

A.2 Expansions considering Gaussian stochastic variables

In this subsection, we detail the mathematical expression of the polynomial chaos, Haar and wavelet expansions when the input parameter θ follows a Gaussian distribution. Following the Wiener-Askey scheme summarised in Table 2.1, the univariate polynomials ψ_η have the following expression [168]:

$$\psi_\eta(\theta) = \sum_{k=0}^{\lfloor \frac{\eta-1}{2} \rfloor} (-1)^k \frac{(\eta-1)!}{2^k k! (\eta-1-2k)!} \theta^{\eta-1-2k}, \quad (\text{A.10})$$

where $\lfloor \cdot \rfloor$ is the floor operator.

Building the Haar and wavelet expansions requires to know the function F that links the cumulative distribution y (comprised between 0 and 1) of the variable θ to the value of the variable θ . Taking into account the fact that θ is a stochastic variable, the function F can be expressed as follows:

$$F(y) = \frac{1}{2} \left(1 + \operatorname{erf} \left(\frac{y}{\sqrt{2}} \right) \right)^{-1}, \quad (\text{A.11})$$

where erf is the error function. The function F in Equation (A.11) can be approximated by the following formula [169]:

$$F(y) = t - \frac{2.30753 + 0.27061t}{1 + 0.99229t + 0.04481t^2}, \quad (\text{A.12})$$

where $t = \sqrt{\ln \left(\frac{1}{(1-y)^2} \right)}$. This approximation is only valid when $0.5 \leq y \leq 1$ but can be extended to the interval $[0,1]$ using the fact that $F(y) = -F(1-y)$.

Appendix B

Nonlinear functions of random variables

This appendix details the stochastic operations needed in Section 4.3.3. They involve non-polynomial operations of random variables such as square root or cubic root. A Taylor expansion, albeit simpler to compute can require a high number of terms to obtain correct accuracy and is valid only in the vicinity of the centre of the expansion. Hence, we build on the work of Debusschere *et al.*, where a methodology for non-polynomial operation on random quantities is proposed in Ref. [134].

B.1 Algorithm for computation of non-polynomial functions of random variables

We briefly sketch the integration approach for non-polynomial function evaluations in [134]. We consider a function u of a variable x and derivative g . We write the variables x , u and g as follows:

$$x = x(s, \theta) = \sum_{j=0}^P x_j(s) \Psi_j(\theta), \quad (\text{B.1})$$

$$u = u(s, \theta) = \sum_{j=0}^P u_j(s) \Psi_j(\theta), \quad (\text{B.2})$$

$$g = g(s, \theta) = \sum_{j=0}^P g_j(s) \Psi_j(\theta), \quad (\text{B.3})$$

where $P + 1$ is the dimension of the stochastic space, and s parametrises the path across the space of PCE coefficients. Consequently, we can write:

$$\int_{\tilde{s}_1}^{s_2} \frac{\partial u}{\partial s} ds = \int_{\tilde{s}_1}^{s_2} g \frac{\partial x}{\partial s} ds. \quad (\text{B.4})$$

After Galerkin projections and mathematical steps detailed in Ref. [134], Equation (B.4) can be rewritten such that:

$$u_k(s_2) - u_k(s_1) = \sum_{j=0}^P \int_{x_j(s_1)}^{x_j(s_2)} \sum_0^P C_{ijk} g_i dx_j, \quad (\text{B.5})$$

where C_{ijk} is a third order tensor equal to $\langle \Psi_i \Psi_j, \Psi_k \rangle$ and $x_j(s_1)$ is a weighted average between quantities $a = \sum_{j=0}^P a_j \Psi_j$ where the function u has to be evaluated and $\tilde{a} = \sum_{j=0}^P \tilde{a}_j \Psi_j$ where the value of u in \tilde{a} is known. Typically, \tilde{a} is supposed to be the deterministic part of a so that the function u can be easily evaluated at this point. We write $x_j(s) = (a_j - \tilde{a}_j)s + \tilde{a}_j$, and consequently, we can rewrite Equation (B.5) as follows:

$$u_k(s_2) - u_k(s_1) = (a_j - \tilde{a}_j) \sum_{j=0}^P \int_{s_1}^{s_2} \sum_0^P C_{ijk} g_i ds. \quad (\text{B.6})$$

We now replace s_1 by 0 and s_2 by s' . Consequently we obtain:

$$u_k(s') - u_k(0) = (a_j - \tilde{a}_j) \sum_{j=0}^P \int_{\tilde{a}_j}^{(a_j - \tilde{a}_j)s' + \tilde{a}_j} \sum_{i=0}^P C_{ijk} g_i ds. \quad (\text{B.7})$$

We now differentiate this equation with respect to s' . Taking into account that $u_k(0)$ is independent from s' , we obtain the following equation:

$$\dot{u}_k(s') = (a_j - \tilde{a}_j) \sum_{j=0}^P \sum_{i=0}^P C_{ijk} g_i(s'). \quad (\text{B.8})$$

Recalling the aim is to compute $u_k(1)$ for k between 0 and P , we use Equation (B.8) to write:

$$u_k(s' + ds') = u_k(s') + \dot{u}_k(s') ds' = u_k(s') + (a_j - \tilde{a}_j) \sum_{j=0}^P \sum_{i=0}^P C_{ijk} g_i(s') ds'. \quad (\text{B.9})$$

As $u_k(0)$ is trivial to evaluate, because it simply equal to the stochastic component k of the function u evaluate at the deterministic point \tilde{a}_j , it is possible to create an iterative scheme to compute $u_k(1)$ if the knowledge of $u_k(s')$ is enough to compute $g_i(s')$. The procedure is summarised in Algorithm 2.

Algorithm 2 Evaluation of a non-linear function u for a random variable \tilde{a}

- 1: **Initialisation.** Set $s \leftarrow 0$. Set value of step increment ds , evaluate $u(a)$ where a is the mean value of \tilde{a} and $g(a)$.
 - 2: **while** $s \neq 1$ **do**
 - 3: For $k = 0$ to P , evaluate $u_k(s + ds)$ in equation (B.9).
 - 4: For $k = 0$ to P , evaluate and store $g_k(s)$ thanks to the knowledge of $u(s)$.
 - 5: Set $s \leftarrow s + ds$
 - 6: **end while**
-

B.2 Application to square root

In this section, a function $u(x)$ equal to $x^{1/3}$ is considered. Consequently, the function g is equal to $\frac{1}{3}x^{-2/3}$. We can rewrite g as follows:

$$g(x) = \frac{1}{3} \frac{u(x)}{x}. \quad (\text{B.10})$$

Here, it is possible to compute $g(x)$ if $u(x)$ is known as divisions of random variables has already been defined in the literature, see Appendix of [154] for more details. Consequently, Equation (B.9) becomes:

$$u_k(s' + ds') = u_k(s') + \frac{1}{3}(a_j - \tilde{a}_j) \sum_{j=0}^P \sum_{i=0}^P C_{ijk} \left(\frac{u(s')}{x(s')} \right) ds'. \quad (\text{B.11})$$

We benchmark this algorithm on Equation (4.3), assuming the value of $\frac{Q}{P}$ is equal to 0.25, the friction coefficient μ is a random Gaussian variable centered in 0.35 with a standard deviation of 0.025. We use a step $ds = 0.001$ for the discretisation in equation (B.9). We generate the CDF of c -values in equation (4.3) using MC and a PCE approximation of order 4. Figure B.1 shows the performance of our algorithm as only little deviation from MC is observed. This algorithm also allows for the computations of square roots in Equation (4.4).

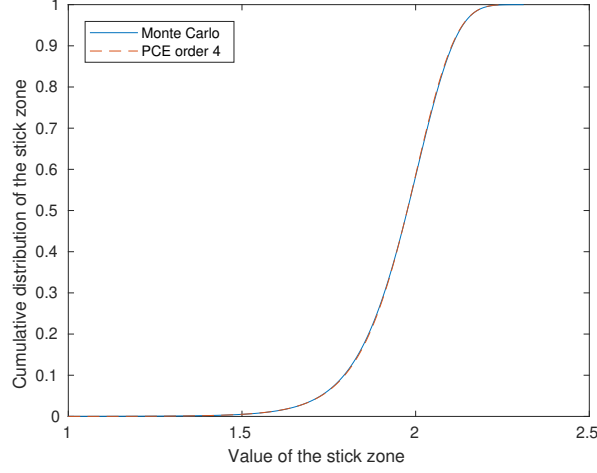


Figure B.1: Comparison of the histogram of the stick zone between MC method and PCE approximation of order 4.

B.3 Application to logarithm

In this section, a function $u(x)$ equal to $\log(x)$ is considered. Consequently, the function g is equal to $\frac{1}{x}$. Trivially, it is possible to compute $g(x)$. Consequently, equation (B.9) becomes:

$$u_k(s' + ds') = u_k(s') + (a_j - \tilde{a}_j) \sum_{j=0}^P \sum_{i=0}^P C_{ijk} \left(\frac{1}{x(s')} \right) ds'. \quad (\text{B.12})$$

We benchmark this algorithm by computing the logarithm of $0.9 + 0.2\mathcal{N}(0, 1) + 0.1\mathcal{N}(0, 1)^2$ where $\mathcal{N}(0, 1)$ is a Gaussian random variable centered in 0 with a standard deviation of 1. We use a step $ds = 0.001$ for the discretisation in Equation (B.9). We generate the CDF of \log -values using MC and a PCE approximation of order 5. Figure B.2 shows the performance of our algorithm as only little deviation from MC is observed. This algorithm also allows for the logarithm for the stochastic area growth constitutive model.

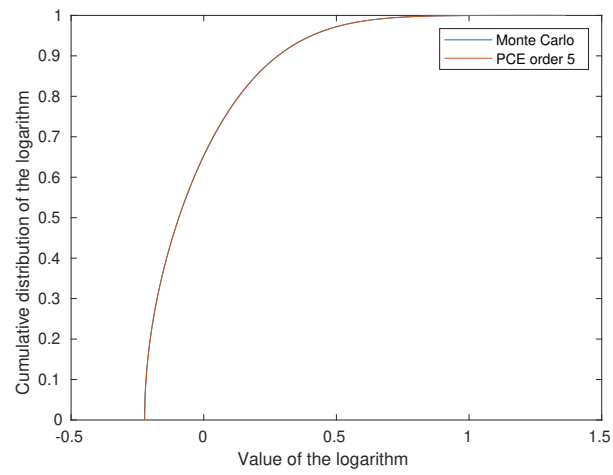


Figure B.2: CDF of logarithm value of a random variable between MC method and PCE approximation of order 5.

Appendix C

Impact of remeshing strategy

This appendix shows that the remeshing strategy used in Section 4.1.3 has little impact on the final results. We illustrate this with a simple example: a plate with random defect in tension. The remeshing step is done by considering four different strategies. The final results are then compared to show the independence of the method with respect to the constitutive law used for the first step.

C.1 Plate in tension with a single defect

As discussed in Chapter 4, the first stochastic transformation maps the reference frame to a new geometry defined stochastically. The transformation \mathbf{F}_{Map} then corrects the subsequent deformation to only capture the mechanics of the material deforming from this intermediate frame. Then we show that this subsequent mechanical deformation is independent of the effective remeshing resulting from \mathbf{F}_{Map} . We consider 2D plate, clamped on its left side and submitted to a deterministic uniform loading on its right side, see Figure C.1. We introduced a stress raiser in the plate: an elliptic hole of random aspect ratio. The peak stress arises at the top hole and the Stress Concentration Factor (SCF) follows an analytical formula that we will use to evaluate the performance of our framework. To obtain

the tensor \mathbf{F}_{Map} , we solve for the stochastic nodal displacement in a boundary-value problem defined in Figure C.2. While the edges in black are clamped, the y -displacement of the green edges is 0. The following Dirichlet Boundary Conditions (BCs) are applied on nodes lying in the red half-circle:

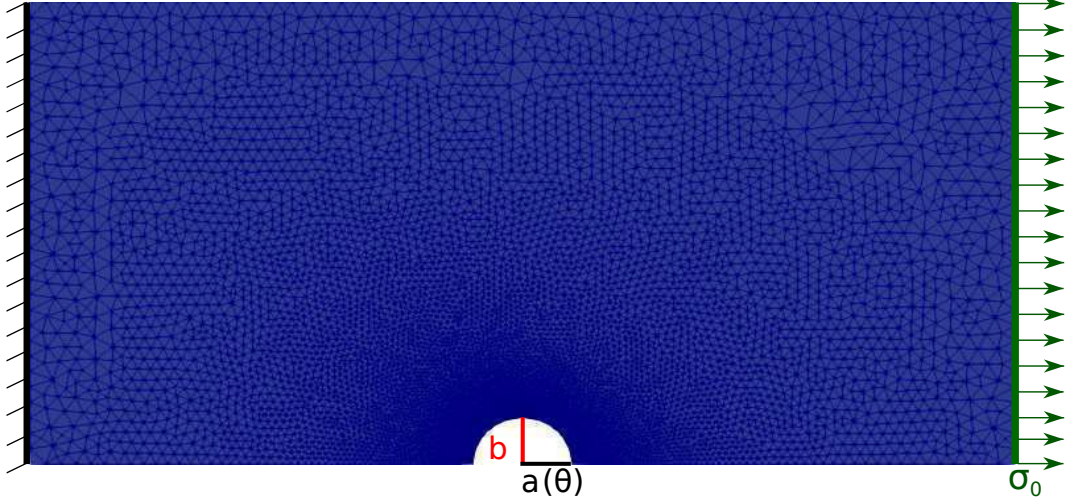


Figure C.1: Plate with a hole of random dimension. On the left-hand side, the component is clamped. On the right-hand side, deterministic pressure σ_0 is applied.

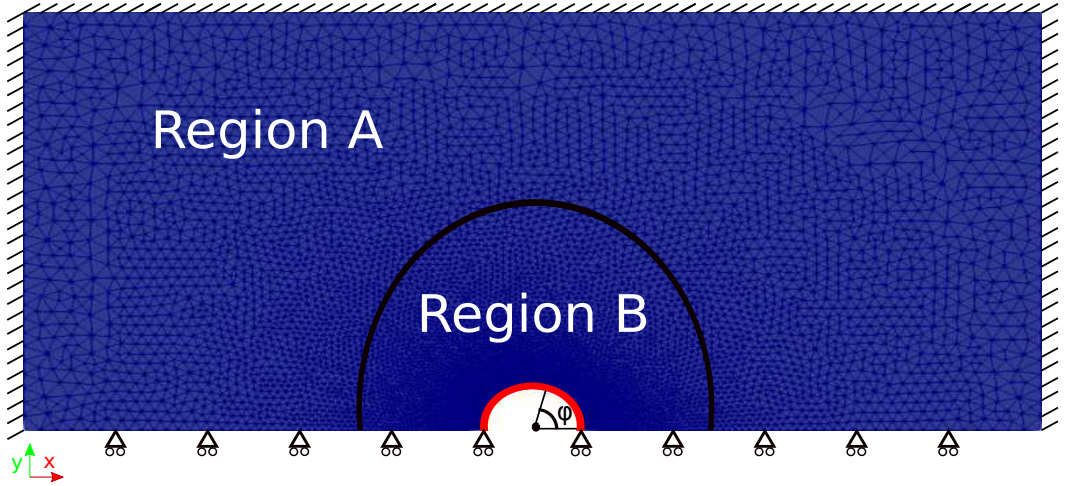


Figure C.2: The rectangular plate is divided in two regions, A and B. The lateral and top edges of the rectangular plate are clamped. The nodes in the bottom edge are only allowed to move in the x -direction. Stochastic BCs, see Equation (C.1), are applied in the red half-ellipse to create the mapping between an initial configuration and a set of random geometries. During the first step of our framework, the bulk of the plate is divided in two regions.

$$\begin{aligned}
BC_x &= \frac{abc\cos(\varphi)}{\sqrt{b^2\cos^2(\varphi) + a^2\sin^2(\varphi)}} - b\cos(\varphi) \\
BC_y &= \frac{absin(\varphi)}{\sqrt{b^2\cos^2(\varphi) + a^2\sin^2(\varphi)}} - b\sin(\varphi),
\end{aligned} \tag{C.1}$$

where φ is the angle between the position vector and the x -axis, b is the long axis, and a is the small axis of the ellipse, equal to $\frac{b}{5}(4 + \theta)$, where θ is a random variable. Here the eccentricity $\epsilon = \frac{b}{a}$ is comprised between -1 and 1. Expressing the BCs using PCE requires a specific algorithm detailed in Ref. [134] and [154] as nonlinear functions of random variables have to be performed. In this first step, the plate is supposed to be a heterogenous material, split in two regions, A and B, see in Figure C.2. We study four cases with different Young's modulus values in region A and B using a Saint Venant-Kirchhoff constitutive model, see Table C.1. Showing that the end result of the computation is independent of the chosen constitutive law and parameters during the first step of the procedure is key to prove the proposed framework's robustness. The FE discretisation and the geometry are detailed in Table C.2. In this case, the SCF, defined as the ratio between the maximum longitudinal stress σ_{xx} and the nominal stress σ_0 is analytically described as follows:

$$SCF = \frac{\max(\sigma_{xx})}{\sigma_0} = 1 + 2\frac{b}{a}, \tag{C.2}$$

where a and b are the axis of the hole, shown in Figure C.1. We leverage the extension of APFEM to random domains and obtain the SCF for elliptic holes of axis a comprised between 0.3 and 0.5 m. The displacements, strain and stress fields were obtained using a fourth-order PCE.

Figure C.3a shows the comparison of the SCF obtained with the aforementioned proposed framework and the analytical solution given in Equation (C.2). Despite discrepancies, we observe a satisfying match between the APFEM and the baseline solution. Discrepancies originate from the approximation of the BCs in Equation (C.1) as PCE using an algorithm first published in Ref. [134]. Note that the terms in Equation (C.1) involve negative power of random variables, higher-order PCE would be required for better accuracy, at the expense of computational cost. We

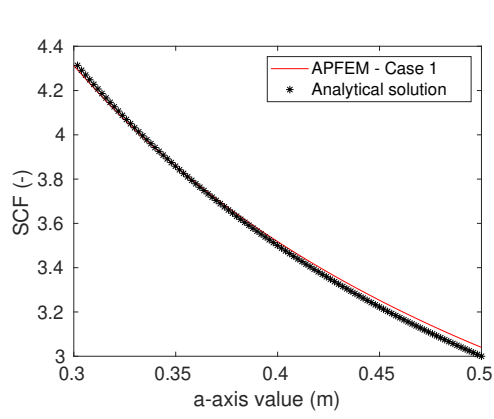
can remark that the results are weakly dependent of the remeshing strategy. As we change the stiffness of the two regions in Figure C.2, our results remain similar as the relative error between APFEM in case 1 and any other cases is smaller than half of a percent, see Figure C.3b. Therefore, we consider that the final result of this method does not depend on the constitutive law or material parameters used in the first step of the computation.

	Region A	Region B
Case 1	$E=10^6$ Pa, $\nu=0.3$	$E=10^6$ Pa, $\nu=0.3$
Case 2	$E=10^7$ Pa, $\nu=0.3$	$E=10^7$ Pa, $\nu=0.3$
Case 3	$E=10^6$ Pa, $\nu=0.3$	$E=10^7$ Pa, $\nu=0.3$
Case 4	$E=10^7$ Pa, $\nu=0.3$	$E=10^6$ Pa, $\nu=0.3$

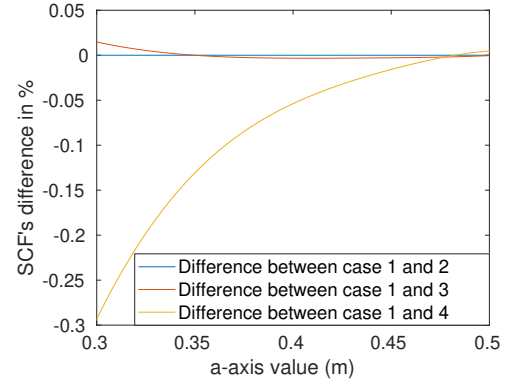
Table C.1: Material parameters for the four different cases during the first step.

Parameters	Value
Geometric features	Length = 10 m, width = 5 m
Number of nodes	32 669
Type of elements	CPS6
Number of elements	16 152
Value of b-axis of the plate	0.5 m
Range of a-axis of the plate	0.3 m to 0.5 m
PCE order	4
σ_0	10 000 Pa
Young's modulus and Poisson's ratio	1E7 Pa, 0.3

Table C.2: FE discretisation and geometric features of the plate.



(a) Comparison of the SCF between APFEM and analytical solution.



(b) Variation in computed SCF for different parameters of the constitutive model during the remeshing step using APFEM.

Figure C.3: Evaluation of a) APFEM's accuracy to capture geometrical uncertainties' effect and b) robustness of APFEM framework with respect to the remeshing step.

References

- [1] P. Love et al. “What Goes up, Shouldn’t Come down: Learning from Construction and Engineering Failures”. In: *Procedia Engineering* 14 (2011), pp. 844–850.
- [2] J. Bigen. “Durability of engineering structures: Design, repair and maintenance”. In: *Woodhead Publishing* ().
- [3] B.C. Rao. “Revisiting classical design in engineering from a perspective of frugality”. In: *Heliyon* 3.5 (2017), e00299.
- [4] J-S. Kim et al. “Development of concurrent engineering system for design of composite structures”. In: *Composite Structures* 50.3 (2000), pp. 297–309.
- [5] M. Eiermann, O.G. Ernst, and E. Ullmann. “Computational aspects of the stochastic finite element method”. In: *Computing and Visualization in science* 10 (2007), pp. 3–15.
- [6] J. McCall. “Genetic algorithms for modelling and optimisation”. In: *Journal of Computational and Applied Mathematics* 184.1 (2005), pp. 205–222.
- [7] K. Krishnapillai and R. Jones. “Three-dimensional structural design optimisation based on fatigue implementing a genetic algorithm and a non-similitude crack growth law”. In: *Finite Elements in Analysis and Design* 45 (2009), pp. 132–47.
- [8] J.M. Peña, A. LaTorre, and A. Jérusalem. “SoftFEM: The Soft Finite Element Method”. In: *International Journal for Numerical Methods in Engineering* 118.10 (2019), pp. 606–630.
- [9] T.S. Mesogitis, A.A. Skordos, and A.C. “Uncertainty in the manufacturing of fibrous thermosetting composites: A review”. In: *Composites: Part A* 57 (2014), pp. 67–75.
- [10] N. Korshunova et al. “Uncertainty quantification of microstructure variability and mechanical behavior of additively manufactured lattice structures”. In: *Computer Methods in Applied Mechanics and Engineering* 385 (2021), p. 114049.
- [11] J. Neggers, O. Allix, and F. Hild. “Big Data in Experimental Mechanics and Model Order Reduction: Today’s Challenges and Tomorrow’s Opportunities”. In: *Archives of Computational Methods in Engineering* 25 (2018), pp. 143–164.
- [12] H. Rappel, L.A.A. Beex, and L. Noels. “Identifying elastoplastic parameters with Bayes’ theorem considering output error, input error and model uncertainty”. In: *Probabilistic Engineering Mechanics* 55 (2019), pp. 28–41.
- [13] D. Wang and Q. Miao. “Smoothness index-guided Bayesian inference for determining joint posterior probability distributions of anti-symmetric real Laplace wavelet parameters for identification of different bearing faults”. In: *Journal of Sound and Vibration* 345 (2015), pp. 250–266.

- [14] Q. Zhiping and Z. Zhang. “Fatigue crack propagation analysis in structures with random parameters based on polynomial chaos expansion method”. In: *Theoretical and Applied Fracture Mechanics* 105 (2020).
- [15] JP. Boyd. “Chebyshev and fourier spectral methods”. In: (2001).
- [16] B. Sudret and A. Der Kiureghian. “A. Stochastic finite elements and reliability: a state-of-the-art report”. In: (2000), pp. 1–173.
- [17] D. Moens and M. Hanss. “Non-probabilistic finite element analysis for parametric uncertainty treatment in applied mechanics: Recent advances”. In: *Finite Elements in Analysis and Design* 47.1 (2011), pp. 4–16.
- [18] M.G.R. Faes and D. Moens. “Recent Trends in the Modeling and Quantification of Non-probabilistic Uncertainty”. In: *Archives of Computational Methods in Engineering* 27 (2019), pp. 633–671.
- [19] S.S. Rao and L. Berke. “Analysis of Uncertain Structural Systems Using Interval Analysis”. In: *AIAA Journal* 35 (1997).
- [20] X.Y. Long et al. “An interval analysis method for fatigue crack growth life prediction with uncertainty”. In: *Computers & Structures* 210 (2018), pp. 1–11.
- [21] M. Xu and Z. Qiu. “A dimension-wise method for the static analysis of structures with interval parameters”. In: *Science China Physics, Mechanics & Astronomy* 57 (2014), pp. 1934–1945.
- [22] B.Y. Ni and C. Jiang. “Interval field model and interval finite element analysis”. In: *Computer Methods in Applied Mechanics and Engineering* 360 (2020), p. 112713.
- [23] R. Ghanem and P.D. Spanos. “Stochastic Finite Elements: A Spectral Approach”. In: *Springer-Verlag* 0 (1991).
- [24] S. Acharjee and N. Zabaras. “Uncertainty propagation in finite deformations—A spectral stochastic Lagrangian approach”. In: *Computer Methods in Applied Mechanics and Engineering* 195 (2006), pp. 2289–2312.
- [25] Y.M. Marzouk, H.N. Najm, and L.A. Rahn. “Stochastic spectral methods for efficient Bayesian solution of inverse problems”. In: *Journal of Computational Physics* 224.2 (2007), pp. 560–586.
- [26] B.V. Rosic and M. Hermann. “Variational Theory and Computations in Stochastic Plasticity”. In: *Archives of Computational Methods in Engineering* 22 (2015), pp. 457–509.
- [27] G. Stefanou. “The stochastic finite element method: Past present and futures”. In: *Computer Methods in Applied Mechanics and Engineering* 1998 (2009), pp. 1031–1051.
- [28] R. Sheikholeslami and S. Razavi. “Progressive Latin Hypercube Sampling: An efficient approach for robust sampling-based analysis of environmental models”. In: *Environmental Modelling & Software* 93 (2017), pp. 109–126.
- [29] M. Mahdi, B. Ataie-Ashtiani, and H. Janssen. “Efficiency enhancement of optimized Latin hypercube sampling strategies: Application to Monte Carlo uncertainty analysis and meta-modeling”. In: *Advances in Water Resource* 76 (2015), pp. 127–139.

- [30] W.Li K.Q Ye and A.Sudjianto. “Algorithmic construction of optimal symmetric Latin hypercube designs”. In: *Journal of Statistical Planning and Inference* 90.1 (2000), pp. 145–159.
- [31] I.M. Sobol’. “Quasi-Monte Carlo methods”. In: *Progress in Nuclear Energy* 24 (1990), pp. 55–61.
- [32] M. Giles et al. “Monte Carlo and Quasi-Monte Carlo Methods 2006”. In: (2006), pp. 343–358.
- [33] G. Blatman and B. Sudret. “Adaptive sparse polynomial chaos expansion based on least angle regression”. In: *Journal of Computational Physics* 230.6 (2011), pp. 2345–2367.
- [34] A.H.S. Ang. “Probability concepts in engineering planning and design”. In: *Risk, and Reliability, Desision* (1984).
- [35] O. Ditlevsen. *Uncertainty modeling with applications to multidimensional civil engineering systems*. McGraw-Hill International Book Company, 1981.
- [36] C. Soize. “Uncertainty Quantification; An Accelerated Course with Advanced Applications in Computational Engineering.” In: *Interdisciplinary Applied Mathematics* 47 (2017).
- [37] B.R. Ellingwood and K. Kinali. “Quantifying and communicating uncertainty in seismic risk assessment”. In: *Structural Safety* 31.2 (2009), pp. 179–187.
- [38] K.J. Beven et al. “Epistemic uncertainties and natural hazard risk assessment – Part 1: A review of different natural hazard areas”. In: *Natural Hazards and Earth System Sciences* 18.10 (2018), pp. 2741–2768.
- [39] Z. Wang and R. Ghanem. “An extended polynomial chaos expansion for PDF characterization and variation with aleatory and epistemic uncertainties”. In: *Computer Methods in Applied Mechanics and Engineering* 382 (2021), p. 113854.
- [40] F.M. Hemez, J.M Booker, and J.R. Langenbrunner. “Answering the question of sufficiency: How much uncertainty is enough”. In: (2007), pp. 11–13.
- [41] L.A Zadeh. “Fuzzy sets as a basis for a theory of possibility”. In: *Fuzzy sets and systems* 1.1 (1978), pp. 3–28.
- [42] A. Kaufmann and M.M. Gupta. “Introduction to fuzzy arithmetic: Theory and applications, 1991”. In: *VanNostrand Reinhold, New York* (1991).
- [43] D. Dubois and H. Prade. “POSSIBILITY THEORY: AN APPROACH TO COMPUTERIZED PROCESSING OF UNCERTAINTY”. In: *International Journal of General Systems* 15.2 (1989), pp. 168–170.
- [44] Y. He, M. Mirzargar, and R.M. Kirby. “Mixed aleatory and epistemic uncertainty quantification using fuzzy set theory”. In: *International Journal of Approximate Reasoning* 66 (2015), pp. 1–15.
- [45] Y. He and M.Y. Hussaini. “Mixed aleatory and epistemic uncertainty propagation using Dempster–Shafer theory”. In: *Journal of Computational and Applied Mathematics* (2023), p. 115234.
- [46] L. Huilin et al. “Numerical simulation of bubble and particles motions in a bubbling fluidized bed using direct simulation Monte-Carlo method”. In: *Powder Technology* 169 (2006), pp. 159–171.

- [47] M. Kohns J. Marx and K. Langenbach. “Vapor-liquid equilibria of binary mixtures containing Stockmayer-type model fluids from Monte-Carlo simulations”. In: *Fluid Phase Equilibria* 568 (2023), p. 113742.
- [48] B.I. Epureanu Z. He and C. Pierre. “Convergence predictions for aeroelastic calculations of tuned and mistuned bladed disks”. In: *Journal of Fluids and Structures* 24.5 (2008), pp. 732–749.
- [49] T. Argentini et al. “Monte Carlo analysis of total damping and flutter speed of a long span bridge: Effects of structural and aerodynamic uncertainties”. In: *Journal of Wind Engineering and Industrial Aerodynamics* 128 (2014), pp. 90–104.
- [50] S. Murugan et al. “Helicopter aeroelastic analysis with spatially uncertain rotor blade properties”. In: *Aerospace Science and Technology* 16.1 (2012), pp. 29–39.
- [51] P. Rodrigues, O. Gicquel, and R. Vicquelin B. Franzelli N. Darabiha. “Analysis of radiative transfer in a turbulent sooting jet flame using a Monte Carlo method coupled to large eddy simulation”. In: *Journal of Quantitative Spectroscopy and Radiative Transfer* 235 (2019), pp. 187–203.
- [52] Mark J. Ablowitz and Justin T. Cole. “Nonlinear optical waveguide lattices: Asymptotic analysis, solitons, and topological insulators”. In: *Physica D: Nonlinear Phenomena* 440 (2022), p. 133440.
- [53] P.A. Mello et al. “Transport of waves in disordered waveguides: A potential model”. In: *Physica A: Statistical Mechanics and its Applications* 386.2 (2007), pp. 603–610.
- [54] P.A Martin. *Multiple scattering: interaction of time-harmonic waves with N obstacles*. 107. Cambridge University Press, 2006.
- [55] J.A Kong et al. *Scattering of electromagnetic waves: numerical simulations*. John Wiley & Sons, 2004.
- [56] L. Tsang, J.A. Kong, and K.H. Ding. *Scattering of electromagnetic waves: theories and applications*. John Wiley & Sons, 2004.
- [57] H. Lopez-Menchon et al. “A parallel Monte Carlo method for solving electromagnetic scattering in clusters of dielectric objects”. In: *Journal of Computational Physics* 463 (2022), p. 111231.
- [58] Z. Lu and Y. Liu. “Experimental investigation of random loading sequence effect on fatigue crack growth”. In: *Materials & Design* 32.10 (2011), pp. 4773–4785.
- [59] W.F. Wu and C.C. Ni. “Statistical aspects of some fatigue crack growth data”. In: *Engineering Fracture Mechanics* 74.18 (2007), pp. 2952–2963.
- [60] C.D Chen et al. “The effects of material variations on aircraft inspection schedules based on stochastic crack growth model”. In: *International Journal of Fatigue* 30.5 (2008), pp. 861–869.
- [61] Thomas Svensson. “Prediction uncertainties at variable amplitude fatigue”. In: *International Journal of Fatigue* 19.93 (1997), pp. 295–302.
- [62] Y. Liu and S. Mahadevan. “Probabilistic fatigue life prediction using an equivalent initial flaw size distribution”. In: *International Journal of Fatigue* 31.3 (2009), pp. 476–487.

- [63] Y. Liu and S. Mahadevan. “Stochastic fatigue damage modeling under variable amplitude loading”. In: *International Journal of Fatigue* 29.6 (2007), pp. 1149–1161.
- [64] Masanori Matsuishi and Tatsuo Endo. “Fatigue of metals subjected to varying stress”. In: *Japan Society of Mechanical Engineers, Fukuoka, Japan* 68.2 (1968), pp. 37–40.
- [65] M.A. Miner. “Cumulative Damage in Fatigue”. In: *Journal of Applied Mechanics* 3.6 (1945), pp. 159–164.
- [66] Y.Liu. “Stochastic modeling of multiaxial fatigue and fracture [Ph. D. Thesis]”. In: *USA: Vanderbilt University* (2006).
- [67] Y.M Low. “A variance reduction technique for long-term fatigue analysis of offshore structures using Monte Carlo simulation”. In: *Engineering Structures* 128 (2016), pp. 283–295.
- [68] W.X Wang et al. “Experimental investigation on test methods for mode II interlaminar fracture testing of carbon fiber reinforced composites”. In: *Composites Part A: Applied Science and Manufacturing* 40.9 (2009), pp. 1447–1455.
- [69] A.J. Brunner, B.R.K Blackman, and J.G. Williams. “Calculating a damage parameter and bridging stress from GIC delamination tests on fibre composites”. In: *Composites Science and Technology* 66.6 (2006), pp. 785–795.
- [70] H.K. Jeong and R.A. Shenoi. “Probabilistic strength analysis of rectangular FRP plates using Monte Carlo simulation”. In: *Computers & Structures* 76.1 (2000), pp. 219–235.
- [71] M.B. Whiteside, S.T. Pinho, and P. Robinson. “Stochastic failure modelling of unidirectional composite ply failure”. In: *Reliability Engineering & System Safety* 108 (2012), pp. 1–9.
- [72] P.D. Soden, M.J Hinton, and A.S. Kaddour. “Biaxial test results for strength and deformation of a range of E-glass and carbon fibre reinforced composite laminates: failure exercise benchmark data”. In: (2004), pp. 52–96.
- [73] Y. Lian, F. Wu, and Y. Han. “Stochastic numerical analysis for static performance of composite laminates based on resampling method”. In: *Composite Structures* 311 (2023), p. 116819.
- [74] M. Rocas, A. García-González, and X. Larráyoz. “Nonintrusive Stochastic Finite Elements for Crashworthiness with VPS/ Pamcrash”. In: *Archives of Computational Methods in Engineering* 27 (2020), pp. 1337–1362.
- [75] J. Bruyère et al. “Statistical tolerance analysis of bevel gear by tooth contact analysis and Monte Carlo simulation”. In: *Mechanism and Machine Theory* 42.10 (2007), pp. 1326–1351.
- [76] R. Caflisch. “Monte Carlo and quasi-Monte Carlo methods”. In: *Acta Numerica* 7 (1998), pp. 1–49.
- [77] L.Palluotto et al. “Assessment of randomized Quasi-Monte Carlo method efficiency in radiative heat transfer simulations”. In: *Journal of Quantitative Spectroscopy and Radiative Transfer* 236 (2019), p. 106570.

- [78] E.R. van Dam B.G. Husslage G. Rennen and D. den Hertog. “Space-filling Latin hypercube designs for computer experiments”. In: *Optimization and Engineering* 12 (2011), pp. 611–630.
- [79] J.C. Helton and F.J. Davis. “Latin hypercube sampling and the propagation of uncertainty in analyses of complex systems”. In: *Reliability Engineering & System Safety* 81 (2003), pp. 23–69.
- [80] M. Hadigol and A. Doostan. “Least squares polynomial chaos expansion: A review of sampling strategies”. In: *Computer Methods in Applied Mechanics and Engineering* 332 (2018), pp. 382–407.
- [81] M. Giles. “Multilevel Monte Carlo methods”. In: *Acta numerica* 24 (2015), pp. 259–328.
- [82] A.Cliffe et al. “Multilevel Monte Carlo Methods and Applications to Elliptic PDEs with Random Coefficients”. In: *Computing and Visualization in Science* 14.1 (2011), pp. 3–15.
- [83] S. Krumscheid, F. Nobile, and M. Pisaroni. “Quantifying uncertain system outputs via the multilevel Monte Carlo method — Part I: Central moment estimation”. In: *Journal of Computational Physics* 414 (2020), p. 109466.
- [84] V. Rey, S. Krumscheid, and F. Nobile. “Quantifying uncertainties in contact mechanics of rough surfaces using the multilevel Monte Carlo method”. In: *International Journal of Engineering Science* 138 (2019), pp. 50–64.
- [85] K. Deep et al. “A real coded genetic algorithm for solving integer and mixed integer optimization problems”. In: *Applied Mathematics and Computation* 212.2 (2009), pp. 505–518.
- [86] N. Wiener. “The Homogeneous Chaos”. In: *American Journal of Mathematics* 4 (), pp. 897–936.
- [87] R.H. Cameron and W.T Martin. “Transformations of Wiener Integrals under Translations”. In: *Annals of mathematics* 45 (1944), pp. 386–396.
- [88] H.Ogura. “Orthogonal functionals of the Poisson process”. In: *IEEE Transactions on Information Theory* 18.4 (1972), pp. 473–481.
- [89] R.A. Askey and J.A. Wilson. “Some basic hypergeometric orthogonal polynomials that generalize Jacobi polynomials”. In: *Memoirs of the American Mathematical Society* 54 (1985).
- [90] D. Xiu and G. Karniadakis. “The Wiener-Askey Polynomial Chaos for Stochastic Differential Equations”. In: *SIAM Journal on Scientific Computing* 24 (2002), pp. 619–644.
- [91] S. Oladyshkin, F.P.J. de Barros, and W. Nowak. “Global sensitivity analysis: A flexible and efficient framework with an example from stochastic hydrogeology”. In: *Advances in Water Resources* 37 (2012), pp. 10–22.
- [92] S. Oladyshkin and W. Nowak. “Data-driven uncertainty quantification using the arbitrary polynomial chaos expansion”. In: *Reliability Engineering and System Safety* 106 (2012), pp. 189–190.
- [93] K.K. Phoon, H.W. Huang, and S.T. Quek. “Simulation of second-order processes using Karhunen–Loeve expansion”. In: *Computers & structures* 80.12 (2002), pp. 1049–1060.

- [94] K.K. Phoon, H.W. Huang, and S.T. Quek. "Simulation of strongly non-Gaussian processes using Karhunen–Loeve expansion". In: *Probabilistic Engineering Mechanics* 20.2 (2005), pp. 188–198.
- [95] L.Cam. "The central limit theorem around 1935". In: *Statistical Science* 1.1 (1986), pp. 78–91.
- [96] G.Golub and J.Welsch. "Calculation of Gauss quadrature rules". In: *Mathematics of Computation* 23 (1969), pp. 221–230.
- [97] C.Clenshaw and A.Curtis. "A method for numerical integration on an automatic computer". In: *Numerical Mathematics* 2 (1960), pp. 19–205.
- [98] L. Bruno, C. Canuto, and D. Fransos. "Stochastic aerodynamics and aeroelasticity of a flat plate via generalised Polynomial Chaos". In: *Journal of Fluids and Structures* 25.7 (2009), pp. 1158–1176.
- [99] A. Camacho et al. "Uncertainty quantification in reservoir simulation models with polynomial chaos expansions: Smolyak quadrature and regression method approach". In: *Journal of Petroleum Science and Engineering* 153 (2017), pp. 203–211.
- [100] S. Smolyak. "Quadrature and interpolation formulas for tensor products of certain classes of functions". In: *Soviet Mathematics* 4 (1963), pp. 240–243.
- [101] H. Cheng and A. Sandu. "Collocation Least-Squares Polynomial Chaos Method". In: *Proceedings of the 2010 Spring Simulation Multiconference* (2010), pp. 1–6.
- [102] J.YunYuan. "Numerical methods for generalized least squares problems". In: *Journal of Computational and Applied Mathematics* 66.1-2 (1996), pp. 571–584.
- [103] S. Isukapalli, A. Roy, and P.G. Georgopoulos. "Stochastic Response Surface Methods (SRSMs) for Uncertainty Propagation: Application to Environmental and Biological Systems". In: *Risk Analysis* 18.3 (1998), pp. 351–363.
- [104] A.Tatang et al. "An efficient method for parametric uncertainty analysis of numerical geophysical models". In: *Journal of geophysical research* 102.18 (1997), pp. 925–932.
- [105] S. Huang, M. Sankaran, and R. Ramesh. "Collocation-based stochastic finite element analysis for random field problems". In: *Probabilistic engineering mechanics* 22 (2007), pp. 194–205.
- [106] B. Sudret. "Global sensitivity analysis using polynomial chaos expansions". In: *Reliability engineering & system safety* 93.7 (2008), pp. 964–979.
- [107] K. Sepahvand and S. Marburg. "Spectral stochastic finite element method in vibroacoustic analysis of fiber-reinforced composites". In: *Procedia Engineering* 199 (2017), pp. 1134–1139.
- [108] X. Peng et al. "Uncertainty analysis of composite laminated plate with data-driven polynomial chaos expansion method under insufficient input data of uncertain parameters". In: *Composite Structures* 209 (2019), pp. 625–633.
- [109] R.H. Gallagher. "Perturbation procedures in nonlinear finite element structural analysis". In: (1975), pp. 75–89.

- [110] W.K. Liu, T. Belytschko, and A. Mani. “Probabilistic finite elements for nonlinear structural dynamics”. In: *Computer Methods in Applied Mechanics and Engineering* 56.1 (1986), pp. 61–81.
- [111] M. Kamiński. “Stochastic second-order perturbation approach to the stress-based finite element method”. In: *International Journal of Solids and Structures* 38.21 (2001), pp. 3831–3852.
- [112] H.Z. Huang and H.B. Li. “Perturbation finite element method of structural analysis under fuzzy environments”. In: *Engineering Applications of Artificial Intelligence* 18.1 (2005), pp. 83–91.
- [113] I. Doltsinis and Z. Kang. “Perturbation-based stochastic FE analysis and robust design of inelastic deformation processes”. In: *Computer Methods in Applied Mechanics and Engineering* 195.19 (2006), pp. 2231–2251.
- [114] A.K. Onkar, C.S. Upadhyay, and D. Yadav. “Probabilistic failure of laminated composite plates using the stochastic finite element method”. In: *Composite Structures* 77.1 (2007), pp. 79–91.
- [115] M. Kamiński and T.D. Hien. “Stochastic finite element modeling of transient heat transfer in layered composites”. In: *International Communications in Heat and Mass Transfer* 26.6 (1999), pp. 801–810.
- [116] M. Kamiński and G.F. Carey. “Stochastic perturbation-based finite element approach to fluid flow problems”. In: *International Journal of Numerical Methods for Heat & Fluid Flow* 15.7 (2005), pp. 671–695.
- [117] M. Kamiński. “Generalized perturbation-based stochastic finite element method in elastostatics”. In: *Computers & Structures* 85.10 (2007), pp. 586–594.
- [118] M. Kamiński. “Perturbation-based stochastic finite element method using polynomial response function for the elastic beams”. In: *Mechanics Research Communications* 36.3 (2009), pp. 381–390.
- [119] M. Kamiński and M. Solecka. “Optimization of the truss-type structures using the generalized perturbation-based Stochastic Finite Element Method”. In: *Finite Elements in Analysis and Design* 63 (2013), pp. 69–79.
- [120] F. Wu et al. “A Modified Computational Scheme for the Stochastic Perturbation Finite Element Method”. In: *Latin American Journal of Solids and Structures* 12.Lat. Am. j. solids struct., 2015 12(13) (2015), pp. 2480–2505.
- [121] Z. Shao, X. Li, and P. Xiang. “A new computational scheme for structural static stochastic analysis based on Karhunen–Loève expansion and modified perturbation stochastic finite element method.” In: *Computational Mechanics* 63 (2023), pp. 69–79.
- [122] J. H. Bramble and S. R. Hilbert. “Estimation of Linear Functionals on Sobolev Spaces with Application to Fourier Transforms and Spline Interpolation”. In: *SIAM Journal on Scientific Computing* 7.1 (1970), pp. 112–124.
- [123] S. Roux, D. Vandembroucq, and F. Hild. “Effective toughness of heterogeneous brittle materials”. In: *European Journal of Mechanics-A/Solids* 22.5 (2003), pp. 743–749.

- [124] Z. Yang and X.F. Xu. “A heterogeneous cohesive model for quasi-brittle materials considering spatially varying random fracture properties”. In: *Computer methods in applied mechanics and engineering* 197.45-48 (2008), pp. 4027–4039.
- [125] C. Schwab and R.A. Todor. “Karhunen–Loève approximation of random fields by generalized fast multipole methods”. In: *Journal of Computational Physics* 217.1 (2006), pp. 100–122.
- [126] W. Betz, I. Papaioannou, and D. Straub. “Numerical methods for the discretization of random fields by means of the Karhunen–Loève expansion”. In: *Computer Methods in Applied Mechanics and Engineering* 271 (2014), pp. 109–129.
- [127] Y. Chien and K.S. Fu. “On the generalized Karhunen–Loève expansion”. In: *IEEE Transactions on Information Theory* 13 (1967), pp. 518–520.
- [128] R. Takhanov. “On the speed of uniform convergence in Mercer’s theorem”. In: *Journal of Mathematical Analysis and Applications* 518.2 (2023), p. 126718.
- [129] A.B. Bakushinskii. “A numerical method for solving Fredholm integral equations of the 1st kind”. In: *USSR Computational Mathematics and Mathematical Physics* 5.4 (1965), pp. 226–233.
- [130] M.F. Ngah and A. Young. “Application of the spectral stochastic finite element method for performance prediction of composite structures”. In: *Composite Structures* 78.3 (2007), pp. 447–456.
- [131] N.Z. Chen and C. Guedes Soares. “Spectral stochastic finite element analysis for laminated composite plates”. In: *Computer Methods in Applied Mechanics and Engineering* 197.51 (2008), pp. 4830–4839.
- [132] P.B. Nair and A.J. Keane. “Stochastic Reduced Basis Methods”. In: *AIAA Journal* 40.8 (2002), pp. 1653–1664.
- [133] P. Surya Mohan, P.B. Nair, and A.J. Keane. “Multi-element stochastic reduced basis methods”. In: *Computer Methods in Applied Mechanics and Engineering* 197.17 (2008), pp. 1495–1506.
- [134] B.J. Debuschere, H. Najm, and P. Pebay. “Numerical challenges in the use of polynomial chaos representations for stochastic processes”. In: *Society for Industrial and Applied Mathematics* 26.2 (2004), pp. 698–719.
- [135] O.P. Le Maître et al. “Uncertainty propagation using Wiener–Haar expansions”. In: *Journal of Computational Physics* 197.1 (2004), pp. 28–57.
- [136] O.P. Le Maître and O.M. Knio. “A stochastic particle-mesh scheme for uncertainty propagation in vortical flows”. In: *Journal of Computational Physics* 226.1 (2007), pp. 645–671.
- [137] H.N. Najm. “Uncertainty Quantification and Polynomial Chaos Techniques in Computational Fluid Dynamics”. In: *Annual Review of Fluid Mechanics* 41 (2009), pp. 35–52.
- [138] O.P. Le Maître et al. “Multi-Resolution-Analysis Scheme for Uncertainty Quantification in Chemical Systems”. In: *Society for Industrial and Applied Mathematics* 29 (2007), pp. 864–889.

- [139] H.N. Najm et al. “Uncertainty quantification in chemical systems”. In: *International Journal for Numerical Methods in Engineering* 80.6-7 (), pp. 789–814.
- [140] X.Wang et al. “Direct numerical simulation and large eddy simulation on a turbulent wall-bounded flow using lattice boltzmann method and multiple GPUs”. In: *Mathematical Problems in Engineering* (2014), pp. 1–10.
- [141] Loïc Giraldi et al. “To Be or Not to Be Intrusive? The Solution of Parametric and Stochastic Equations—the “Plain Vanilla” Galerkin Case”. In: *SIAM Journal on Scientific Computing* 36.6 (2014), A2720–A2744.
- [142] B. Li et al. “Surface wrinkling of mucosa induced by volumetric growth: Theory, simulation and experiment”. In: *Journal of the Mechanics and Physics of Solids* 59.4 (2011), pp. 758–774.
- [143] D.F. Walnut. “An Introduction to Wavelets Analysis”. In: *Applied and Numerical Harmonic Analysis* (2002).
- [144] B.K. Alpert. “A class of bases in L^2 for the sparse representation of integral operators”. In: *SIAM journal on mathematical analysis* (1993), pp. 246–262.
- [145] O.P. Le Maitre, H. Najm, and R. Ghanem. “Multi-resolution analysis of Wiener-type uncertainty propagation schemes”. In: *Journal of Computational Physics* 197 (2004), pp. 502–531.
- [146] M. Rosenblatt. “Remarks on a Multivariate Transformation”. In: *The Annals of Mathematical Statistics* 23.3 (1952), pp. 470–472.
- [147] C.J. Geyer. “Practical Markov Chain Monte Carlo”. In: *Statistical Science* 7 (1996), pp. 473–483.
- [148] W.R. Gilks and S. Richardson. “Markov Chain Monte Carlo in Practice”. In: *Chapman & Hall* (1996).
- [149] L. Liu et al. “Elastic and failure response of imperfect three-dimensional metallic lattices: the role of geometric defects induced by Selective Laser Melting”. In: *Journal of the Mechanics and Physics of Solids* 107 (2017), pp. 160–184.
- [150] A. Nouy et al. “An extended stochastic finite element method for solving stochastic partial differential equations on random domains”. In: *Computer Methods in Applied Mechanics and Engineering* 197.51 (2008), pp. 4663–4682.
- [151] D. Pivovarov and P. Steinmann. “Modified SFEM for computational homogenization of heterogeneous materials with microstructural geometric uncertainties”. In: *Computational Mechanics* 57 (2016).
- [152] H. Leipholz and J.W. Hutchinson. “Theory of Elasticity”. In: *Journal of Applied Mechanics* 42.4 (1975), pp. 911–911.
- [153] B. Pan and W. Cui. “An overview of buckling and ultimate strength of spherical pressure hull under external pressure”. In: *Marine Structures* 23.3 (2010), pp. 227–240.
- [154] Y. Ammouche and A. Jérusalem. “A modular nonlinear stochastic finite element formulation for uncertainty estimation”. In: *Computer Methods in Applied Mechanics and Engineering* 396 (2022), p. 115044.

- [155] X. Zheng et al. “Ultralight, ultrastiff mechanical metamaterials”. In: *Science* 344.6190 (2014), pp. 1373–1377.
- [156] X. Yu et al. “Mechanical metamaterials associated with stiffness, rigidity and compressibility: A brief review”. In: *Progress in Materials Science* 94 (2018), pp. 114–173.
- [157] R. Hasan et al. “Comparison of the Drop Weight Impact Performance of Sandwich Panels with Aluminium Honeycomb and Titanium Alloy Micro Lattice Cores”. In: 24 (Aug. 2010), pp. 413–418.
- [158] S.M. Ahmadi et al. “Mechanical behavior of regular open-cell porous biomaterials made of diamond lattice unit cells”. In: *Journal of the Mechanical Behavior of Biomedical Materials* 34 (2014), pp. 106–115.
- [159] S. Bonfanti et al. “Automatic design of mechanical metamaterial actuators”. In: *Nature Communications* 11.1 (2020).
- [160] C. Cattaneo. “Sul contatto de due corpi elastici: Distribuzione locale degli sforzi”. In: *Rendiconti dell’Accademia nazionale dei Lincei* 6 (1938), pp. 342–349.
- [161] R.D Mindlin. “Compliance of elastic bodies in contact”. In: (1949).
- [162] S. Lin, J. Sun, and Y. Peng. “Analysis of axial fretting mode and mechanical model for a four-row tapered roller bearing”. In: *International Journal of Mechanical Sciences* 228 (2022), p. 107463.
- [163] A.P. Sanders and R.M. Brannon. “Assessment of the applicability of the Hertzian contact theory to edge-loaded prosthetic hip bearings”. In: *Journal of Biomechanics* 44.16 (2011), pp. 2802–2808.
- [164] Y. Bing et al. “Medical imaging based in silico head model for ischaemic stroke simulation”. In: *Journal of the Mechanical Behavior of Biomedical Materials* 101 (2020), p. 103442.
- [165] K. Karhunen. “Zur Spektraltheorie stochastischer prozesse”. In: 1946.
- [166] K. Karhunen. “Über lineare Methoden in der Wahrscheinlichkeitsrechnung”. In: 1947.
- [167] R.W. Ogden and R. Hill. “Large deformation isotropic elasticity – on the correlation of theory and experiment for incompressible rubberlike solids”. In: *Proceedings of the Royal Society of London. A. Mathematical and Physical Sciences* 326.1567 (1972), pp. 565–584.
- [168] B.B. Saha. “On a generating function of Hermite polynomial”. In: *Yokohama Mathematical Journal* (1969), pp. 73–76.
- [169] M. Abramowitz and I.A. Stegun. “Handbook of Mathematical Functions with Formulas, Graphs, and Mathematical Tables”. In: *Probabilistic Engineering Mechanics* 20 (1964), pp. 188–198.